Multi-Dimensional Correlation Exploited Cooperative Wireless Communications

by

Xiaobo Zhou

submitted to
Japan Advanced Institute of Science and Technology
in partial fulfillment of the requirements
for the degree of
Doctor of Philosophy

Supervisor: Professor Tadashi Matsumoto

School of Information Science
Japan Advanced Institute of Science and Technology

July, 2013

Abstract

In this thesis, cooperative wireless communications are intensively investigated from the perspective of exploiting correlations among multiple sources. The primary goal is to create theoretical bases and establish practical coding frameworks for cooperative wireless communications that exploit multi-dimensional correlations, and finally achieve new paradigm shift in wireless communication system design. Particularly, we focus on three representative problems to demonstrate the impact of the source correlations on the performance of the cooperative wireless communication systems and how we can best utilize the correlation knowledge among the distributed multiple sources.

Creation of the design concept and the algorithms of the conventional point-to-point (P2P) systems are the basis for solving the problems arising in cooperative wireless communications. Initially, the problem of transmitting binary Markov sources from a single source to a single destination over wireless channels is studied. The achievable compression rate region is determined by the source coding theorem. The performance limits in Additive White Gaussian Noise (AWGN) channels and outage probability in Rayleigh fading channels are then derived. Furthermore, we propose a new joint source-channel (JSC) decoding scheme, based on serial-concatenated convolutional codes (SCCC). By combining the trellis diagrams of Markov source and the outer code, a super trellis is constructed to exploit the time-domain correlation of the source. A novel modified version of Bahl-Cocke-Jelinek-Raviv (BCJR) algorithm is derived based on this super trellis and used for decoding of the joint outer code.

Then, we investigate the problem of transmitting Markov source over a one-way single relay channel, which consists of one source, one relay and one destination. The relay just extracts and forwards the source information sequence to the destination, even though the extracted information sequence may contain some errors. Therefore, the information sent from the source and relay nodes are correlated, which is referred to as source-relay correlation. The achievable compression rate region of this system is determined by the Slepian-Wolf theorem. Lower bound of the performance limit in AWGN channels and the outage probability in block Rayleigh fading channels can be derived based on the achievable compression rate region. We also propose a distributed joint source-channel (DJSC) decoding scheme to exploit the source-relay correlation and the source memory simultaneously. In our proposed technique, a Log-likelihood Ratio (LLR) updating function, which is supported by the Slepian-Wolf theorem, is used to estimate and exploit the source-relay correlation, while the JSC technique proposed above is used to exploit the source memory.

Finally, we consider the problem of transmitting two correlated sources over orthogonal multiple access relay channel (MARC). The MARC consists of two sources communicating with a common destination with the assistance of a single relay. The role of the relay is to perform network coding, followed by channel coding, to assist the two sources to improve the probability of successful signal reception at the destination. In this case, the achievable compression rate region is derived based on the theorem for source coding with side information. The performance limits in AWGN channels and the outage probability

in block Rayleigh fading channels are derived based on the achievable compression rate region. Furthermore, we propose a novel joint source-channel-network (JSCN) decoding technique to fully exploit the correlation between the two sources, as well as the benefit of network coding. In our proposed technique, modified versions of boxplus operation that takes into account the correlation between the two sources are derived for the relay and source nodes.

In the three problems described above, the impacts of source correlations on the performance of the corresponding systems are investigated through asymptotic analysis. The convergence properties of the proposed JSC and DJSC techniques are verified through Extrinsic Information Transfer (EXIT) chart analysis. Moreover, the effectiveness of the proposed JSC, DJSC, and JSCN decoding techniques and the accuracy of the theoretical analysis are verified through a series of simulations, including bit-error-rate (BER) performance in AWGN channels and frame-error-rate (FER) performance in Rayleigh fading channels.

Keywords: Cooperative wireless communications, source correlation, achievable compression rate region, performance limit, outage probability, relay channel, multiple access relay channel, Slepian-Wolf theorem, source coding with side information theorem

Acknowledgments

First of all, I would like to express my deepest gratitude to my supervisor, Professor Tadashi Matsumoto, who introduce me to Wireless Communications three years ago. I am grateful to him for his patient guidance, inspiring instructions and warm encouragement throughout my graduate research, and for the international platform that he provided which broadens my horizons. I also highly appreciate the positive and friendly atmosphere he fosters in our group, which is nutritious and healthy for theoretical and creative research.

I am grateful to Associate Professor Azman Osman Lim for his able guidance and useful suggestions, which helped me in completing the sub-theme research. Deep sense of gratitude are also due to Assistant Professor Khoirul Anwar, without his knowledge and assistance this thesis would not have been completed. I would also like to take this opportunity to express my gratitude to the members of examination committee of my doctoral dissertation, Professor Ping Li from City University of Hong Kong, Professor Markku Juntti from University of Oulu, Associate Professor Takeo Fujii form The University of Electro-Communications, Professor Mineo Kaneko form JAIST and Associate Professor Brian Michael Kurkoski form JAIST, for their valuable comments and suggestions to improve the quality of this thesis.

I wish to devote my sincere thanks to all my colleagues of Information Theory and Signal Processing Laboratory, Kisho Fukawa, N. Imazato, Qianxing Wang, Ormsub Soulisak, Yasuhiro Takano, Valtteri Tervo, Pen-Shun Lu, Hui Zhou, Ade Irawan, Meng Cheng, Xin He, Shen Qian, Kun Wu, Muhammad Reza Kahar Aziz, Ricardo Antonio Parrao Hernandez and Francisco Javier Cuadros Romero, for their kind help and friendship. The discussions, chats and laughters with them made my life in JAIST much more easier and colorful. Special thanks go to the exchange student, Mohd Azri Mohd Izhar form Universiti Teknologi Malaysia (UTM), Malaysia, for the stimulating discussions and cooperation.

In addition, I would like to express my gratitude to the Graduate Research Program (GRP) of JAIST for providing me with financial support such that I can focus on my research. I also devote my sincere appreciation to all the staff of JAIST for their friendly and heartwarming assistance, which make my daily life and research smooth and comfortable.

Finally, I would like to express my sincere gratitude to my parents and my brother for their love, support and encouragement. I would also like to express my sincere gratitude to my wife, Yuanzhe Liu, for her unconditional love and support. Without her understanding and accompany, I would never complete this work.

Contents

List of Figures

List of Tables

Chapter 1

Introduction

In this chapter, we first of all briefly introduce the basic concept of cooperative wireless communications. The motivation of the research on exploiting multi-dimensional correlations among multiple sources in cooperative wireless communications and literature review on existing results of some techniques used in this research is then presented. The contribution of this research is also provided, which is followed by the organization of the dissertation.

1.1 Cooperative Wireless Communications

The fundamental goal of future ubiquitous communications systems is to transmit information data efficiently and reliably from multiple sources to multiple destinations over wireless channels, where signal fading is the major channel impairment [1]. In order to increase the data rate through spatial multiplexing and to mitigate the fading effect through spatial diversity, multiple-input multiple-output (MIMO) techniques where multiple antennas are employed at the transmitter and/or receiver sides have been widely acknowledged and adopted in various wireless standards [2]. There are a great number of papers available on the performance limits, capacity analysis and practical coding schemes on MIMO systems, and a survey on MIMO techniques can be found in [3]. However, in future cellular networks or wireless sensor/mesh networks, multiple antennas may not be supported due to the bandwidth, size and energy limitations. To overcome these limitations, cooperative wireless communications have emerged as a promising technique for future communication systems [4, 5].

Due to the broadcast nature of wireless signals, a signal transmitted from a source node to a particular destination node in a wireless network can be "overheard" at the neighboring nodes. These neighboring nodes can process signals they overhear and transmit towards the destination. The basic idea of cooperative wireless communications is to enhance power and spectrum efficiencies and improve communication reliability, by allowing wireless nodes in a wireless network to overhear and help the information transmission of each other. These neighboring nodes that overhear and help in information transmission are usually referred to as *relays* (or partners, helpers). It is easily to identify that, in cooperative wireless communications, multiple nodes in a wireless network form a *virtual multiple antenna system* by sharing the single antenna of each node [6]. Therefore, spatial diversity of the MIMO techniques can be achieved by allowing node cooperation in cooperative wireless communications. Moreover, compared with MIMO techniques,

cooperative wireless communications is advantageous in terms of deployment flexibility and hardware feasibility [7].

The basic idea of cooperative wireless communications can be traced back to relay channel introduced by Van der Meulen [8] in 1970s, where a three terminal relay channel is investigated. Shortly after that, capacity of the relay networks was intensively investigated by Cover and Gamal in [9], where the results constructed the theoretical basis for the subsequent research work on cooperative communications. Since then, various cooperative wireless communication schemes have been proposed to exploit the advantages in terms of the capacity, diversity, the error rate, the outage probability, etc. [10].

Generally, there are two ways to achieve cooperation in a wireless network: (1) deploy extra relay nodes to assist the communication between source nodes and their corresponding destinations, (2) allow the nodes in the same wireless network to hep each other to communicate with their corresponding destinations. Systems using these two ways of operation are referred to as relay networks and cooperative networks, respectively [2]. In relay networks, the only purpose of relay nodes is to forward the information sent from the source nodes, therefore they do not have their own information. On the other hand, in cooperative networks, each node acts as both a source node and a relay node at different transmission phases. Beside this difference, as far as signal processing at relay is concerned, there is no difference between the relay networks and the cooperative networks. Therefore, in this thesis, we use the common terminology "cooperative wireless communications" to represent the general wireless communication system where node cooperation is involved, including both the relay networks and the cooperative networks.

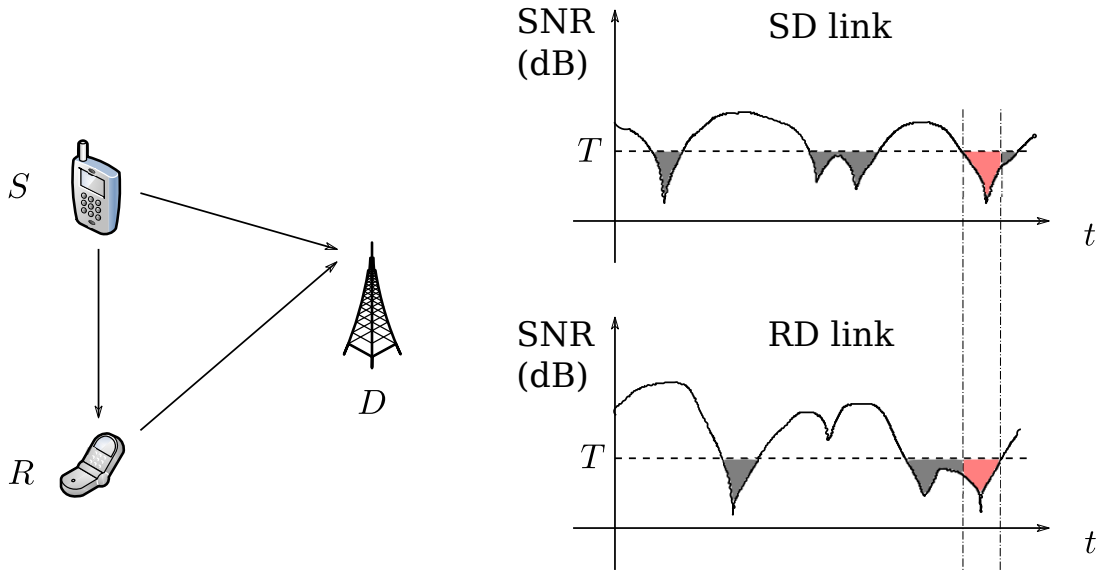

Figure 1.1: An example of a cooperative wireless communication system.

We demonstrate the basic concept of cooperative wireless communication by considering a simple example of relay system, shown in Fig. 1.1, where a source node S wants to communicate with a destination node D with the help of a relay node R over wireless channels. In the first time slot, S broadcasts its signal to both R and D, and at the second time slot, R will forward the overheard signal to D. Thus D has two copies of the same information. Because of the channel variation, the transmission fails when the channel experiences a deep fade, i.e., when the instantaneous signal-to-noise ration (SNR) of the

SD link falls below a certain threshold T, which is denoted by the gray region in Fig. 1.1. However, if R can overhear the signals from S and send it to D, then the transmission fails only if the instantaneous SNR of both SD and RD links fall below T, as shown in Fig. 1.1. Hence, through cooperation between S and R, spatial diversity can be achieved, by which the probability that the transmission fails is significantly reduced.

The relay protocol specifies the processing performed by the relay node upon its received signals. In the above example, the relay node decodes and re-encodes the received signal, then forwards the coded sequence to the destination node. However, the signal processing at the relay node should not necessarily be decoding, re-encoding and forwarding. Based on the operations at the relay node, there are several prominent relay protocols [11], which are listed as follow:

- **Amplify-and-Forward**
  Amplify-and-forward (AF) (also called scale-and-forward) is one of the simplest relay protocols [12, 13]. For the AF protocol, each relay node simply scales its received signal according to its power constraint and forwards the scaled signal to the destination. The destination node make decision by properly combining signals transmitted from the source and relay nodes, and thereby spatial diversity can be achieved by the AF protocol. The major problem of the AF protocol is that the noise at the relay node is also amplified. The outage probability and bit-error-rate (BER) performance of the AF protocol is presented in [12] and the impact of relay location on the system performance is investigated in [14]. It is shown in [14] that when the relay node is located in the middle of the source and destination nodes, optimum performance can be achieved.

- **Compress-and-Forward**
  Compress-and-Forward (CF) (also called estimated-and-forward, or quantize-and-forward) is another widely investigated protocol. For the CF protocol, the relay node retransmits a quantized and compressed version of the received signal to the destination node. Furthermore, the relay takes advantages of the statistical dependence between the signal received at the relay node and that received at the destination node. Although CF is not as popular as AF, some practical aspects of CF can be found in [15–17], where the relay use Wyner-Ziv source coding [18] to exploit side information at the destination.

- **Decode-and-Forward**
  Decode-and-Forward (DF) has drawn more attention than AF and CF, and it is well-studied among all the relay protocols. For the DF protocol, after receiving signals transmitted from the source node, the relay node first decodes the received signals and then re-encodes before transmitting it to the destination node. Therefore additioned error protection to the original information can be provided. A lot of practical implementations of the DF protocol have been proposed, using different code families, such as convolutional code [19], Turbo codes [20–22] and low density parity check (LDPC) codes [23, 24]. It is found that, when the channel quality of the source-relay link is good, DF based cooperation scheme outperforms AF and CF based schemes. However, AF and CF based cooperative schemes are more advantageous if the source-relay link suffers from deep fade [7].

The relay node can work in either full-duplex mode or half-duplex mode. Under half-duplex constraint, the receiving and transmitting at the relay node are carried out in different time slots. Due to its simplicity of implementation, half-duplex relaying is assumed in a large number of existing works on cooperative wireless communications [21, 25–29]. However, the half-duplex relaying suffers from loss in bandwidth efficiency because it requires resource partitioning for signal reception and transmission. To overcome the drawback of half-duplex relaying, full-duplex relaying is considered in [30–34], where the relay node receives signals from the source node and transmits signals to the destination node at the same time and in the same frequency band. With full-duplex mode, higher spectral efficiency can be achieved, at the price of extra hardware implementation and increased energy consumption. Full-duplex relaying has been considered impractical in the past due to the strong self-interference caused by the transmitter to its own receiver, but recent advances on antenna technology and signal processing make it feasible [35]. Recently, a relay scheme that uses relay selection and half-duplex relays with buffers to mimic full-duplex relaying is proposed in [36].

In cooperative wireless communications, the source and relay nodes can transmit through either orthogonal channels or non-orthogonal channels [2]. In orthogonal transmissions, the signals transmitted from the source and relay nodes can be separated at the destination node, thus there is no interference and the receiver processing is simple. Some related works can be found in [37–44]. In non-orthogonal transmissions, the source and relay nodes transmit to the destination node at the same time and the same frequency. Hence, the signal received at the destination node is a combination of the signals transmitted from the source and relay nodes. Some practical code designs for cooperative wireless communications over non-orthogonal channels are proposed in [45–47]. Generally, they can achieve higher throughput than orthogonal channels. However, the choice of orthogonal or non-orthogonal channels depends on both SNR and power allocation, which are investigated in [48, 49].

1.2 Motivations and Research Background

1.2.1 Motivations

Wireless sensor networks (WSNs) [50] made up of a great number of densely deployed low-energy consuming wireless nodes (e.g. micro cameras and small relays) have attracted a lot of attention recently, and its potential applications cover a vast area of human activities, such as wireless video surveillance, environmental monitoring, health care system, and many other possible applications [51]. An example of a simple WSN is depicted in Fig. 1.2, where several wireless sensors are deployed in a forest area for monitoring. There are several inherent properties within WSNs that make the problem interesting: (1) the correlation exists between the data collected at the wireless nodes, (2) the wireless nodes can exchange information to increase their efficiency or flexibility through cooperation, (3) the wireless nodes have energy consumption limit, and hence their computational capabilities are also limited. Therefore the signaling complexity as well as the transmitting power has to be as low as possible.

The problem of optimal code design for WSNs that makes efficient use of the advantage of correlation knowledge among sources as well as achieving spatial diversity through node cooperation falls into the category of cooperative communication for correlated sources

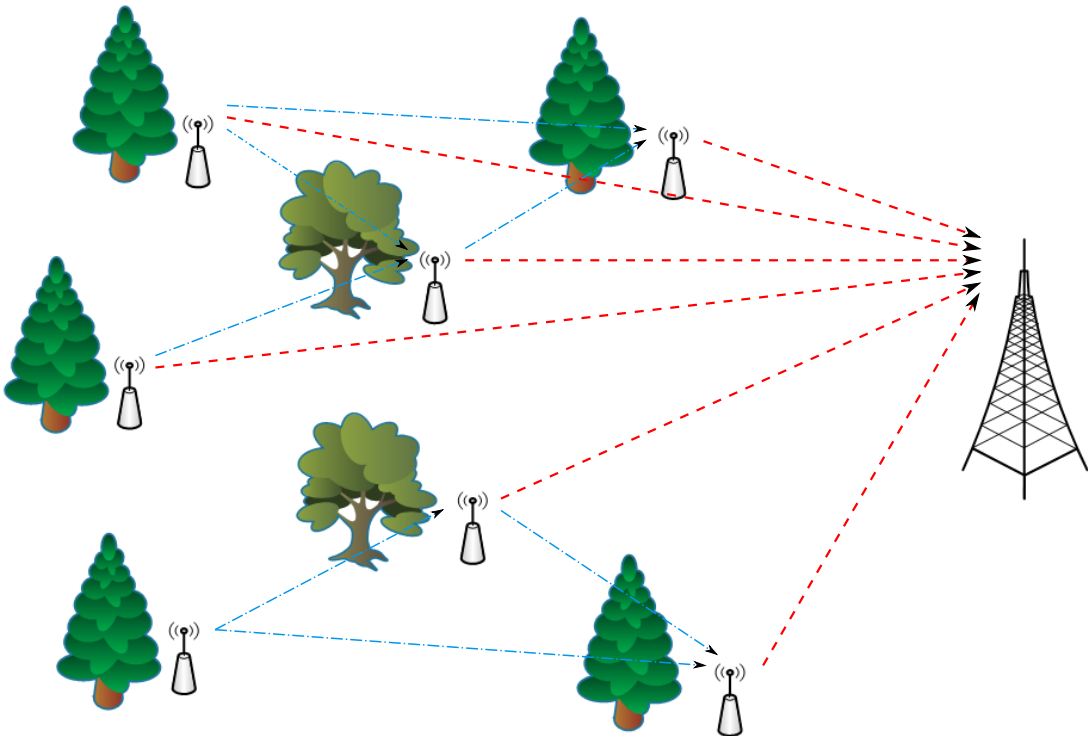

Figure 1.2: An example of a simple WSN.

[52–54]. It has been shown in [55] that the problem of transmitting correlated sources over the cooperative networks involves the issues of joint source-channel (JSC) coding, distributed source coding (DSC) [56] and network coding [57]. At the initial stage, JSC, DSC and network coding were performed separately [55]. JSC and DSC exploits the correlation among sources for efficient source compression while network coding provides cooperative diversity for fading mitigation. However, it is well known that in practical cooperative networks such as WSNs with limited complexity, separate design of source, channel and network coding may not be optimal [58].

Recently, joint source-channel-network (JSCN) coding has emerged as a promising technique for correlated sources transmission over the cooperative networks. This problem was originally investigated in [59], where a general network of discrete memoryless channels (DMCs) with multiple relay nodes and a single sink node is considered. Later, multicasting of correlated sources over a network of noiseless channels were considered in [52], where error exponents are provided. Reference [53] provides theorems with their proofs that can be used as a theoretical basis for solving the problem of network information flow with correlated sources. Following the theoretical investigations described above, some practical JSCN coding schemes have also been proposed [60–63]. A JSCN coding scheme for bidirectional wireless relays based on fountain code is proposed in [62], and JSCN coding schemes for multicasting are presented in [55, 58, 61].

However, there are still many open problems in cooperative wireless communications exploiting multi-dimensional correlations among correlated sources, based on different network topologies and cooperative strategies. In the next subsection, we provide brief reviews on state-of-the-art technologies in JSC, DSC and network coding which are involved in this research, respectively.

1.2.2 Joint Source-Channel Coding

In conventional point-to-point (P2P) systems, source coding and channel coding are usually designed independently. The optimal design of conventional system has largely relied on the design criteria supported by the Shannon's separation theorem [64]. However, there are several impractical limitations while utilizing the separation theorem [65], which prevent communication systems from achieving desired performance in practice. As a consequence, JSC optimal design has drawn considerable attentions over the last two decades [66–69].

In the majority of the approaches to JSC decoding, variable-length code (VLC) is employed as source encoder and the implicit residual redundancy after source encoding is additionally used for error correction in the decoding process. A common idea is to represent the VLC as a symbol-level or bit-level trellis and decode it with maximum *a posteriori* probability (MAP) algorithm by modifying the Bahl-Cocke-Jelinek-Raviv (BCJR) algorithm [70, 71]. The extended work of this category is presented in [72–74], where convolutional code (CC) is replaced by more powerful Turbo code. Quite recently, Multiple Label Mapping (MLM) is investigated in [75] to eliminate the boundary problem due to the variable length source coding, and the use of Burrows-Wheeler Transform (BWT) is investigated in [76], both with the aim of achieving efficient JSC code design.

Instead of utilizing the residual redundancy after source encoding, there are several techniques which focus on exploiting the memory structure of the source in the decoding process directly. There are two advantageous points with this class of JSC design: (1) no source encoding is needed and hence it can be employed in universal applications, while it simplifies the encoder structure and reduces power consumption at the transmitter, (2) the error correction capability of the system, as a whole, can further be improved. An approach of combining Hidden Markov Model (HMM) with the Turbo code design framework is presented in [77,78], while combining HMM in the framework of LDPC code design in [79–81]. Besides HMM, Markov Chain (MC) is also used to describe the source and combined with Turbo code, which is presented in [82].

1.2.3 Distributed Source Coding

Source coding is one of the most important signal processing component in communication systems. In conventional source coding techniques, a single encoder or several encoders collaborate with each other to exploit the redundancy of the source in order to perform compression, which is usually referred to as centralized source coding [56]. However, the advance of wireless sensor/mesh networks and ad-hoc networks brought new challenges to the source coding problem: the source information to be compressed appears at several separate terminals and it is not always feasible to communicate among these terminals. The resulting source coding problem is often referred to as distributed source coding (DSC) [83]. The first fundamental theory about DSC was established in Slepian and Wolf's pioneer work [84], where two correlated sources coding problem was considered. Slepian and Wolf proved that as long as joint decoding is performed, separate encoding can be as efficient as joint encoding for lossless compression, and the admissible rate region for separate encoding is also derived. The first practical framework for distributed source coding using syndromes (DISCUS) was introduced in [85]. Later on, many excellent schemes for DSC were proposed, which are based on irregular repeat accumulate (IRA) codes [86–88], Turbo codes [89, 90] and LDPC codes [91–94].

The DSC concept can be applied to relay system to achieve better performance. With DF relaying, the information forwarded by the relay node is a replica of that transmitted from the source node, therefore the performance of the relay system can be further improved if signaling and coding at the source and relay nodes are performed in the framework of DSC. Based on this concept, a variety of distributed coding structures have been successfully developed over the past several years for wireless relay systems, which are based on distributed Turbo codes (DTC) [22, 95] or Distributed LDPC codes [24].

With DF relaying protocol, decoding errors may occur at the relay node, depending on the quality of the source-relay link. In conventional DF systems, the recovered data sequence is discarded if errors are detected after decoding at the relay node. It is believed that if the relay re-encodes this erroreous data sequence and forwards it to the destination, error propagation will occur, which leads to even worse performance. However, even with some errors occurring in the information part, the data sequence transmitted from the source and relay nodes are still highly correlated, therefore Slepian-Wolf's correlated source coding theorem can be well utilized in this situation. Reference [96] formulates this issue from the viewpoint of Slepian-Wolf theorem, where the authors assume the relay does not aim to perfectly correct the errors in the source-relay link, instead, it just simply *extracts*[1] information part from the received signals, interleaves, re-encodes and then forwards to the destination node. The extracted data may contain errors, but by iterative processing with the Log-likelihood Ratio (LLR) updating function [88], the error probability can be estimated and further utilized at the destination node. This scheme is referred to as *extract-and-forward* (ErF) relaying in [96]. The ErF concept is adopted and combined with bit-interleaved coded modulation with iterative detection (BICM-ID) in [97]. The outage probability of the ErF relay system in block Rayleigh fading channel is evaluated in [98, 99], where the impacts of not only the source correlation but also the correlation of the link variation are theoretically analyzed.

1.2.4 Network Coding

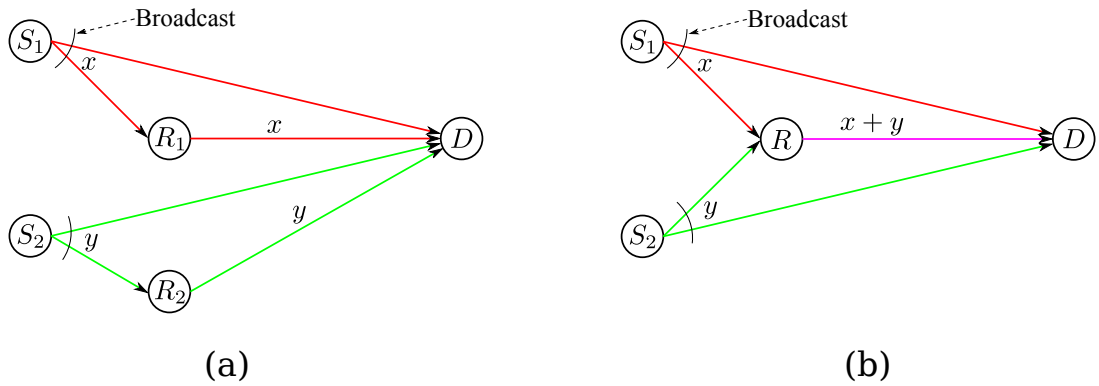

Figure 1.3: Examples of simple relay networks. (a) The conventional relay strategy. (b) A network coded relay strategy.

In cooperative wireless communications, multiple source nodes are communicating

[1]Full iterative decoding is not performed at the relay with the aim of reducing the computational burden on the relay node. Instead, the relay performs only 1 round of iteration to obtain a tentative estimate of the source information sequence.

with multiple destination nodes with the help of multiple relay nodes. Here we consider a simple network model where two source nodes S_1 and S_2 are communicating with a common destination D with the help of several relay nodes. According to the early cooperative communication protocols (AF, CF and DF, etc.), two relay nodes R_1 and R_2 are needed to help the data transmission of S_1 and S_2, respectively, as shown in Fig. 1.3(a), thus diversity gain can be achieved with each data transmission. However, the signal sent from S_2 can also be overheard at R_1, due to the broadcasting property of the wireless medium. Therefore, a new strategy for information transmission in networks has been proposed, as shown in Fig. 1.3(b), which is referred to as network coding [100]. With network coding, a single relay R is used to help S_1 and S_2 simultaneously by forwarding the combination of signals received from S_1 and S_2 to D, thus the same diversity gain can be achieved.

The concept of network coding was first introduced in [57], which shows that bandwidth can be saved with network coding for multicasting in a wired network. Since then, network coding has been applied to various cooperative communication schemes [101–103]. It has been shown that, despite of diversity gain, performance gains in terms of throughput, energy/spectrum efficiency and reliability can be achieved with network coding. According to the relay strategy, there are mainly two types of network coding: analog network coding and q-ary network coding. In analog network coding, AF is adapted to combine the analog signals transmitted from the sources, some related work can be found in [104, 105]. The outage behavior and optimum power allocation for analog network coding are investigated in [106–108]. On the other hand, DF is employed in q-ary network coding, where the relay node first decodes the signals received from the sources, performs superposition of the information part, re-encodes and then forwards the encoded sequence to the destination node. Some practical approaches based on bit-wise Exclusive-OR (XOR) operation for binary network coding are presented in [101–103, 109]. Also, some literature focus on designing linear block codes defined over $GF(q)$ for network coding [110–113], where q represents the size of finite alphabet set.

1.3 Summary of Contribution

Our research investigates cooperative wireless communications from the perspective of exploiting correlation among multiple sources, by considering three representative problems: (1) binary Markov source transmission in P2P communications, (2) binary Markov source transmission in one-way relay system, and (3) correlated sources transmission over multiple access relay channel (MARC). In all the three problems considered, the relay nodes work in half-duplex mode. Although the system models are quite simple, our work provides both theoretical and practical contributions to the existing research on wireless cooperative communications. The main contributions of this thesis can be summarized as follows:

A. Theoretical Contributions

- The performance limits of Problem (1) in Additive White Gaussian Noise (AWGN) channels and the outage probability in Rayleigh fading channels are theoretically analyzed.

- For Problem (2), it is found that the Slepian-Wolf theorem can be used to determine the achievable compression rate region. Lower bound of the performance limits in AWGN channels and the outage probability in Rayleigh fading channels are theoretically derived based on the achievable compression rate region.

- For Problem (3), the achievable compression rate region is determined by the theorem for source coding with side information, which is found to be a 3D space. The performance limits in AWGN channels and the outage probability in Rayleigh fading channels are derived based on the achievable rate region.

- The impact of source correlation on the performance of corresponding systems are investigated through asymptotic analysis.

B. Practical Contributions

- For Problem (1), a new JSC decoding technique is proposed to exploit the source memory, which is based on serial-concatenated convolutional codes (SCCC). A modified version of Bahl-Cocke-Jelinek-Raviv (BCJR) algorithm is derived for the joint decoding of the Markov source and the outer code.

- The JSC technique is applied to Problem (2) and a distributed joint source-channel (DJSC) decoding scheme is proposed to exploit the source memory and the source-relay correlation simultaneously.

- We propose a novel JSCN decoding technique for Problem (3) to fully exploit the correlation between the two sources and the benefit of network coding.

- We use of Extrinsic Information Transfer (EXIT) chart analysis to evaluate the convergence property of the techniques proposed for Problem (1) and (2). Also, code parameter optimization is performed based on EXIT chart analysis for Problem (1).

- Simulations are performed to evaluate the superiority of the proposed techniques that exploit source correlations, and the impact of source correlations on the system performance.

1.4 Dissertation Organization

The dissertation is organized as follow:

In **Chapter 1** (this chapter), we have introduced the basic concept of cooperative wireless communications, motivation of the research and some research backgrounds. We have also summarized the contributions of this research and presented the structure of the dissertation.

Chapter 2 reviews the concept of entropy and mutual information. A general modern P2P communication system is described, where the issues of lossless source coding theorem, noisy channel coding theorem, channel models and channel capacity are discussed. Also, EXIT chart analysis which can be used for evaluating the convergence property of communication systems is introduced.

Chapter 3 investigates problem of transmitting binary Markov source in P2P communications, where the source memory is exploited in the joint decoding process at the decoder. The performance limits in AWGN channels and the outage probability in Rayleigh fading channels are first derived to evaluate the impact of exploiting source memory. Then a new JSC decoding scheme based on SCCC to exploit the source memory is presented. The convergence property of the proposed technique is evaluated through EXIT chart analysis, where the code parameters are optimized. The superiority of the proposed JSC technique and the accuracy of the theoretical analysis are verified through computer simulations.

Chapter 4 is devoted to the problem of transmitting Markov source over a one-way single relay system, which is based on ErF relaying strategy. In ErF relay system, the information sent from the source and relay nodes are correlated, which is referred to source-relay correlation. Both the source-relay correlation and the memory structure of the Markov source can be exploited at the destination node. The Slepian-Wolf theorem is used to determine the achievable compression rate region of this system. The lower bound of the performance limits in AWGN channels and the outage probability in Rayleigh fading channels are derived based on the achievable compression rate region. Then the DJSC decoding scheme that exploits the source-relay correlation and source memory simultaneously is present. 3D EXIT chart analysis is presented to evaluate the convergence property of the proposed DJSC technique. Results of simulations for BER and frame-error-rate (FER) performance evaluations, as well as application to image transmissions are presented.

Chapter 5 focuses on the problem of transmitting two correlated sources over orthogonal MARC, where binary XOR operation is employed at the relay node. First, the achievable compression rate region is derived based on the theorem for source coding with side information. The performance limits in AWGN channels and the outage probability in Rayleigh fading channels are then derived based on the achievable compression rate region. A JSCN decoding scheme that fully exploits the correlation between the two sources and the benefit of network coding is also presented. Simulation results of the BER and FER performance are also presented.

Chapter 6 summarizes the work in this dissertation, and provides insights into the future work.

Chapter 2

Preliminaries

In this chapter, we briefly provide explanations and definitions of background knowledge exploited in this research. First we introduce the concept of entropy and mutual information. Then we describe a general model of communication system, and several fundamental issues related, i.e., the lossless source coding theorem, the noisy channel coding theorem, modulation/demodulation schemes, channel models and channel capacity, are presented. Finally, the basic concept of EXIT chart analysis, which is used to evaluate the convergence property of the communication systems, is provided in detail.

2.1 Entropy and Mutual Information

In Information theory, the concept of *entropy* was first introduced by Shannon in [64], which is used as a measure of the uncertainty or ambiguity of a random variable. Consider a discrete random variable X drawing i.i.d. from a finite alphabet $\mathscr{X}$ with probability mass function $p(x) = \Pr\{X = x\}, x \in \mathscr{X}$. The entropy of X is defined by

$$H(X) = -\sum_{x \in \mathscr{X}} p(x) \log p(x). \tag{2.1}$$

If the log is to the base 2, entropy is expressed in bits. For the completeness, we use the convention that $0 \log 0 = 0$, and $H(X)$ is always non-negative.

This definition can be easily extended to a pair of random variables. Let X and Y be a pair of discrete random variables with a joint distribution $p(x, y)$. The joint entropy of X and Y is expressed as

$$H(X, Y) = -\sum_{x \in \mathscr{X}} \sum_{y \in \mathscr{Y}} p(x, y) \log p(x, y). \tag{2.2}$$

The conditional entropy of X given Y can be further described as

$$\begin{aligned} H(X|Y) &= \sum_{y \in \mathscr{Y}} p(y) H(X|Y = y) \\ &= -\sum_{y \in \mathscr{Y}} p(y) \sum_{x \in \mathscr{X}} p(x|y) \log p(x|y) \\ &= -\sum_{y \in \mathscr{Y}} \sum_{x \in \mathscr{X}} p(x, y) \log p(x|y). \end{aligned} \tag{2.3}$$

Obviously, the joint entropy of a pair of random variables is the summation of the entropy of one (X or Y) and the conditional entropy of the other (Y or X, conditioned on X or Y, respectively), which is also called the chain rule of entropy [114], expressed as

$$\begin{aligned} H(X,Y) &= H(X) + H(Y|X) \\ &= H(Y) + H(X|Y). \end{aligned} \tag{2.4}$$

The mutual information measures the common information that two random variables contain. The mutual information between X and Y is defined by

$$I(X;Y) = \sum_{x\in\mathscr{X}} \sum_{y\in\mathscr{Y}} p(x,y) \log \frac{p(x,y)}{p(x)p(y)}, \tag{2.5}$$

where $p(x)$ and $p(y)$ are marginal probability mass functions. When the random variables X and Y are statistically independent, $p(x|y) = p(x)$ and hence $I(X;Y) = 0$. In summary, the relationship between entropy and mutual information can be expressed as

$$\begin{aligned} I(X;Y) &= H(X) - H(X|Y) \\ &= H(Y) - H(Y|X) \\ &= H(X) + H(Y) - H(X,Y). \end{aligned} \tag{2.6}$$

2.2 General Model of Communication System

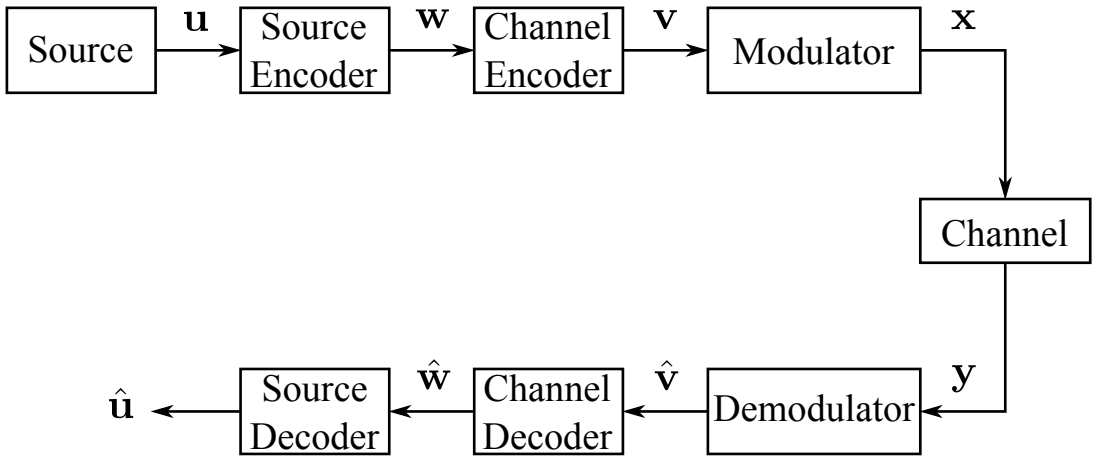

Figure 2.1: System Model of a general communication system.

The block diagram of a general model of a P2P communication system is shown in Fig. 2.1, where all higher layer protocols are removed and only physical layer and error correction components are described. This communication system is designed to transmit the information generated from a source to the destination. The output of the source can be analog or digital (finite alphabet[1]) signals. In modern communication systems, the analog signals are usually first sampled and quantized to convert into digital form. Therefore, we assume that the output of the source $\mathbf{u}$ is a symbol sequence in digital

[1]This thesis only assume binary representation of the source.

form. The information sequence $\mathbf{u}$ is first encoded by a source encoder to *remove the redundancy* for compression, and then encoded by a channel encoder to *add redundancy* for error correcting. The channel encoded sequence $\mathbf{v}$ is mapped into a sequence of signal waveforms $\mathbf{x}$ to be transmitted through the channel, according to the modulation scheme of the system. After receiving signals from the channel, the destination will perform demodulation, channel decoding and source decoding to obtain the estimate of $\mathbf{u}$.

2.2.1 Source Coding Theorem

The source encoder in Fig. 2.1 removes all redundant information from $\mathbf{u}$ (if any) and obtains a compressed binary version of the data in $\mathbf{w}$, with the aim of reducing the amount of data to be transmitted, which is equivalent to minimizing the transmission power and bandwidth. The compression rate R_s represents the number of bits per symbol needed to describe the source. In general, there are two different categories of source coding, lossless and lossy. In lossless source coding, the goal is to minimize the number of bits in such a way that the source symbols can be exactly recovered from the compressed version of the data. On the contrary, in lossy source coding, certain level of distortion is allowed when recovering the source symbols. In this thesis, we only consider the lossless source coding problem. The fundamental bound on R_s that achieving lossless source coding is given in the following theorem first proved by Shannon [64].

Theorem 2.1 (Lossless source coding theorem) *For a sequence $\{X_i\}_{i=1}^{\infty}$ of discrete random variables drawing i.i.d. from a source X according to the density mass function $p(x)$. There exists a lossless source code for this sequence if the compression rate $R_s \geq H(X)$.*

This theorem is also called Shannon's first theorem. According to this theorem, for any compression rate $R_s < H(X)$, lossless source coding is not possible. Cover and Thomas extended this theorem to any stationary stochastic sources [114, Theorem 5.4.2], where $H(X)$ represents the entropy rate of the stochastic sources. There are many approaches for lossless source coding, such as Huffman coding [64], Shannon-Fano-Elias coding [114] and Lempel-Ziv coding [115].

2.2.2 Channel Coding Theorem

After source encoding, the channel encoder in Fig. 2.1 adds redundancy to $\mathbf{w}$ for more reliable communication. The code rate of the channel encoder is denoted by $R_c = L_w/L_v$, where L_v is the number of bits in the channel encoding output $\mathbf{v}$. The condition on R_c for reliable communication, if source coding and modulation is not considered, is specified by the following theorem.

Theorem 2.2 (Noisy Channel Coding Theorem) *Reliable Communication over a discrete memroyless channel is possible if the communication rate R_c satisfies $R_c \leq C$, where C is the channel capacity[2]. At rates higher than channel capacity, reliable communication is impossible.*

[2]Discussion on channel capacity will be detailed in Section 2.2.5.

The noisy channel coding theorem is also referred to as Shannon's second theorem [64], which is the fundamental theorem of communication theory. Note that Shannon's proof of this theorem employs a method called *random coding*. In this method, the codes are constructed randomly and the performance of the system is averaged over them, which proves the existence of good codes with which the error probability can be made arbitrarily small, if $R_c \leq C$. In Shannon's landmark paper [64], it is stated that although this theorem shows the existence of good codes, it does not provide any way of constructing these good codes. Ever since the Shannon's original paper, a variety of techniques have been proposed to construct good channel code, such as Hamming code, convolutional code. Most recently, many excellent codes approaching the capacity have been applied in modern communication systems, such as Turbo-like codes and LDPC codes.

2.2.3 Modulation and Demodulation

As shown in Fig. 2.1, a general modulator takes every m bits from $\mathbf{v}$ and maps the m-bit vector on to one symbol x_i in $\mathbf{x}$ in the complex domain, where i is the time index. The set of all possible symbols for x_i is denoted as $S = \{s_1, s_2, \cdots, s_M\}$, $M = 2^m$, which is also called the symbol constellation. The most commonly used modulation schemes are M-ary phase shift keying (MPSK) where the M symbols lie on a circle, and quadrature amplitude modulation (QAM) where the symbols are equally spaced in the two dimensions [115]. Examples of symbol constellation for BPSK (binary PSK, $M = 2$), QPSK (quadrature PSK, $M = 4$), 8PSK and 16QAM are shown in Fig. 2.2.

The modulated symbol sequence $\mathbf{x}$ is transmitted through the channel and corrupted by the noise. At the destination, the received signal sequence $\mathbf{y}$ is fed into the demodulator to calculate the extrinsic LLRs of all the bits of symbol x_i. Further improvement of decoding can be achieved by invoking the soft-decision feedback from the channel decoder's output to the demodulator in an iterative manner [116]. This concept is known as Bit-Interleaved Coded Modulation with Iterative Decoding (BICM-ID) [117]. For an arbitrary constellation, the extrinsic LLRs of the k-th bit of symbol x_i that generated from the demodulator can be expressed as [118]

$$\begin{aligned} L_e(x_i^k) &= \ln \frac{\Pr(y_i|x_i^k = 1)}{\Pr(y_i|x_i^k = 0)} \\ &= \ln \frac{\sum\limits_{x_i \in S_1^k} p(y_i|x_i) \prod_{j=1, j\neq k}^{m} \exp[x_i^j \cdot L_a(x_i^j)]}{\sum\limits_{x_i \in S_0^k} p(y_i|x_i) \prod_{j=1, j\neq k}^{m} \exp[x_i^j \cdot L_a(x_i^j)]}, \end{aligned} \tag{2.7}$$

where S_1^k and S_0^k are subsets of the symbol constellations having the k-th bit being 1 and 0, respectively. $L_a(x_i^j)$ represents the LLRs fed back from the channel decoder corresponding to the j-th bit of x_i. The output extrinsic LLRs of the demodulator are then forwarded to the channel decoder for next iteration in BICM-ID.

In this thesis, we only consider BPSK modulation, where bit "0" is mapped to "-1" and bit "1" to "$+1$". However, the extension of the results presented in this thesis to higher order modulation is quite straightforward. Using (2.7), it can easily be found that for BPSK, the extrinsic LLRs in AWGN channels can be expressed as

$$L_e(x_i) = \ln \frac{\Pr(y_i|x_i = 1)}{\Pr(y_i|x_i = 0)} = \frac{4\sqrt{E_s}}{N_0} y_i, \tag{2.8}$$

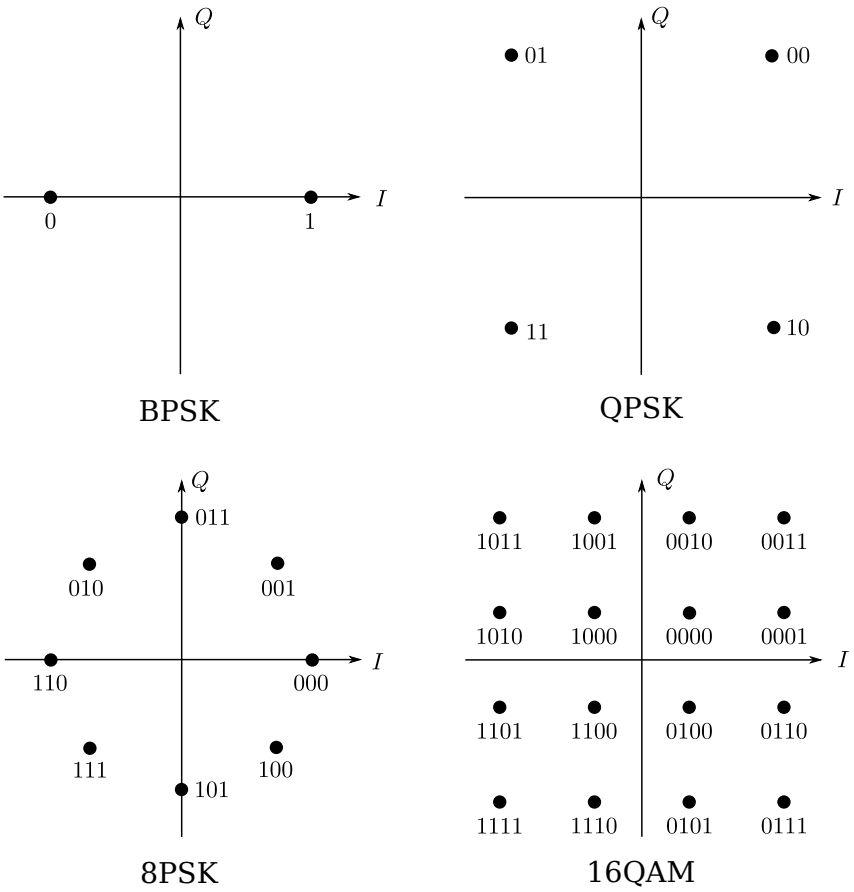

Figure 2.2: Symbol constellation for BPSK, QPSK, 8PSK and 16QAM with Gray mapping.

where E_s and N_0 denotes the average energy per symbol and the two-sided spectral density of the noise, respectively. It can be seen from (2.8) that, the demodulator needs to know both E_s and N_0 to calculate the extrinsic LLRs of $\mathbf{x}$ based on $\mathbf{y}$.

2.2.4 Channel Model

As noted in previous subsection, the modulated symbol sequence $\mathbf{x}$ is transmitted through wireless channels where it suffers from various impairments such as fading, interference, and/or distortions due to practical limitations [119]. In Information theory and wireless communications, there are a variety of models that can be used to describe the statistical properties of the wireless channels, such as Binary Symmetric Channel (BSC), Binary Erasure Channel (BEC), AWGN channel, block Raleigh fading channel and Frequency-selective fading channel. In this thesis, we only consider the most widely used AWGN channel and block Rayleigh fading channel models.

AWGN Channel

If $\mathbf{x}$ is transmitted through AWGN channel, a random Gaussian noise vector $\mathbf{n}$ is added to $\mathbf{x}$. The received signal sequence at the destination can be expressed as

$$\mathbf{y} = \mathbf{x} + \mathbf{n}. \tag{2.9}$$

The Gaussian random variables in $\mathbf{n}$ are i.i.d with zero-mean, with the variance of $\sigma_w^2 = \frac{N_0}{2}$ per dimension.

Block Rayleigh Fading Channel

In block Rayleigh fading channel, the change in signal power over the transmission phase due to multi-path fading and shadowing (also referred to as channel gain) is also considered. The received signal sequence at the destination is defined as

$$\mathbf{y} = h \cdot \mathbf{x} + \mathbf{n}, \tag{2.10}$$

where h represents the complex channel gain. With the block Rayleigh fading assumption, the channel gain h remains constant over one block, but changes independently block-by-block. We can model h as a zero-mean, circularly symmetric complex Gaussian random variable with unit variance. Hence, the magnitude $|h|^2$ is exponentially-distributed with $E[|h|^2] = 1$.

2.2.5 Channel Capacity

Channel capacity defines the maximum number of bits per dimension (or bits per channel use) that could be reliably transmitted through a noisy channel [64]. The most widely used channel model is the time-discrete Gaussian channel, where the output of the channel is the sum of the input and the noise, described as

$$y = x + z, \tag{2.11}$$

where x, y and z are all one-dimensional random variables, and z is a zero-mean one-dimensional Gaussian noise with variance σ_z^2. Note that the channel input x and the

noise z are independent of each other. The capacity of this Gaussian channel is defined as

$$C = \max_{p(x)} I(x;y). \tag{2.12}$$

According to (2.6), $I(x;y)$ can be expanded as

$$\begin{aligned} I(x;y) &= H(y) - H(y|x) \\ &= H(y) - H(x+z|x) \\ &= H(y) - H(z|x) \\ &= H(y) - H(z), \end{aligned} \tag{2.13}$$

since z is independent of x. Now, $H(z) = \frac{1}{2}\log(2\pi e\sigma_z^2)$, and the maximization of $I(x;y)$ is equivalent to maximize $H(y)$. According to [114, Theorem 8.6.5], the maximum of $H(y)$ is achieved if y follows Gaussian distribution. In this case, obviously x also follows Gaussian distribution with variance of σ_x^2. Now $H(y)$ is bounded by $\frac{1}{2}\log(2\pi e(\sigma_x^2+\sigma_z^2))$, and the capacity of the Gaussian channel is

$$\begin{aligned} C &= \max_{p(x)} I(x;y) \\ &= \max_{p(x)} H(y) - H(z) \\ &= \frac{1}{2}\log(2\pi e(\sigma_x^2+\sigma_z^2)) - \frac{1}{2}\log(2\pi e\sigma_z^2) \\ &= \frac{1}{2}\log\left(1+\frac{\sigma_x^2}{\sigma_z^2}\right). \end{aligned} \tag{2.14}$$

It is shown in [64] that the entropy of a multi-dimensional Gaussian variable with equal variances in all dimensions is equal to the number of dimensions times the entropy of the one-dimensional Gaussian distribution. In practical communication systems, the channel is assumed to be complex Gaussian channel. In this case, the noise is two-dimensional and the variance in each dimension is $\sigma_z^2 = N_0/2$. For complex Gaussian input, $\sigma_x^2 = E_s/2$ and the capacity is

$$C = \log\left(1+\frac{E_s}{N_0}\right). \tag{2.15}$$

For real Gaussian input (imaginary part not used), $\sigma_x^2 = E_s$ and the capacity can be expressed as

$$C = \frac{1}{2}\cdot\log\left(1+2\frac{E_s}{N_0}\right). \tag{2.16}$$

2.3 EXIT Chart Analysis

The extrinsic information transfer (EXIT) chart of soft-input soft-output (SISO) decoders was first introduced by Stephan ten Brink [120, 121] as a novel tool for the better understanding of convergence property of iterative decoding schemes. The exchange of extrinsic information can be visualized as a decoding trajectory in the EXIT chart, which enables the prediction of the turbo cliff position. Moreover, with the aid of EXIT chart, the code optimization falls into the problem of the EXIT curve matching. Hence, EXIT chart analysis plays an important role in designing, analyzing and optimizing of iterative decoding schemes.

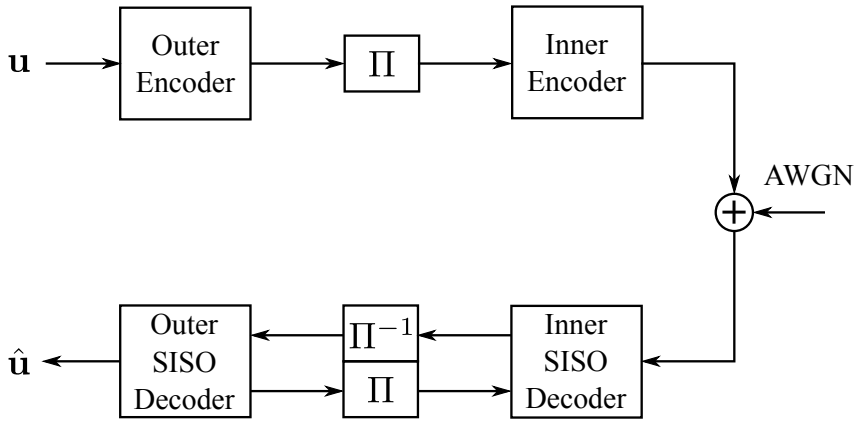

Figure 2.3: A serially concatenated codes and iterative decoder.

We consider a serial-concatenated codes with iterative decoding to present the basic concept of EXIT chart, which is shown in Fig. 2.3. The output LLRs of the inner decoder are generated on the received signals from the channel and the extrinsic information generated from the outer decoder, while the LLRs output from the outer decoder are calculated using the extrinsic LLRs generated from the inner decoder as input. Note that the interleaver Π keeps the output LLRs from the outer and inner decoders uncorrelated with each other over many iterations. Moreover, the probability density function (pdf) of the extrinsic LLRs approaches the Gaussian-like distribution as the number of iterations increased [120]. Therefore, it is appropriate to model the extrinsic LLRs as output of an equivalent Gaussian channel, where the known transmitted information bit x is suffering from zero-mean Gaussian noise n_l with variance σ_l^2, which can be expressed as

$$L = \mu_l x + n_l, \tag{2.17}$$

with $\mu_l = \sigma_l^2/2$ denoting the mean of LLRs. According to (2.5), the mutual information between the information bits X and the LLRs L can be calculated as

$$\begin{aligned} I(X;L) &= \sum_{x=-1,+1} \int_{-\infty}^{+\infty} p(x,l) \log \frac{p(x,l)}{p(x)p(l)} dl \\ &= \sum_{x=-1,+1} \int_{-\infty}^{+\infty} p(l|x)p(x) \log \frac{p(l|x)}{p(l)} dl. \end{aligned} \tag{2.18}$$

With the assumption $p(x=+1) = p(x=-1) = \frac{1}{2}$ and $p(l) = \frac{1}{2}[p(l|x=+1) + p(l|x=-1)]$, we can obtain

$$I(X;L) = \frac{1}{2} \sum_{x=-1,+1} \int_{-\infty}^{+\infty} p(l|x) \log \frac{2p(l|x)}{p(l|x=+1) + p(l|x=-1)} dl. \tag{2.19}$$

Recall that L is Gaussian distributed and according to (2.17), the conditional pdf of the LLRs L is

$$p(l|x) = \frac{1}{\sqrt{2\pi}\sigma_l} \exp\left[-\frac{(l - \frac{\sigma_l^2}{2}x)^2}{2\sigma_l^2} \right], \tag{2.20}$$

with the following symmetry and consistency properties as follow:

$$\text{Symmetry}: \quad p(-l|x=+1) = p(l|x=-1), \tag{2.21}$$

$$\text{Consistency}: \quad p(-l|x=+1) = e^{-l} \cdot p(l|x=+1). \tag{2.22}$$

With (2.20), (2.22) and (2.22), the mutual information $I(X;L)$ can be further expressed as

$$\begin{aligned} I(X;L) &= 1 - \int_{-\infty}^{+\infty} p(l|x=+1)\log[1+e^{-l}]dl \\ &= 1 - \int_{-\infty}^{+\infty} \frac{1}{\sqrt{2\pi}\sigma_l} \exp\left[-\frac{(l-\frac{\sigma_l^2}{2})^2}{2\sigma_l^2}\right] \log[1+e^{-l}]dl \\ &= I(\sigma_l) \end{aligned} \tag{2.23}$$

According to [120], it is found that $I(X;L)$ is a function of the square-root variance σ_l of LLRs, which is specified by the so called J-function defined as

$$J(\sigma) = I(\sigma_l = \sigma), \tag{2.24}$$

with the following property:

$$\lim_{\sigma\to 0} J(\sigma) = 0, \text{and} \quad \lim_{\sigma\to\infty} J(\sigma) = 1, \quad \sigma > 0. \tag{2.25}$$

The J-function can not be expressed in closed form, instead, it can be calculated by numerical methods. It is well known that the J-function can be approximated as [122]

$$J(\sigma) \approx (1 - 2^{-H_1\sigma^{2H_2}})^{H_3}, \tag{2.26}$$

with its inverse function

$$\sigma = J^{-1}(I) = \left[-\frac{1}{H_1}\log_2(1 - I^{\frac{1}{H_3}})\right]^{\frac{1}{2H_2}}, \tag{2.27}$$

where $H_1 = 0.3037$, $H_2 = 0.8935$, and $H_3 = 1.1064$, which are obtained by least square curve fitting. The functions $J(\cdot)$ and $J^{-1}(\cdot)$ convert the square-root variance σ of LLRs to mutual information, and vice versa, respectively. By using these functions, it is convenient to measure the output mutual information of the inner and outer codes. If the square-root variance σ of LLRs is not provided, mutual information can be calculated by histogram measurement [120] according to (2.19).

An example of the EXIT chart of the iterative system shown in Fig. 2.3 is depicted in Fig. 2.4. The green and blue curves indicate the EXIT curves of the outer and inner decoders, respectively. Both of them use the output LLRs via interleaver/deinterleaver of the other side as the *a priori* information. The red curve between the EXIT curves of the outer and inner decoders is called trajectory, which visualizes the real mutual information exchange between the outer and inner decoders. If the tunnel between the two EXIT curves is kept open, the trajectory can finally reach the $(1,1)$ mutual information point and successful transmission is guaranteed. Otherwise, a transmission failure results.

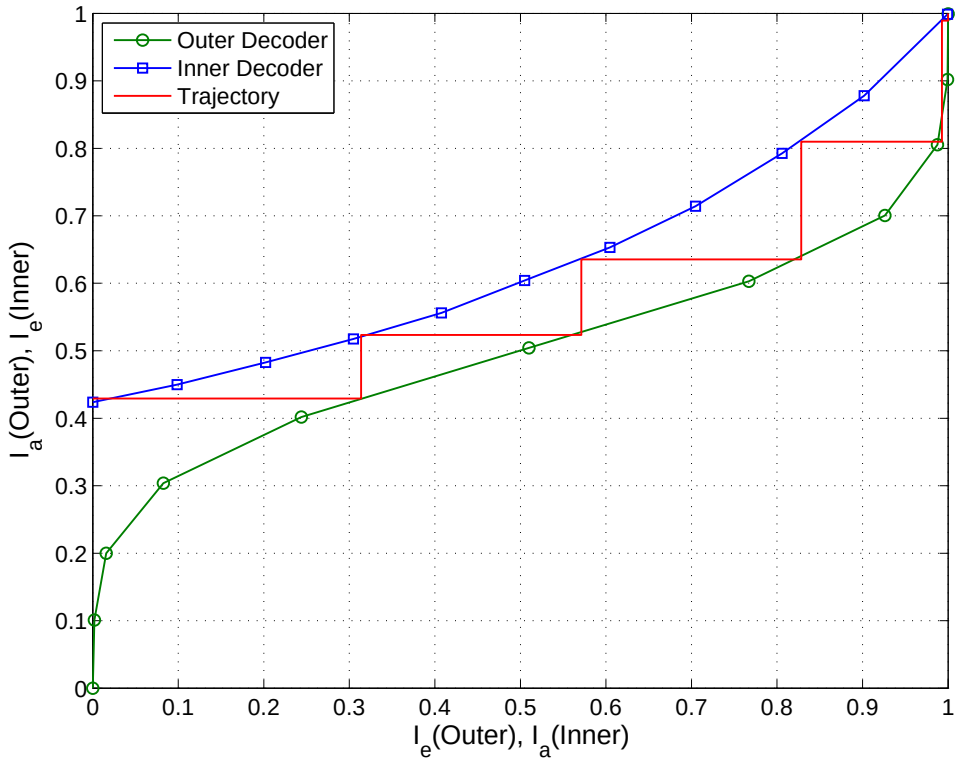

Figure 2.4: An example of EXIT chart.

2.4 Summary

In this chapter, some background knowledge of this research is provided. The definitions of entropy and mutual information are introduced first of all. Then the lossless source coding theorem, the noisy channel coding theorem, modulation/demodulation schemes, channel models and channel capacity, are presented. Finally, the basic concept of EXIT chart analysis that plays an important role in code optimization and convergence analysis in this research, is provided.

Chapter 3

Markov Source Transmission in Point-to-Point Communications

In this chapter, we consider the problem of transmitting binary Markov source over wireless channels in P2P communications. First of all, a brief description of the system model assumed in this chapter is presented. Then, the theoretical analysis, including the performance limits in AWGN channels and the outage probability in Rayleigh fading channels are provided. We then propose a practical framework for JSC that exploits the memory structure of the Markov source. The JSC decoding strategy that involves a modified version of BCJR algorithm, will be detailed. The convergence property of the proposed technique is evaluated by EXIT chart analysis, with the aim of searching for code parameters with which the decoder can achieve close-limit performance. Finally, simulation results are presented to confirm the superiority of the proposed technique and verify the results of the theoretical analysis.

3.1 System Model

The source we consider in this chapter is a stationary state emitting binary Markov source S generating output sequence $\mathbf{u}$, with the property that the current binary value is determined only by its previous counterpart, as

$$\Pr\{u_t|u_{t'}, 1 \leq t' < t\} = \Pr\{u_t|u_{t-1}\}, \tag{3.1}$$

where u_t denotes the t-th symbol of $\mathbf{u}$. This can be conveniently described by using the transition matrix

$$A = [a_{i,j}] = \begin{bmatrix} a_{00} & a_{01} \\ a_{10} & a_{11} \end{bmatrix} = \begin{bmatrix} p_1 & 1-p_1 \\ 1-p_2 & p_2 \end{bmatrix}, \tag{3.2}$$

with the transition probability defined as

$$a_{i,j} = \Pr\{u_t = j|u_{t-1} = i\}, \quad i,j \in \{0,1\}. \tag{3.3}$$

The entropy rate [114] of this stationary Markov source is

$$H^M(p_1,p_2) = -\sum_{i,j\in\{0,1\}} \mu_i a_{i,j} \log a_{i,j} = \mu_0 \cdot H_b(p_1) + \mu_1 \cdot H_b(p_2), \tag{3.4}$$

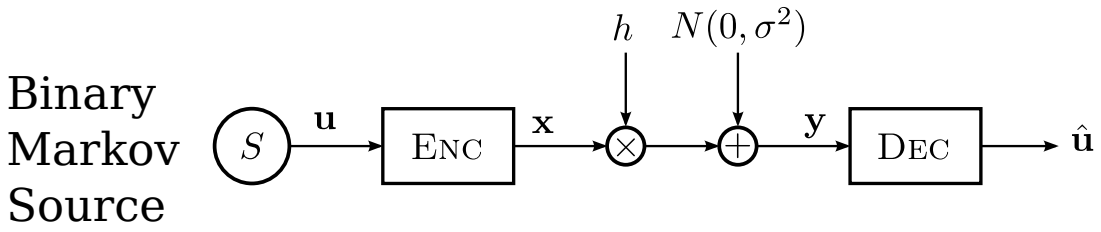

Figure 3.1: Block diagram of the binary Markov source transmission.

where $\mu_0 = \frac{1-p_2}{2-p_1-p_2}$ and $\mu_1 = \frac{1-p_1}{2-p_1-p_2}$ are the stationary distribution for the two states that emit "0" and "1", respectively. $H_b(x) = -x\log(x) - (1-x)\log(1-x)$ denotes the binary entropy function. For symmetric Markov source, $p_1 = p_2 = p$ and hence $\mu_0 = \mu_1 = 0.5$ holds, which yields

$$H^M(p_1, p_2) = H_b(p). \tag{3.5}$$

The block diagram of the system model is illustrated in Fig. 3.1. At the transmitter side, the binary data sequence $\mathbf{u}$, generated from the Markov source, is first encoded by channel encoder Enc and then modulated by BPSK to obtain the modulated sequence $\mathbf{x}$. In this chapter, $\mathbf{x}$ is transmitted over wireless channel that suffers from AWGN and frequency flat block Rayleigh fading. The received signal sequence at the receiver can be expressed as

$$\mathbf{y} = h \cdot \mathbf{x} + \mathbf{n}, \tag{3.6}$$

where h represents the complex channel gain and $\mathbf{n}$ zero-mean i.i.d. complex Gaussian noise vector with variance σ^2. At the receiver side, the received signal sequence $\mathbf{y}$ is fed into decoder Dec for JSC decoding, which will be detailed in Subsection 3.3.

3.2 Theoretical Analysis

Suppose the Markov source is compressed at rate R_s. According to Theorem 2.1, the source can be recovered with arbitrarily small probability of error as long as R_s satisfies $R_s \geq H^M(p_1, p_2)$.

3.2.1 Performance Limits in AWGN Channels

According to Shannon's separation theorem, if the total information transmission rate satisfies [88]

$$R_s \cdot R_c \leq C, \tag{3.7}$$

then error probability at the receiver side can be arbitrarily reduced, where R_c denotes the spectrum efficiency which takes into account the rate of channel coding and the modulation scheme. C is the channel capacity. Since we assume BPSK modulation, which is a one-dimensional modulation scheme, the channel capacity is defined as

$$C = \frac{1}{2}\log_2(1 + 2SNR), \tag{3.8}$$

where $SNR = E_s/2\sigma^2$.

Combining (3.7) and (3.8), we can obtain the performance limit of the considered problem in AWGN channel. The threshold limit for the corresponding Markov source and spectrum efficiency R_c is

$$SNR_{lim} = \frac{2^{2H^M(p_1,p_2)\cdot R_c} - 1}{2}. \tag{3.9}$$

3.2.2 Outage Probability in Rayleigh Fading Channels

As described in Section 3.1, the instantaneous SNR of the channel is denoted by $\gamma = |h|^2 E_s/2\sigma^2$, where E_s represents the per-symbol power of $\mathbf{x}$. The pdf of γ is

$$p(\gamma) = \frac{1}{\Gamma}\exp(-\frac{\gamma}{\Gamma}), \tag{3.10}$$

where $\Gamma = E_s/2\sigma^2$ denotes the average SNR of the channel. Assume the channel encoder Enc is close limit achieving, according to (3.7) and (3.8), the relationship between the threshold instantaneous SNR and its corresponding R_s is given by

$$R_s = \Phi(\gamma) = \frac{1}{2R_c}\log_2(1+2\gamma), \tag{3.11}$$

with its inverse function

$$\gamma = \Phi^{-1}(R_s) = \frac{2^{2R_sR_c} - 1}{2}. \tag{3.12}$$

It is easy to identify that the outage happens if $R_s < H(S)$, and the outage probability of the proposed system can be expressed as

$$\begin{aligned} P_{out} &= \Pr\{0 \le R_s < H(s)\} \\ &= \Pr\{\Phi^{-1}(0) \le \gamma < \Phi^{-1}[H^M(p_1,p_2)]\} \\ &= \int_{\Phi^{-1}(0)}^{\Phi^{-1}[H^M(p_1,p_2)]} p(\gamma)d\gamma \\ &= \Big[-\exp(-\frac{\gamma}{\Gamma})\Big]_{\Phi^{-1}(0)}^{\Phi^{-1}[H^M(p_1,p_2)]} \\ &= 1 - \exp\left[-\frac{2^{2H^M(p_1,p_2)\cdot R_c} - 1}{2\Gamma}\right]. \end{aligned} \tag{3.13}$$

For Markov sources, $0 \le H^M(p_1,p_2) < 1$. It can be seen from (3.13) that the outage probability is reduced by utilizing the unsaturated entropy of Markov source, compared with the i.i.d. source.

By using the Taylor expansion, and taking the first two parts of the exponential function part of (3.13), as

$$e^{-x} = \sum_{n=0}^{\infty}\frac{(-x)^n}{n!} \approx 1 - x, \quad \text{as} \quad x \to 0, \tag{3.14}$$

P_{out} in (3.13) can be approximated as

$$P_{out} = 1 - \exp\left[-\frac{2^{2H^M(p_1,p_2)\cdot R_c} - 1}{2\Gamma}\right] \approx \frac{2^{2H^M(p_1,p_2)\cdot R_c} - 1}{2\Gamma}, \tag{3.15}$$

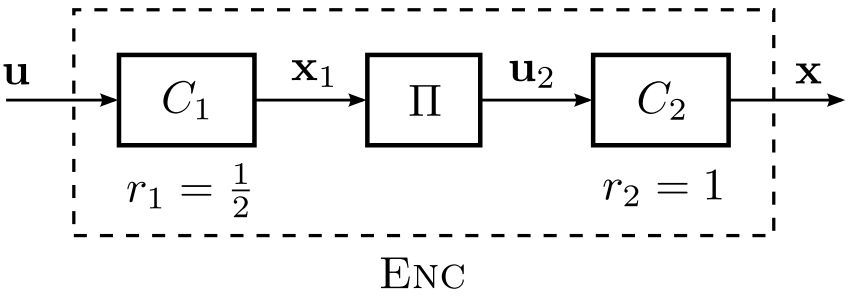

Figure 3.2: Coding structure of ENC. C_1 and C_2 are convolutional codes and Π is random interleaver.

for large enough average SNR Γ. It can be observed from (3.15) that P_{out} is inversely proportion to Γ and hence no diversity gain can be achieved when the average SNR Γ becomes large.

3.3 Practical Code Design

In the theoretical analysis, we have assumed the channel encoder ENC has close-limit performance, and the source correlation can be exploited in the joint decoding process at the destination node. In this section, we propose the coding/decoding framework based on some practical channel codes for transmitting binary Markov sources.

3.3.1 Coding Structure

The block diagram for the coding structure of ENC is illustrated in Fig. 3.2. We use SCCC, where a rate $r_1 = 1/2$ outer code C_1 and a rate $r_2 = 1$ inner code C_2 are serially concatenated, yielding an overall rate $r_1 r_2 = 1/2$. The information sequence generated from the binary Markov source is fed directly to C_1 to obtain the output sequence $\mathbf{x}_1$. The output of C_1, including systematic and parity bits, are then bit-interleaved by a random interleaver Π and encoded by C_2 to get $\mathbf{x}$. The inner code C_2 is a rate-1 recursive convolutional code with doping[1] rate Q, where every Q-th output bit is replaced by its corresponding systematic bit.

3.3.2 Joint Source-Channel Decoding Strategy

The block diagram for the decoder structure of DEC is shown in Fig. 3.3. The Markov source model and the outer code trellis are integrated to form a super trellis. Then a modified BCJR algorithm is derived and employed at D_1 to perform joint decoding of the outer code and Markov source based on the super trellis, as indicated by the gray square in Fig. 3.3. Moreover, the standard BCJR algorithm is employed at D_2 to perform the decoding of the inner code. Iterative decoding is invoked between two SISO modules D_1 and D_2, according to the Turbo decoding principle. Finally, hard decision is made on the output of D_1.

[1]The terminology "doping" was first proposed by ten Brink in [120] to express the notion that a small portion of the coded bits are substituted by their systematic counterpart, without changing the code rate. Here we use "code doping" rather than "doping" for the sake of clarity.

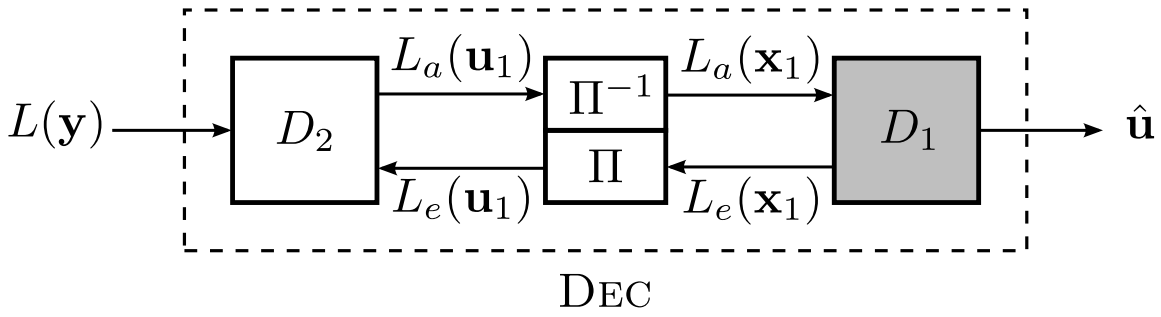

Figure 3.3: Decoder structure of DEC. D_1 and D_2 are the decoder for C_1 and C_2, respectively. Π^{-1} is deinterleaver.

In this section, we derive the modified version of the BCJR algorithm that takes into account the memory structure of Markov source. Hence, in this section, we ignore momentarily the serially concatenated structure and only focus on the decoding process of one decoder using the BCJR algorithm.

Standard BCJR Algorithm

First of all, we briefly describe the standard BCJR decoding algorithm, originally developed to perform the MAP algorithm [123] for CC. For a CC with memory length v, there are 2^v states in its trellis diagram, which are indexed by m, $m = 0, 1, \cdots, 2^v - 1$. The input to the encoder is denoted as $\mathbf{u} = u_1 u_2 \cdots u_t \cdots u_L$, of which the length is L. Let's assume that $r_1 = 1/2$ for the simplicity. Then, the output of the encoder is denoted as $\{\mathbf{x}_t\} = \{\mathbf{x}_t^{v1}, \mathbf{x}_t^{v2}\}$. The coded binary sequence is BPSK mapped, and then transmitted over an AWGN channel. The received signal is a noise corrupted version of the BPSK mapped sequence, denoted as $\{\mathbf{y}_t\} = \{\mathbf{y}_t^{v1}, \mathbf{y}_t^{v2}\}$. The received sequence during time duration from t_1 to t_2 is denoted as $\mathbf{y}_{t_1}^{t_2} = \mathbf{y}_{t_1}, \mathbf{y}_{t_1+1}, \cdots, \mathbf{y}_{t_2}$.

When making modifications on the BCJR algorithm, we do not assume that the code is either systematic or non-systematic. Because the BCJR decoder can calculate the extrinsic LLRs of coded and uncoded (information) bits by giving labeling properly in the trellis diagram of the code corresponding to its input-output relationship [124]. The BCJR algorithm evaluates the conditional LLR for $\{x_t^{v1}\}$ based on the whole received sequence $\mathbf{y}_1^L$, which is defined by

$$L(x_t^{v1}) = \log \frac{\Pr\{x_t^{v1} = 1 | \mathbf{y}_1^L\}}{\Pr\{x_t^{v1} = 0 | \mathbf{y}_1^L\}} = \log \frac{\Pr\{x_t^{v1} = 1, \mathbf{y}_1^L\}}{\Pr\{x_t^{v1} = 0, \mathbf{y}_1^L\}}. \tag{3.16}$$

To compute the LLR of x_t^{v1}, we use the joint probability

$$\sigma_t(m', m) = \Pr\{S_{t-1} = m', S_t = m, \mathbf{y}_1^L\}, \tag{3.17}$$

and rewrite (3.16) as

$$L(x_t^{v1}) = \log \frac{\Pr\{x_t^{v1} = 1, \mathbf{y}_1^L\}}{\Pr\{x_t^{v1} = 0, \mathbf{y}_1^L\}} = \log \frac{\sum_{(m',m) \in B_t^1} \sigma_t(m', m)}{\sum_{(m',m) \in B_t^0} \sigma_t(m', m)}, \tag{3.18}$$

where B_t^j denotes the set of transitions $S_{t-1} = m' \to S_t = m$ such that the output on that transition is $x_t^{v1} = j, j \in (0, 1)$.

In order to compute (3.17), three parameters indicating the probabilities defined as below have to be introduced:

$$\alpha_t(m) = \Pr\{S_t = m, \mathbf{y}_1^t\}, \tag{3.19}$$

$$\beta_t(m) = \Pr\{\mathbf{y}_{t+1}^L | S_t = m\}, \tag{3.20}$$

$$\gamma_t(\mathbf{y}_t, m', m) = \Pr\{S_t = m, \mathbf{y}_t | S_{t-1} = m'\}. \tag{3.21}$$

Now we have

$$\sigma_t(m', m) = \alpha_{t-1}(m')\gamma_t(\mathbf{y}_t, m', m)\beta_t(m). \tag{3.22}$$

It is easy to show that $\alpha_t(m)$ and $\beta_t(m)$ can be computed via the following recursive formulae

$$\alpha_t(m) = \sum_{m'} \alpha_{t-1}(m')\gamma_t(\mathbf{y}_t, m', m), \tag{3.23}$$

$$\beta_t(m) = \sum_{m'} \beta_{t+1}(m')\gamma_{t+1}(\mathbf{y}_t, m, m'). \tag{3.24}$$

Since the encoder always starts from zero state, the appropriate boundary conditions for α are $\alpha_0(0) = 1$ and $\alpha_0(m) = 0,\ m \neq 0$. The boundary conditions for β depends on whether the trellis diagram is terminated by transmitting the tail bits or not. If we leave the encoder unterminated, the corresponding conditions for β are $\beta_L(m) = 1/2^v,\ m = 0, 1, \cdots, 2^v - 1$; otherwise, $\beta_L(0) = 1$ and $\beta_L(m) = 0$, for all $m \neq 0$. In our system, we use a long and random enough interleaver, so that LLRs can be regarded as statistically independent.

From the above descriptions, it is found that γ plays a crucial role in computing the LLRs. Because y_t^{v1} and y_t^{v2} are statistically independent, γ can be computed by

$$\gamma_t(\mathbf{y}_t, m', m) = \Pr\{S_t = m | S_{t-1} = m'\} \Pr\{y_t^{v1} | x_t^{v1}\} \Pr\{y_t^{v2} | x_t^{v2}\}, \tag{3.25}$$

The first term $\Pr\{S_t = m | S_{t-1} = m'\}$ is determined by the 0/1 appearance probabilities of the both input and output bits, as:

$$\Pr\{S_t = m | S_{t-1} = m'\} = \Pr\{u_t\} \Pr\{x_t^{v1}\} \Pr\{x_t^{v2}\}, \tag{3.26}$$

where the input/output bits, $u_t/(x_t^{v1}, x_t^{v2})$, are associated with trellis branch of $S_{t-1(m')} \to S_t(m)$. It should be mentioned that the input to the encoder is assumed to be memoryless in standard BCJR algorithm, i.e., $\Pr\{u_t | u_{t-1}\} = \Pr\{u_t\}$. We can rewrite (3.18) as

$$L(x_t^{v1}) = L_{ap}(x_t^{v1}) + L_{ch}(x_t^{v1}) + L_{ex}(x_t^{v1}), \tag{3.27}$$

where

$$L_{ap}(x_t^{v1}) = \log \frac{\Pr\{x_t^{v1} = 1\}}{\Pr\{x_t^{v1} = 0\}}, \tag{3.28}$$

$$L_{ch}(x_t^{v1}) = \log \frac{\Pr\{y_t^{v1} | x_t^{v1} = 1\}}{\Pr\{y_t^{v1} | x_t^{v1} = 0\}}, \tag{3.29}$$

$$L_{ex}(x_t^{v1}) = \log \frac{\sum_{(m',m) \in B_t^1} \alpha(m')\gamma(y_t^{v2}, m', m)\beta(m)}{\sum_{(m',m) \in B_t^0} \alpha(m')\gamma(y_t^{v2}, m', m)\beta(m)}, \tag{3.30}$$

are called the *a priori* LLR, the channel LLR, and the extrinsic LLR, respectively. If the decoder is not connected to the channel such as the outer code of SCCC, it can not get any information about the coded bits from the channel, which means $L_{ch} = 0$ and $L(X_t^{v1}) = L_{ap}(x_t^{v1}) + L_{ex}(x_t^{v1})$. The same result can be obtained for x_t^{v2}.

In iterative decoding, the time position of $L_{ex}(x_t^{v1})$ and $L_{ex}(x_t^{v2})$ are rearranged by the interleaver and fed into the other decoder.

Representation of Super Trellis

We denote the state of the outer encoder at time index t as S_t^c. Similarly, there are two states in order-1 binary Markov source, and the state at the time index t is denoted as S_t^s, $S_t^s \in \{0, 1\}$. For a binary Markov model described in section 3.1, the source model and its corresponding trellis diagram are illustrated in Fig. 3.4(a). The output value at a time instant t from the source is the same as the state value of S_t^s. The trellis branches represent the state transition probabilities, which is defined by (3.3). On the other hand, for the outer code, the branches in its trellis diagram indicate input/output characteristics.

At the time instant t, the state of the source and the state of the outer code can be regarded as a new state (S_t^s, S_t^c), which leads to the super trellis diagram. A simple example of combining binary Markov source with a recursive convolutional code (RSC) with generator polynomial $(G_r, G) = (3, 2)_8$ is depicted in Fig. 3.4. At each state (S_t^s, S_t^c), the input to the outer encoder is determined, given the state of the Markov source. Actually, the new trellis branches represent both state transition probabilities of the Markov source and input/output characteristics of the outer code defined in its trellis diagram.

Modified BCJR Algorithm for Super Trellis

In the original BCJR algorithm, the information bits are assumed to be memoryless. However, with the presence of the source correlation, the BCJR algorithm can well be modified to best ultilize the redundancy inherent within the Markov source.

Again, the aim of the modified BCJR algorithm is to calculate conditional LLRs of the coded bits $\{x_t^{v1}\}$, based on the whole received sequence $\mathbf{y}_1^L$, which is specified by (3.18). To achieve this goal, variables α, β and γ have to be modified as

$$\begin{aligned} \alpha_t^*(m, i) &= \Pr\{S_t = m, u_t = i, \mathbf{y}_1^t\}, \\ \beta_t^*(m, i) &= \Pr\{\mathbf{y}_{t+1}^L | S_t = m, u_t = i\}, \\ \gamma_t^*(\mathbf{y}_t, m', i', m, i) &= \Pr\{S_t = m, U_t = i, \mathbf{y}_t | S_{t-1} = m', u_{t-1} = i'\}. \end{aligned} \tag{3.31}$$

Then the joint probability σ can then be derived as

$$\sigma_t(m', m) = \sum_{i', i} \alpha_{t-1}^*(m', i') \gamma_t^*(\mathbf{y}_t, m', i', m, i) \beta_t^*(m, i). \tag{3.32}$$

As mentioned above, the new trellis branch contains information of input/output relationship corresponding to the state transition $S_t^c = m' \to S_t^c = m$, specified by the outer code trellis, as well as of the state transition probabilities depending on Markov source.

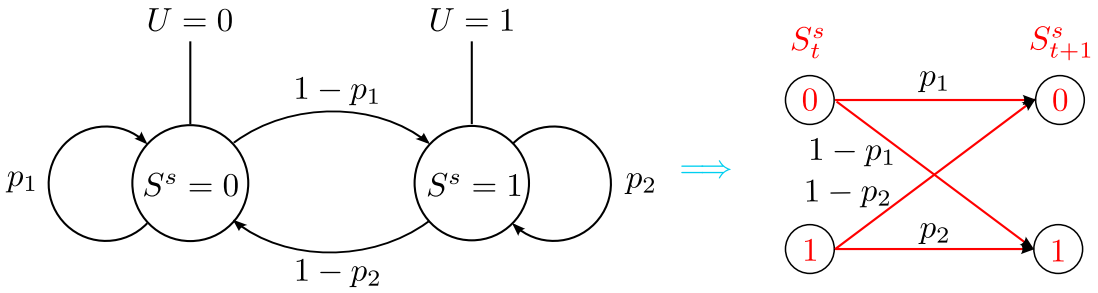

(a)

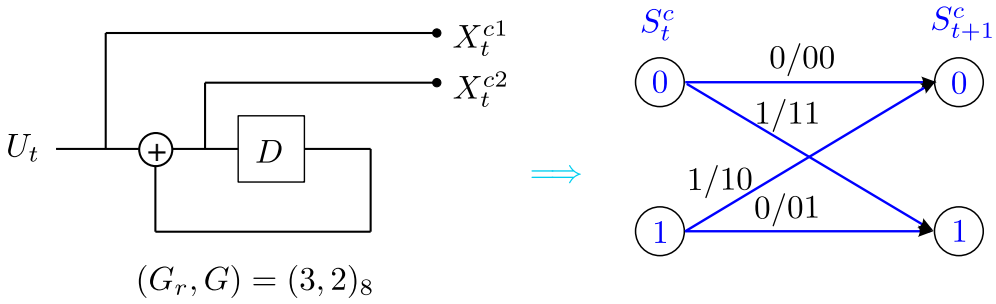

(b)

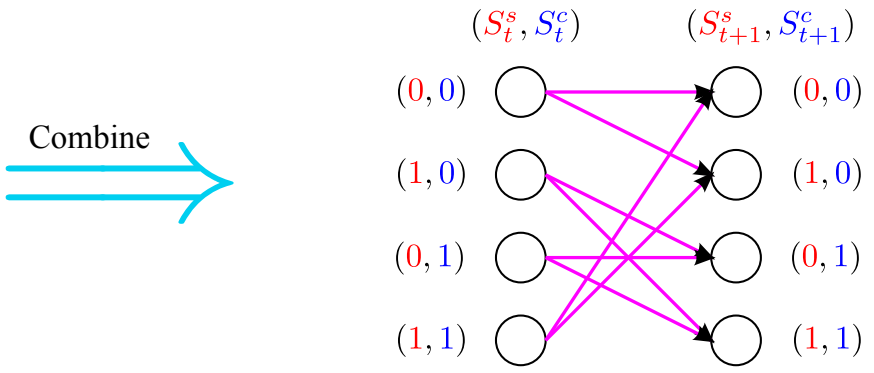

(c)

Figure 3.4: Trellis diagram for (a) binary Markov source, (b) RSC code with generator polynomial$(G_r, G) = (3, 2)_8$, (c) joint outer code.

Therefore, $\gamma_t^*(\mathbf{y}_t, m', i', m, i)$ can be decomposed as

$$\gamma_t^*(\mathbf{y}_t, i', m', i, m) = \begin{cases} a_{i',i}\gamma_t(\mathbf{y}_t, m', m), & \text{if } (i', m') \in E_t(i, m); \\ 0, & \text{otherwise,} \end{cases} \tag{3.33}$$

where $a_{i',i}$ is defined in (3.3), and $\gamma_t(\mathbf{y}_t, m', m)$ is defined in (3.25). $E_t(i, m)$ is the set of states $\{(S_{t-1}^s, S_{t-1}^c)\}$ that have a trellis branch connected with state $(S_t^s = i, S_t^c = m)$. It is now found that the transition probability $\Pr\{u_t = i | u_{t-1} = i'\}$ is utilized in the computation of $\gamma_t^*(\mathbf{y}_t, m', i', m, i)$.

Once $\gamma_t^*(\mathbf{y}_t, m', i', m, i)$ is obtained, α^* and β^* can also be calculated in the same way as in the standard BCJR algorithm, as

$$\begin{aligned} \alpha_t^*(m, i) &= \sum_{m', i'} \alpha_{t-1}^*(m', i')\gamma_t^*(\mathbf{y}_t, m', i', m, i), \\ \beta_t^*(m, i) &= \sum_{m', i'} \beta_{t+1}^*(m', i')\gamma_{t+1}^*(\mathbf{y}_t, m', i', m, i), \end{aligned} \tag{3.34}$$

Since the outer encoder always starts from the zero state, while the probabilities for the Markov source starts from state "0" or state "1" is equal. Hence, the appropriate boundary conditions for α are $\alpha_0(i, 0) = 1/2,\ i = 0, 1$ and $\alpha_0(i, m) = 0,\ m \neq 0$. Similarly, the boundary conditions for β are $\beta_L(i, m) = 1/2^{v+1},\ i = 0, 1; m = 0, 1, \cdots, 2^v - 1$.

Combining all the results described above, we can obtain the conditional LLR for x_t^{v1}, as

$$L(x_t^{v1}) = L_{ap}(x_t^{v1}) + L_{ch}(x_t^{v1}) + L_{ex}(x_t^{v1}), \tag{3.35}$$

where

$$L_{ap}(x_t^{v1}) = \log \frac{p(x_t^{v1} = 1)}{p(x_t^{x1} = 0)}, \tag{3.36}$$

$$L_{ch}(x_t^{v1}) = \log \frac{p(y_t^{v1} | x_t^{v1} = 1)}{p(y_t^{v1} | x_t^{v1} = 0)}, \tag{3.37}$$

$$L_{ex}(X_t^{v1}) = \log \frac{\sum_{(m', m) \in B_t^1} \sum_{i', i} \alpha_{t-1}^*(i', m')\gamma_t^*(y_t^{v2}, i', m', i, m)\beta_t^*(i, m)}{\sum_{(m', m) \in B_t^0} \sum_{i', i} \alpha_{t-1}^*(i', m')\gamma_t^*(y_t^{v2}, i', m', i, m)\beta_t^*(i, m)}, \tag{3.38}$$

which represents the *a priori* LLR, the channel LLR and the extrinsic LLR, respectively, obtained as the result of the modified BCJR algorithm. B_t^j denotes the set of transitions $S_{t-1} = m' \to S_t = m$ such that the output on that transition is $x_t^{v1} = j, j \in (0, 1)$.The same representation should be applied to $\{x_t^{v2}\}$. Using this modified BCJR algorithm, an optimal decoder can be obtained with the cost of only double the decoding complexity.

Comparing the expressions described above with the standard BCJR algorithm, it is found that with the modified BCJR algorithm, the *a priori* LLR and the channel LLR (actually the channel LLR is 0 for the outer code of serially concatenated codes) stay the same as that in the standard BCJR algorithm, respectively. The statistical structure of the source is exploited inherently within the forward-backward calculations, resulting in improved extrinsic LLR in the presence of source memory, which can be fed directly into the other constituent decoder via interleaver without involving any other computations. It should be noticed that if we apply this modified algorithm for memoryless source, since

$a_{i',i} = 0.5,\ for\ i', i \in (0,1)$, the extrinsic LLR of the modified BCJR algorithm, given by (3.38), is the same as that of the standard BCJR. Moreover, as the source correlation becomes larger, the extrinsic LLR will also becomes larger, which will help the decoder recover the information bits even at lower SNR value range.

3.4 EXIT Chart-Based Code Optimization

In this section, we present results of EXIT chart analysis conducted to identify the impact of source correlation on the decoder of the outer code, as well as the convergence property of the proposed technique. We also use EXIT chart analysis to determine the best matched pair of the outer and inner codes, and the doping rate for inner code.

3.4.1 EXIT Chart Analysis

Outer Code

From the descriptions in Subsection 3.3.2, we know that the source memory helps to increase the output extrinsic information of the outer decoder. As described in Section 3.1, the correlation of the source can be parameterized by the Markov state transition probability p_1 and p_2, $0 < p_1, p_2 < 1$. $p_1 = p_2 = 0.5$ indicates a memoryless source while $p_1, p_2 > 0.5$ (or equivalently $p_1, p_2 < 0.5$) indicates the source with memory. Since the correlation is symmetric on p, we only consider the case $0.5 \leq p_1, p_2 < 1$.

As shown in Fig 3.3, the decoder D_1 of C_1 exploits *a priori* LLRs $L_a(\mathbf{x}_1)$. By using the modified BCJR algorithm, it generates extrinsic LLRs $L_e(\mathbf{x}_1)$. Hence the EXIT function of D_1 is defined as:

$$I_e[\mathbf{x}_1; L_e(\mathbf{x}_1)] = T_{D_1}\{I_a[\mathbf{x}_1; \mathbf{L_e}(\mathbf{x_1})]\}, \tag{3.39}$$

where function $I_e[\mathbf{x}_1; L_e(\mathbf{x}_1)]$ denotes the mutual information between $\mathbf{x}_1$ and its extrinsic LLRs $L_e(\mathbf{x}_1)$, which is obtained by the histogram measurement [121] according to (2.19). Similar definition is applied to $I_a[\mathbf{x}_1; L_a(\mathbf{x}_1)]$.

Now, let us assume memory-1 RSC code used with the generator polynomial $(G_r, G) = (3, 2)_8$ as an example. The EXIT curves with standard BCJR and with the modified BCJR exploiting source with different transition probabilities are illustrated in Fig. 3.5. For the source with $p_1 = p_2 = 0.5$, the EXIT curves with the standard BCJR decoder and our modified BCJR decoders are the same. For the Markov sources with different p_1 and p_2 values, the EXIT curves obtained by using the modified BCJR decoder are pushed down and shifted to the right as $H^M(p_1, p_2)$ decreases, indicating that larger extrinsic information can be obtained. These results are consistent with the consideration provided in Subsection 3.3.2. Note that the contribution of source memory represented by the increase in extrinsic mutual information is larger when *a priori* input $I_A < 0.5$ than when $I_A > 0.5$, and the contribution becomes negligible when $I_A > 0.9$.

Inner Code

D_2 calculates its extrinsic LLRs in the same way as D_1, except that it has a direct connection to the channel. Hence, its EXIT function is defined as

$$I_e[\mathbf{u}_2; L_e(\mathbf{u}_2)] = T_{D_2}\{I_a[\mathbf{u}_2; L_a(\mathbf{u}_2)], SNR\}. \tag{3.40}$$

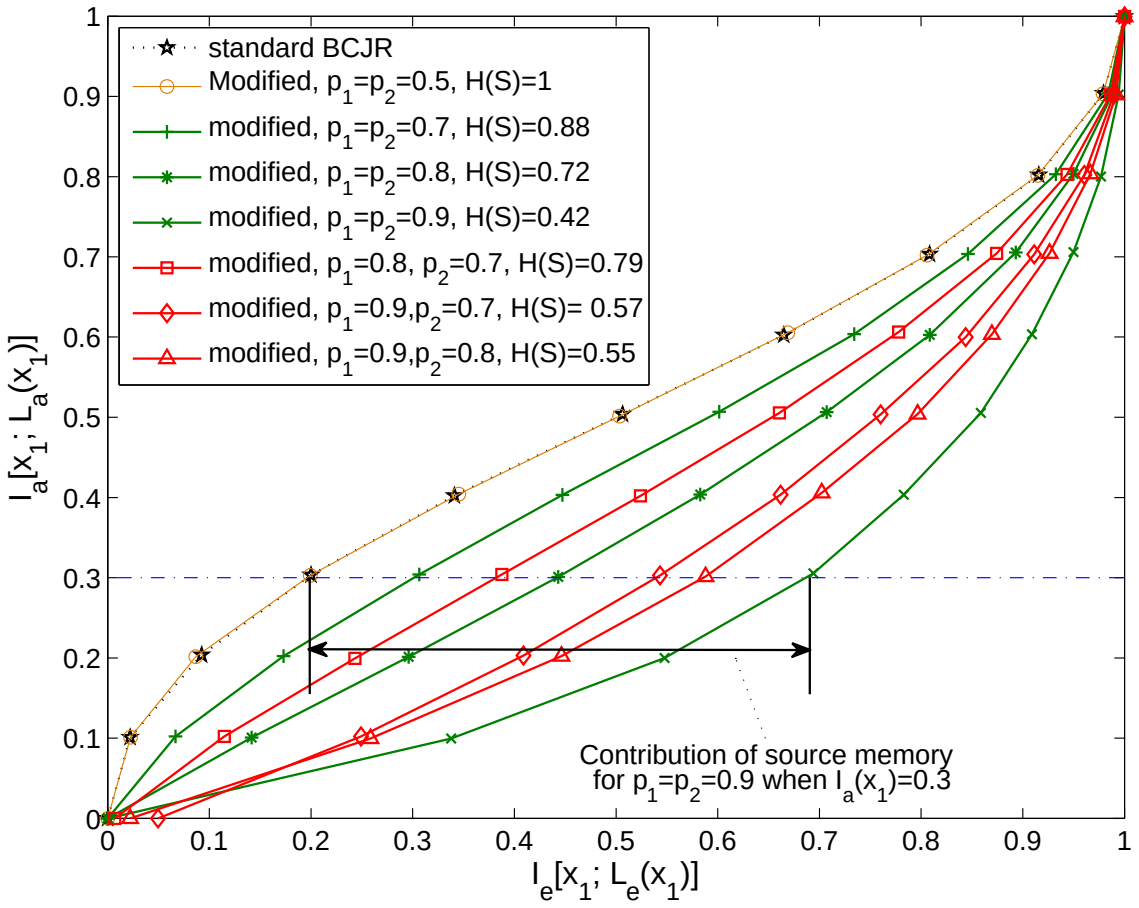

Figure 3.5: An example of extrinsic information transfer characteristic of outer coder, $(G_r, G) = (3, 2)_8$.

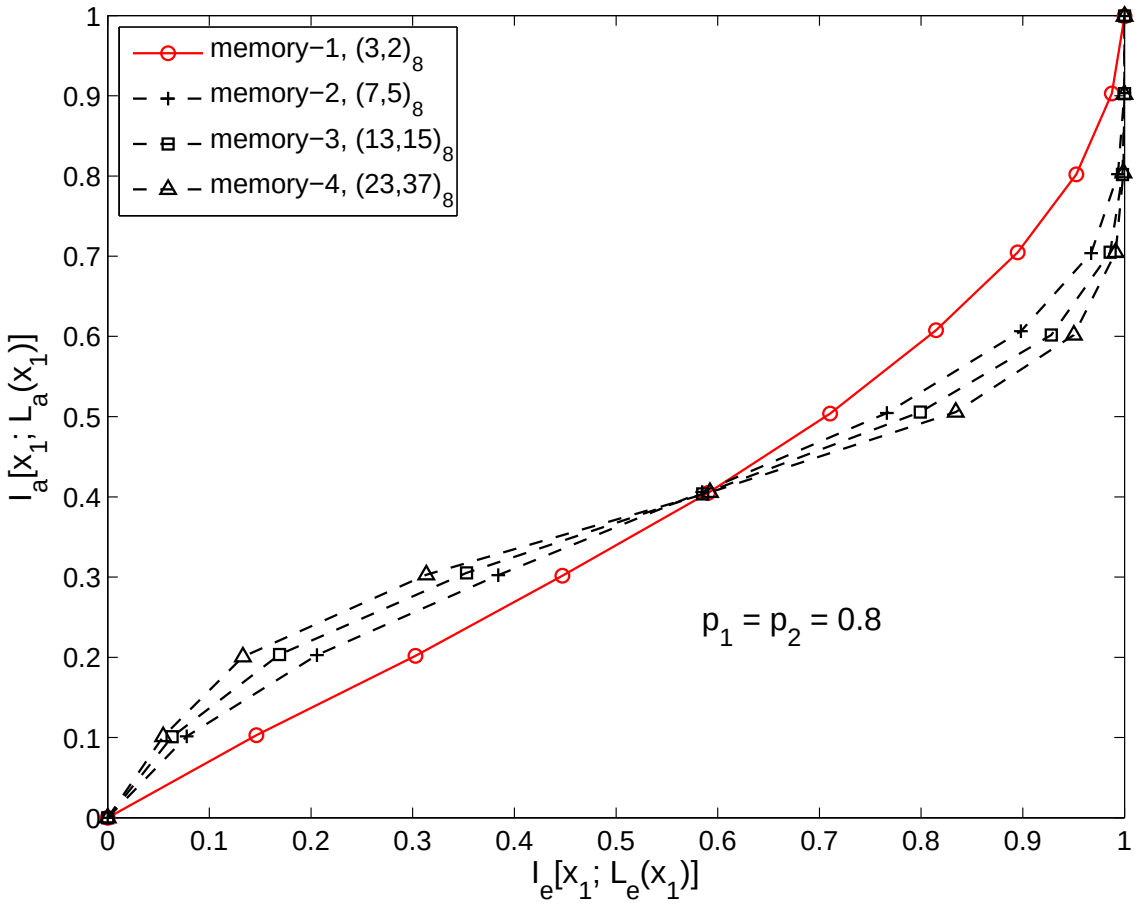

Figure 3.6: An example of observing outer coder for Markov source with $p_1 = p_2 = 0.8$.

Because the mutual information does not change after interleavering/deinterleavering, the following equality holds

$$I_a^{(l)}[\mathbf{x}_1; L_a(\mathbf{x}_1)] = I_e^{(l-1)}[\mathbf{u}_2; L_e(\mathbf{u}_2)], \tag{3.41}$$

$$I_a^{(l)}[\mathbf{u}_2; L_a(\mathbf{u}_2)] = I_e^{(l-1)}[\mathbf{x}_1; L_e(\mathbf{x}_1)], \tag{3.42}$$

where l is the iteration index, i.e., the extrinsic information generated by the first decoder is used as the *a priori* information for the second decoder, and vice versa. In the chain simulations, we evaluated the extrinsic mutual information, iteration-by-iteration, and plotted the obtained mutual information, according to (3.41) and (3.42).

3.4.2 Code Optimization

In this subsection, the code parameters of C_1 and C_2 are optimized from the viewpoint of EXIT curve matching. An example of the code optimization for the state-emitting Markov source with $p_1 = p_2 = 0.8$ is demonstrated in Fig. 3.6. First, the outer code parameters can be determined using the EXIT chart analysis. The EXIT curves of some outer codes with different memory length for Markov source with $p_1 = p_2 = 0.8$ are shown in Fig. 3.6. It can be observed that memory-1 outer code with generator polynomials

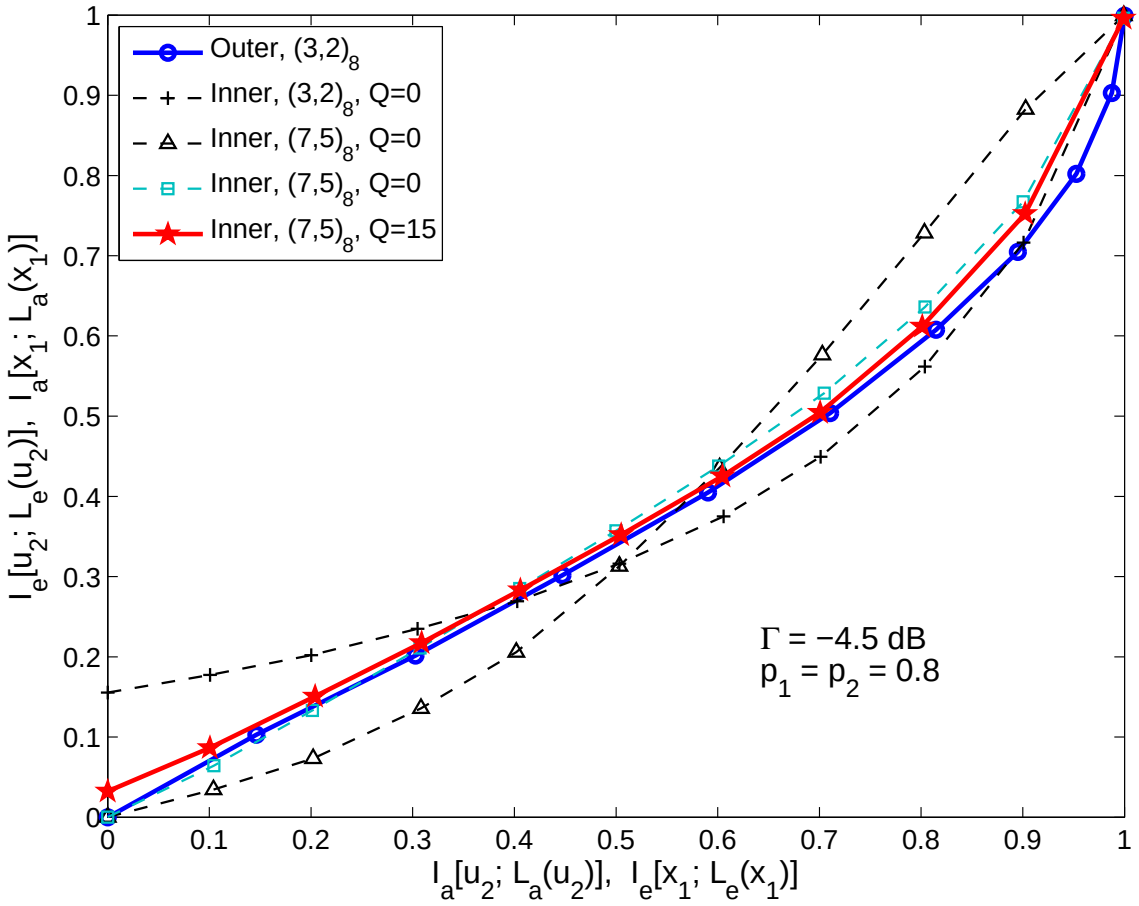

Figure 3.7: An example of determining optimal inner coder and doping rate for Markov source with $p_1 = p_2 = 0.8$.

$(G_r, G) = (3, 2)_8$ exhibits an excellent extrinsic information transfer characteristic, and hence, it is the sub-optimal outer code (the best code among all the tested codes) for Markov source with $p_1 = p_2 = 0.8$.

With this fixed outer code, next we can determine the best inner code that roughly matches with outer code (i.e., the gap between the EXIT curves is minimized among those inner codes parameters), assuming no *code doping* used ($Q = 0$). As shown in Fig. 3.7, at SNR= -4.5 dB, a memory-2 inner code with $(G_r, G) = (6, 7)_8$ has a better matching with outer $(3, 2)_8$ code, compared with the inner $(3, 2)_8$ and $(7, 5)_8$ codes.

After the optimal inner code is obtained, which is best matched with the Markov source memory, the optimal doping rate is identified for the inner code by changing the doping rate to gradually "bend" its EXIT curve, until there is a tunnel open between the EXIT curves of the outer and inner codes. In this example, with $Q = 15$, there is a narrow tunnel open which the trajectory can sneak through until convergence point, as shown in Fig. 3.7. Now those three optimal code parameters are obtained for Markov source with $p_1 = p_2 = 0.8$.

The EXIT chart and trajectory for Markov source with $p_1 = p_2 = 0.8$ by using these optimized code parameters are shown in Fig. 3.8. It is found from Fig. 3.8(a) that with SNR $= -4.5$ dB, the convergence tunnel is still open until a point very close to (1,1) mutual information point, and the trajectory finally reaches the convergence point. The convergence behavior with SNR $= -4.6$ dB is presented in Fig. 3.8(b), where the EXIT curves of the outer and inner codes intersect with each other and the trajectory gets stuck. This observation suggests that the convergence threshold is -4.5 dB for Markov source with $p_1 = p_2 = 0.8$.

The optimization process is performed for the Markov source with different p_1 and p_2 values, and the optimal code parameters are summarized in Table 3.1.

Table 3.1: Optimized Code Parameters for Markov Sources with Different p_1 and p_2 Values

Source Parameters			Code Parameters		
p_1	p_2	$H^M(p_1, p_2)$	Outer	Inner	Q
0.9	0.9	0.47	$(3, 2)_8$	$(6, 7)_8$	25
0.8	0.8	0.72	$(3, 2)_8$	$(6, 7)_8$	15
0.7	0.7	0.88	$(3, 2)_8$	$(6, 7)_8$	4
0.9	0.8	0.55	$(3, 2)_8$	$(6, 7)_8$	25
0.9	0.7	0.57	$(3, 2)_8$	$(6, 7)_8$	25
0.8	0.7	0.79	$(3, 2)_8$	$(6, 7)_8$	10

3.5 Performance Evaluation

3.5.1 BER Performance in AWGN Channels

In this subsection, we evaluate the BER performance versus E_b/N_0 (the energy per bit to noise power spectral density ratio)[2] of the proposed JSC decoding technique based on the results of code optimization provided in the previous section. Both symmetric and

[2]The relationship between E_b/N_0 and SNR is SNR$= R_c \cdot E_b/N_0$.

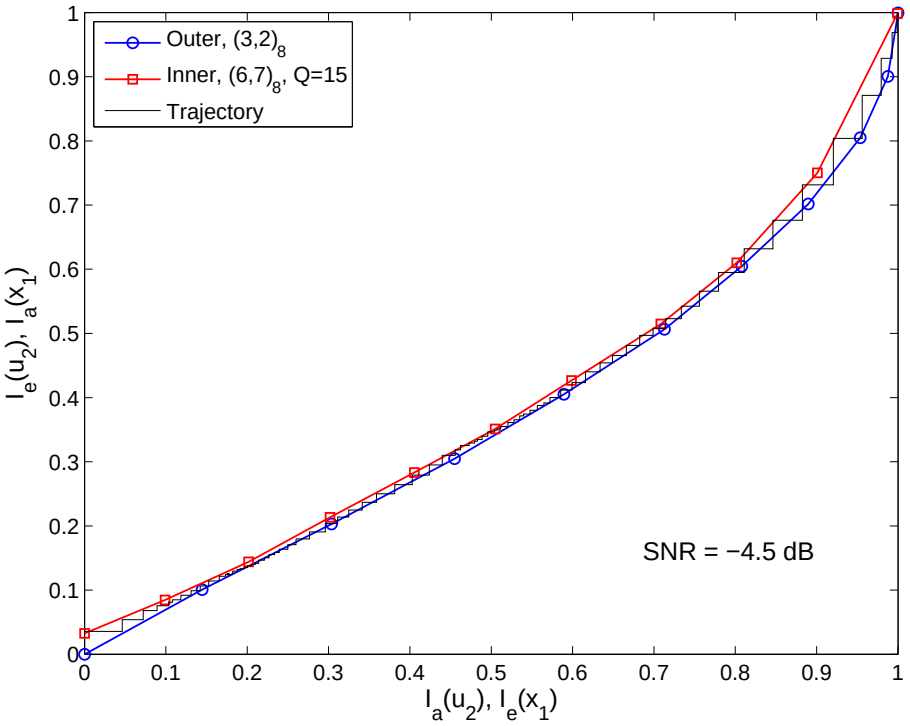

(a) SNR=−4.5 dB

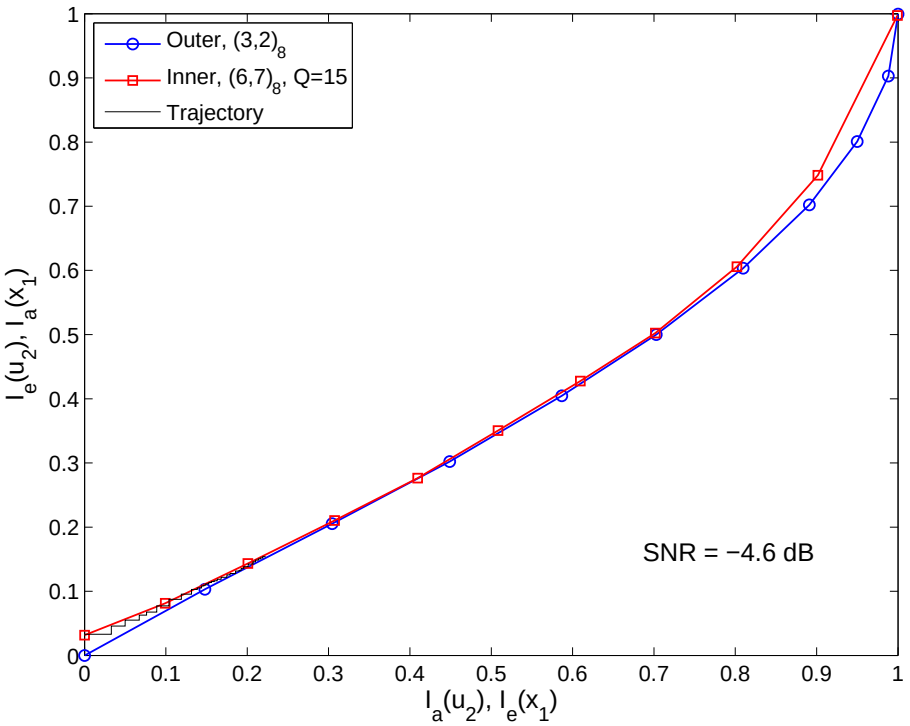

(b) SNR=−4.6 dB

Figure 3.8: EXIT chart and trajectory for Markov source with $p_1 = p_2 = 0.8$.

asymmetric Markov sources are considered. The length of binary sequence generated from the Markov sources is $10,000$ bits, and in total 1000 different blocks were transmitted to guarantee the BER evaluation accuracy.

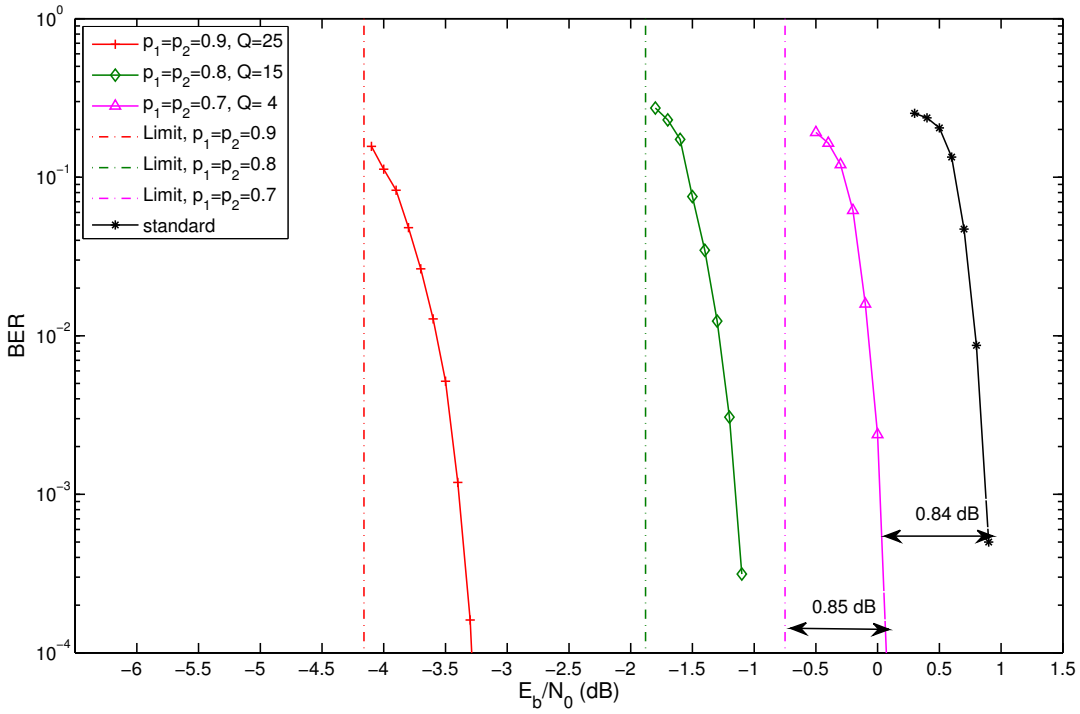

Figure 3.9: BER peformance of the proposed technique for symmetric binary Markov sources in AWGN channels. Code rate is 1/2.

The performance of our proposed JSC decoding technique for transmitting symmetric and asymmetric binary Markov sources are shown in Fig. 3.9 and 3.10, respectively. Simulations are performed for different Markov sources with overall code rate $R_c = 1/2$. Theoretical limits for those cases are also plotted in the same figure. To demonstrate the performance gains obtained by the exploitation of the memory structure, the BER curve of SCCC with the same code parameters, decoded with the standard BCJR algorithm, is also provided in the same figure, which is referred to as "standard". It can be clearly observed that at the BER level of 10^{-4}, when $p_1 = p_2 = 0.7$, our system offers a gain of 0.84 dB over the "standard" system, while achieving a gap to the theoretical limit of 0.85 dB. All the gains and gaps are summarized in Table 3.2, together with the results of the technique proposed in [82], which is referred to as Joint Source Channel Turbo Coding (JSCTC) as a reference.

It can be found from the table that substantial gains can be achieved for different Markov sources with both our proposed SCCC based and [82]'s proposed parallel-concatenated convolutional codes (PCCC) based systems. This implies that exploiting the source redundancy provides us with significant advantage. The gains over the standard BCJR decoding and gaps to the Shannon limits are measured with respect to E_b/N_0, which provide an fair comparison between our proposed JSC technique and the JSCTC technique proposed in [82]. It is found that besides the gap in the case of $p_1 = p_2 = 0.7$, our technique outperforms JSCTC in terms of both gains and the gaps for binary Markov sources.

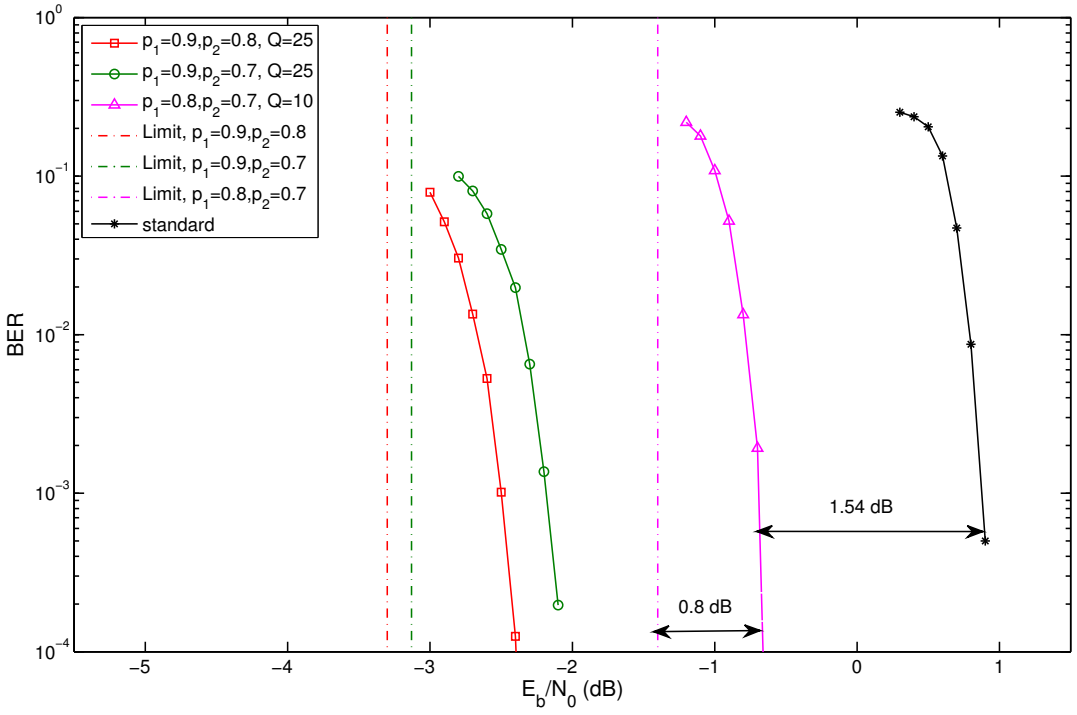

Figure 3.10: BER peformance of the proposed technique for asymmetric binary Markov sources in AWGN channels. Code rate is 1/2.

Table 3.2: BER performance comparison between the proposed system and JSCTC

Source Parameters		JSCTC		Our system	
p_1	p_2	Gain(dB)	Gap(dB)	Gain(dB)	Gap(dB)
0.9	0.9	3.03	1.36	4.24	0.86
0.8	0.8	1.29	0.94	2.04	0.78
0.7	0.7	0.7	0.73	0.84	0.85
0.9	0.8	2.31	1.14	3.24	1.0
0.9	0.7	2.02	1.31	3.04	1.02
0.8	0.7	0.92	0.83	1.54	0.8

It should be emphasized that the derivation of the modified BCJR algorithm is based on the super trellis that represents both the outer code and the binary Markov source, which is more accurate than the method used in JSCTC which is based on approximation. As a consequence, the extrinsic LLRs obtained by the two decoders can be exchanged directly between them in our technique without losing any information, while the extrinsic LLRs generated by the two constitute decoders have to be further modified before being fed into each other in JSCTC. Moreover, JSCTC shown in [82] employs two memory-4 constituent codes, while our proposed system uses a memory-1 outer code (as described in Subsection 3.3.2, the decoding complexity is equivalent to a memory-2 RSC code) and a memory-2 inner coder. Hence, compared with JSCTC, the decoding complexity of our proposed system is significantly reduced.

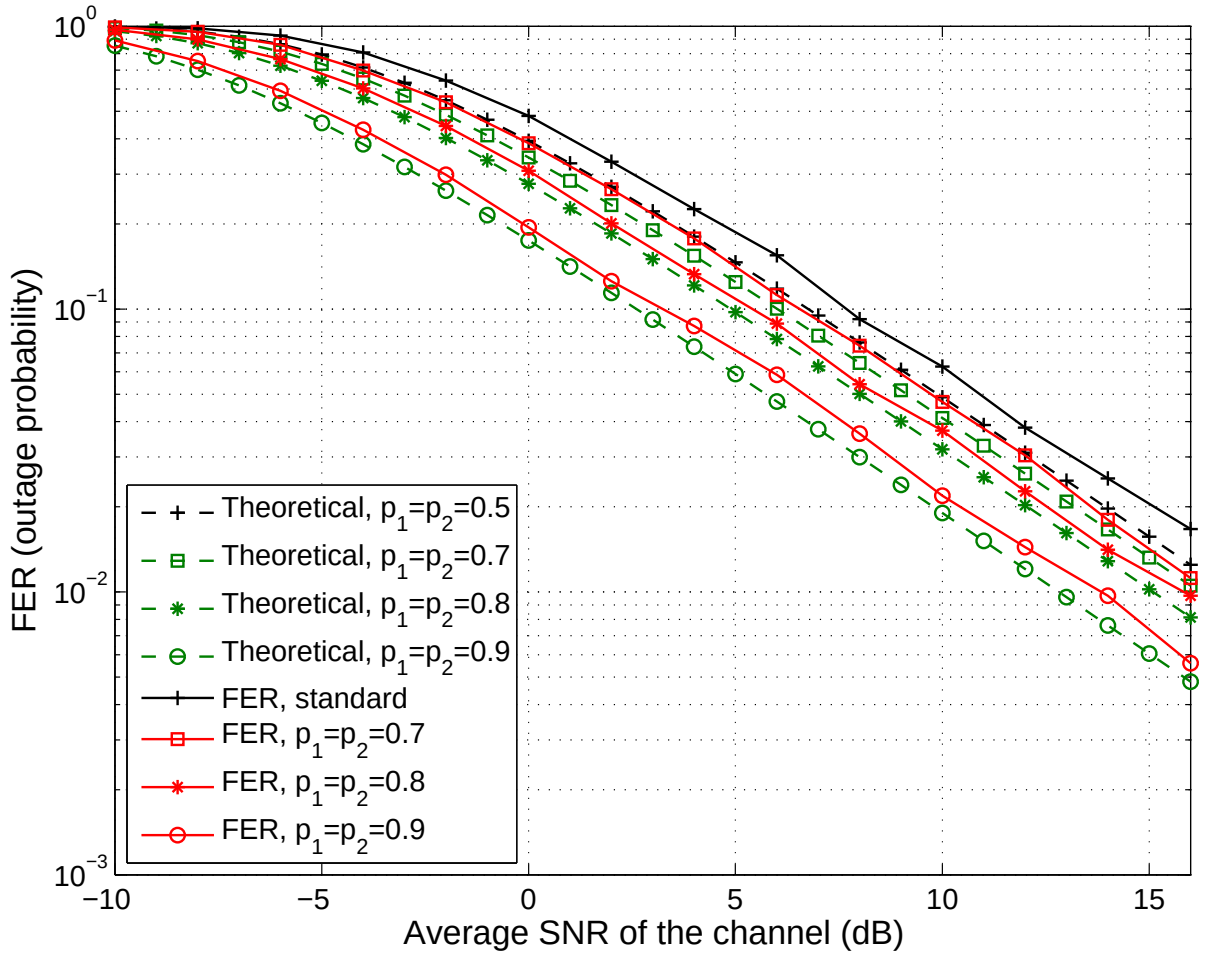

Figure 3.11: FER peformance of the proposed technique for symmetric binary Markov sources in block Rayleigh fading channels.

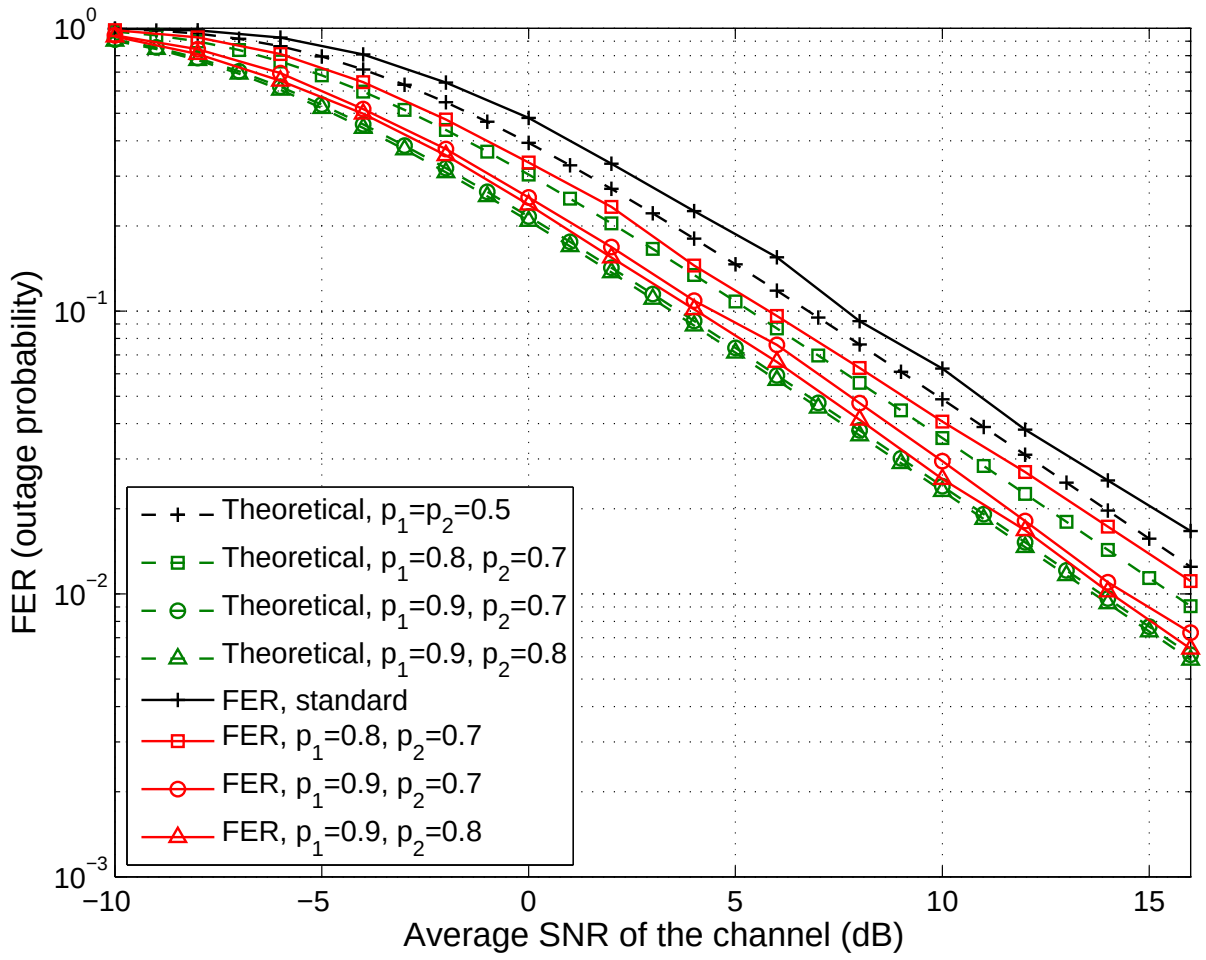

Figure 3.12: FER peformance of the proposed technique for asymmetric binary Markov sources in block Rayleigh fading channels.

3.5.2 FER Performance in Rayleigh Fading Channels

In this subsection, the numerical results of the theoretical outage probability analysis shown in (3.13), and the FER performance of the proposed SCCC-based JSC technique obtained through simulations are presented. The length of binary sequence generated from the Markov sources is 2000 bits, and in total $10,000$ different frames, each having different channel realizations, were transmitted.

The theoretical outage probability and the FER performance of the proposed technique for symmetric Markov sources are shown in Fig. 3.11. It can be observed that the theoretical outage probability decreases as the source memory becomes stronger, since the source memory can be well exploited by the proposed technique. However, all the theoretical outage curves have the same decay (no diversity), regardless of p_1 and p_2 values, this is consistent with the analysis provided in Subsection 3.2.2. It is also shown that the stronger the source memory, the more the FER performance improvement. For the given p_1 and p_2 values, there are around 1 dB gaps between the FER curves obtained through simulations and their corresponding theoretical outage curves.

Similar results can be obtained with the theoretical outage probability and the FER performance of the proposed technique for asymmetric Markov sources, as shown in Fig. 3.12. The decay of the FER curves are consistent with their corresponding outage curves, and there are around 1 dB gaps between them. It can be found from Figs. 3.11 and 3.12 that, our proposed technique is efficient for both symmetric and asymmetric Markov sources. However, we can not achieve diversity gain by exploiting the source memory.

3.6 Summary

In this chapter, we have investigated the problem of transmitting binary Markov source over wireless channels, where the source memory is exploited at the destination.

First of all, we derived the performance limits in AWGN channels and the outage probability in block Rayleigh fading channels, for a channel coding rate R_c and Markov source with given entropy $H^M(p_1, p_2)$. It is found from the theoretical analysis that the source memory helps reducing the outage probability. However, no diversity gain can be achieved with the source memory.

We then proposed a new coding/decoding framework for the problem considered, based on SCCC. To fully exploit the Markov source memory, the trellis of Markov source and that of the outer code are combined to construct a super trellis. A modified BCJR algorithm, suitable for this structure, has been derived based on the super trellis diagram. To further approach the performance limits, code doping is employed for inner code, where the standard BCJR algorithm is used to decode the inner code. The extrinsic information generated by the inner and joint outer decoders is exchanged via interleaver/deinterleaver in the same way as the decoding of serially concatenated codes. The code parameters, including generator polynomials of the outer and inner codes, and the doping rate of inner code, were optimized based on EXIT chart analysis.

It has been shown through BER performance simulations that the proposed technique can achieve equivalent or even better performance than JSCTC technique using PCCC, while requiring much smaller decoding complexity. In addition, the FER curves of the proposed technique obtained through simulations were compared with their corresponding outage curves obtained in the theoretical analysis. It has been found the FER curves are

consistent with their corresponding outage curves, and there are around 1 dB gaps between them.

Chapter 4

Markov Source Transmission over One-Way Relay Channel

In this chapter, we extend the results of **Chapter 3** to the problem of transmitting binary Markov source in a one-way relay system, where a source node is communicating with a destination node with the help of a relay node. The relay strategy is ErF [96], where the relay node only *extracts* and forwards the source message to the destination node, implying imperfect decoding at the relay node. The probability of errors occurring in the source-relay link can be regarded as source-relay correlation, which can be estimated at the destination node and utilized in the decoding process. Moreover, the source memory of the Markov source can also be exploited at the destination.

First of all, we will describe the system model of relay transmission for Markov source. Then, the achievable compression rate region is derived based on the Slepian-Wolf theorem. The performance limits in AWGN channels and the outage probability in block Rayleigh fading channels are derived based on the achievable compression rate region. We also propose a new coding/decoding framework that exploits the source-relay correlation and source memory simultaneously, based on some practical channel codes. Furthermore, the convergence property of the proposed technique is evaluated by EXIT chart analysis. The effectiveness of the proposed technique is verified through a series of simulations, including BER performance in AWGN channels, FER performance in Rayleigh fading channels and image transmission experiments. It is also verified through the numerical results that the accuracy of the theoretical analysis.

4.1 System Model

An abstract model of Markov source transmission in a one-way relay system is illustrated in Fig. 4.1. The Markov source considered is a stationary state emitting binary Markov source, of which the property has already been addressed in **Chapter 3**, and the source memory can be parameterized by the Markov state transition probability p_1 and p_2.

4.1.1 Source-Relay Correlation

At the source node S, the binary data sequence $\mathbf{u}_s$ generated from Markov source is directly fed into the channel encoder ENC_s and then modulated by BPSK to obtain the modulated sequence $\mathbf{x}_s$. The relay node operates in a half-duplex mode and ErF relaying

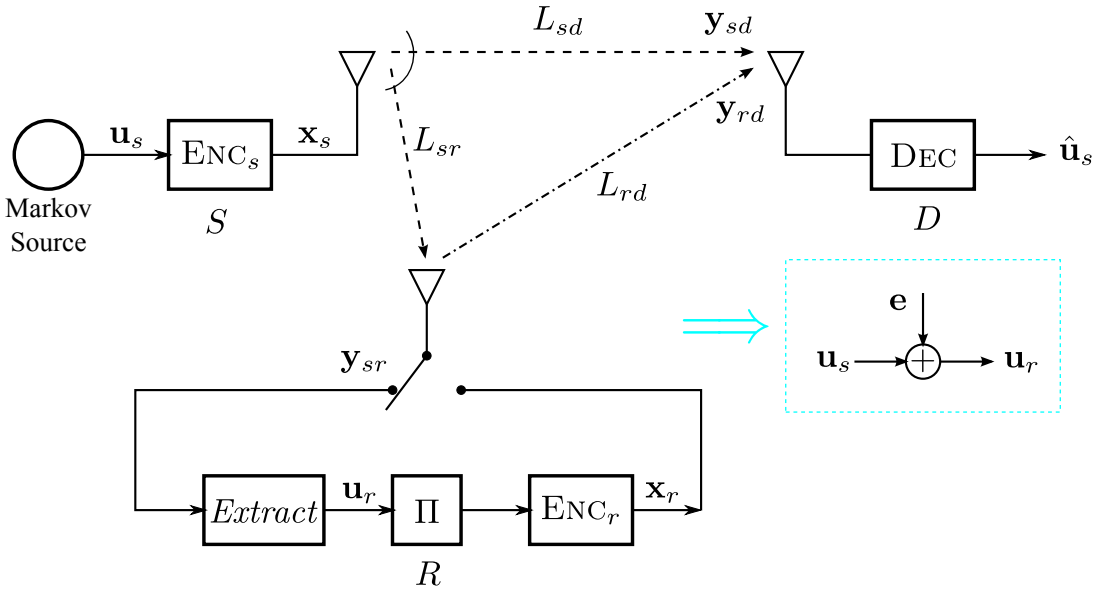

Figure 4.1: Block diagram of the binary Markov source transmission in a one-way relay system and its equivalent bit-flipping model. S, R and D denote the source, relay and destination node, respectively.

strategy is adopted. During the first time slot, the source node broadcasts $\mathbf{x}_s$ to both the relay and destination nodes. After receiving signal $\mathbf{y}_{sr}$ from the source node, the relay node tries to *extract* by a simple decoding method the original data sequence and get an estimate of $\mathbf{u}_s$, which is denoted as $\mathbf{u}_r$. Then $\mathbf{u}_r$ is interleavered, re-encoded by the channel encoder ENC$_r$ and modulated to get the modulated sequence $\mathbf{x}_r$, even though errors may occur between $\mathbf{u}_r$ and $\mathbf{u}_s$. The relay node sends $\mathbf{x}_r$ to the destination node during the second time slot.

As described above, in ErF relay system, the source-relay correlation indicates the correlation between $\mathbf{u_s}$ and $\mathbf{u_r}$, which can be represented by a bit-flipping model, as shown in Fig. 4.1. $\mathbf{u}_r$ can be defined as $\mathbf{u}_r = \mathbf{u}_s \oplus \mathbf{e}$, where $\mathbf{e}$ is an i.i.d. binary random variable vector and $\oplus$ indicates modulus-2 addition. The correlation between $\mathbf{u}_s$ and $\mathbf{u}_r$ is characterized by p_e, where $p_e = \Pr(e^k = 1) = \Pr(u_s^k \neq u_r^k)$ [88]. Here, u_s^k, u_r^k and e^k denote the k-th symbol of $\mathbf{u}_s$, $\mathbf{u}_r$ and $\mathbf{e}$, respectively.

After receiving signals $\mathbf{y}_{sd}$ and $\mathbf{y}_{rd}$ from the source and relay nodes, respectively, the destination node performs joint decoding to exploit both the source-relay correlation and source memory to retrieve the original data sequence sent from the source. This will be detailed in Subsection 4.3.2.

4.1.2 Relay Location and Channel Model

For notational simplicity, the source, relay and destination nodes are indicated as S, R and D, respectively. The link between S and D is denoted as L_{sd}. Similar definitions are applied to L_{sr} and L_{rd}, as shown in Fig. 4.1. R can be located closer to S or to D, or the three nodes keep the same distance with each other. All these three different relay location scenarios are considered in this chapter, as shown in Fig. 4.2. The geometric-gain [125]

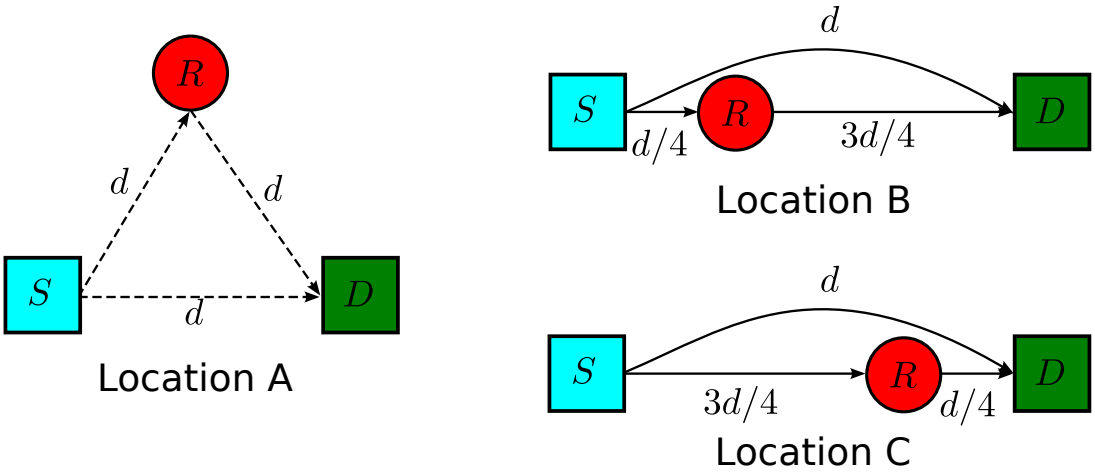

Figure 4.2: Three different relay location scenarios.

G_{xy} of the link L_{ij} can be defined as

$$G_{ij} = (\frac{d_{sd}}{d_{ij}})^l, \tag{4.1}$$

where $ij \in \{sr, sd, rd\}$. The pass loss exponent l is empirically set at 3.52 [125]. According to (4.1), the geometric-gain of the source-destination link G_{sd} is normalized to 1 without the loss of generality.

The received signals at the relay and at the destination nodes can be expressed as

$$\mathbf{y}_{sr} = \sqrt{G_{sr}} \cdot h_{sr} \cdot \mathbf{x}_s + \mathbf{n}_r, \tag{4.2}$$

$$\mathbf{y}_{sd} = \sqrt{G_{sd}} \cdot h_{sd} \cdot \mathbf{x}_s + \mathbf{n}_d, \tag{4.3}$$

$$\mathbf{y}_{rd} = \sqrt{G_{rd}} \cdot h_{rd} \cdot \mathbf{x}_r + \mathbf{n}_d, \tag{4.4}$$

where h_{sr}, h_{sd} and h_{rd} denote the complex block Rayleigh fading channel gains of L_{sr}, L_{sd} and L_{rd}, respectively. According to the block fading assumption, they are constant in each block. Notations $\mathbf{n}_r$ and $\mathbf{n}_d$ represent the zero-mean AWGN noise vectors at the relay and the destination with variances σ_r^2 and σ_d^2, respectively. If we normalize the noise power at R and D to 1, the relationship between the average SNR of the L_{sr} L_{rd} and L_{sd} with the three different relay location scenarios, denoted as Γ_{sr}, Γ_{rd} and Γ_{sd}, respectively, can be decided as[1]:

(1) for location A,

$$\begin{cases} \Gamma_{sr} = \Gamma_{sd}, \\ \Gamma_{rd} = \Gamma_{sd}, \end{cases} \tag{4.5}$$

(2) for location B,

$$\begin{cases} \Gamma_{sr} = \Gamma_{sd} + 21.19 \text{ dB}, \\ \Gamma_{rd} = \Gamma_{sd} + 4.4 \text{ dB}, \end{cases} \tag{4.6}$$

(3) for location C,

$$\begin{cases} \Gamma_{sr} = \Gamma_{sd} + 4.4 \text{ dB}, \\ \Gamma_{rd} = \Gamma_{sd} + 21.19 \text{ dB}. \end{cases} \tag{4.7}$$

[1]Note that $10\log_{10}(4^{3.52}) = 21.19$ dB, and $10\log_{10}[(\frac{4}{3})^{3.52}] = 4.4$ dB.

4.2 Theoretical Analysis

As described above, the source-relay correlation can be characterized by the error probability p_e. With block Rayleigh fading assumption, p_e is also kept constant over one block, but varies between different blocks. In fact, the value of p_e depends largely on the quality of L_{sr} and the extracting method used at R. Therefore, it is impractical to derive the *pdf* of p_e. Hence, in this section, we assume that p_e is a constant number and the impact of the variation of the quality of L_{sr} in not considered. The lower bound of the outage probability of the proposed system is obtained by assuming $p_e = 0$. Furthermore, we assume that the channel encoders ENC_s and ENC_r are both close-limit achieving, corresponding to their rates.

4.2.1 Slepian-Wolf Theorem

Let $\{X_i, Y_i\}_{i=1}^{\infty}$ be a sequence of i.i.d. discrete random pairs with a joint *pdf*, i.e., $(X_i, Y_i) \sim p(x, y)$. According to Theorem 2.1, we known that a rate $H(X, Y)$ is sufficient if X and Y are encoded together for lossless compression. For example, we can first compress X into $H(X)$ bits per symbol and then compress Y into $H(Y|X)$ bits per symbol based on the complete knowledge of X at both the encoder and the decoder.

However, if we want to encode X and Y separately and decode them jointly, determining the sufficient rates for lossless compression of X and Y is not so straightforward. Clearly, X and Y can be separately encoded with a overall rate $R = R_x + R_y = H(X) + H(Y)$, but this is greater than $H(X, Y)$ when X and Y are correlated. This problem has been theoretically investigated by Slepian and Wolf in their landmark paper [84], of which the results can be described as follow.

Theorem 4.1 (Slepian-Wolf) *For a sequence $\{X_i, Y_i\}_{i=1}^{\infty}$ of discrete random pairs (X_i, Y_i) drawing i.i.d. $\sim p(x, y)$, where $X_i \in \mathscr{X}$ and $Y_i \in \mathscr{Y}$. Then for any rate pair that satisfy*

$$\begin{cases} R_x & \geq & H(X|Y), \\ R_y & \geq & H(Y|X), \\ R_x + R_y & \geq & H(X, Y), \end{cases} \tag{4.8}$$

there exists an integer n and mappings

$$\begin{array}{rccl} i: & \mathscr{X}^n & \rightarrow & I = \{1, 2, \cdots, 2^{nR_x}\}, \\ j: & \mathscr{Y}^n & \rightarrow & J = \{1, 2, \cdots, 2^{nR_y}\}, \\ g: & I \times J & \rightarrow & \mathscr{X}^n \times \mathscr{Y}^n, \end{array} \tag{4.9}$$

such that

$$\Pr\{g(i(X_1, \cdot, X_n), j(Y_1, \cdots, Y_n)) = (X_i, \cdots, X_n, Y_1, \cdots, Y_n)\} \geq 1 - \varepsilon. \tag{4.10}$$

According to the Slepian-Wolf theorem, an admissible rate region is specified, as shown in Fig. 4.3. As long as the rate pair (R_x, R_y) falls inside the admissible rate region, the error probability ε after joint decoding can be made arbitrarily small.

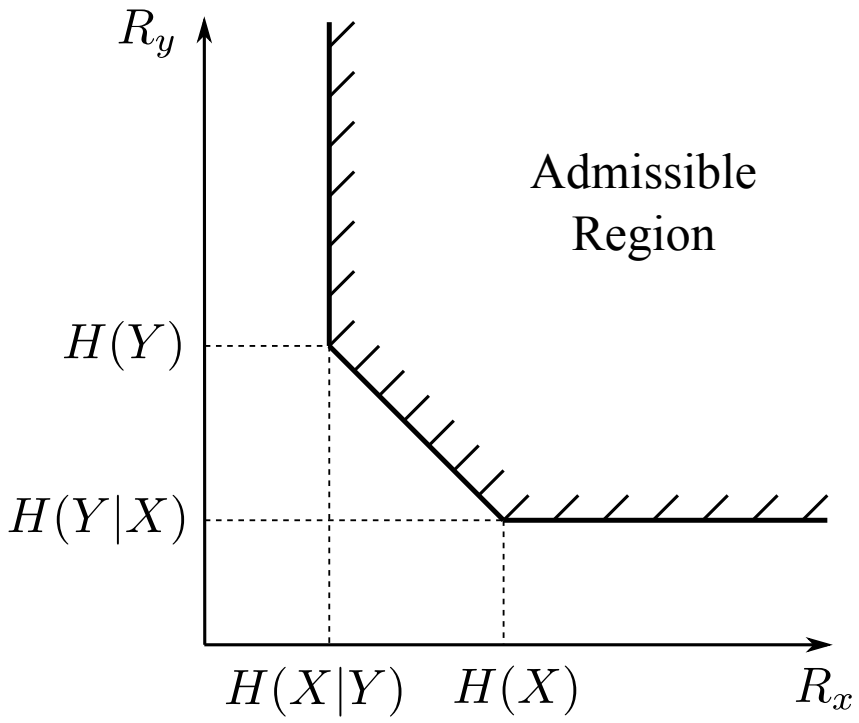

Figure 4.3: The admissible rate region of Slepian-Wolf theorem.

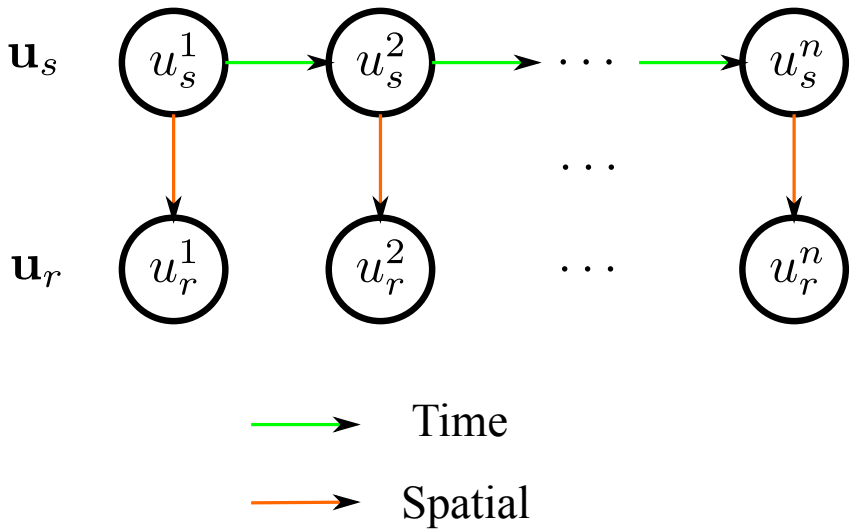

Figure 4.4: The two-dimensional correlation of the proposed system, which are source-relay correlation and the source memory, respectively..

4.2.2 Achievable Compression Rate Region

As described in Section 4.1, $\mathbf{u}_s$ is generated from a binary Markov source and $\mathbf{u}_r$ is a bit-flipped version of $\mathbf{u}_s$. Therefore there are two-dimensional source correlation exists in the proposed system, in terms of both spatial and temporal domains, as shown in Fig. 4.4. Due to the source memory, the random pair (u_s^i, u_r^i) does not follow the i.i.d. property, and $\{u_s^i, u_r^i\}_{i=1}^{\infty}$ is an ergodic process. It has been proved by Cover that the Slepian-Wolf theorem can be applied to arbitrary ergodic process and arbitrary number of correlated sources [126]. Hence we can still use the Slepian-Wolf theorem to determine the achievable compression rate region of the proposed system.

Assume $\mathbf{u}_s$ and $\mathbf{u}_r$ are compressed at rates R_s and R_r, respectively. According to the Slepian-Wolf theorem, successful recovery of both $\mathbf{u}_s$ and $\mathbf{u}_r$ after joint decoding at D is possible if R_s and R_r satisfy

$$\begin{cases} R_s & \geq & H(\mathbf{u}_s|\mathbf{u}_r), \\ R_r & \geq & H(\mathbf{u}_r|\mathbf{u}_s), \\ R_s + R_r & \geq & H(\mathbf{u}_s, \mathbf{u}_r). \end{cases} \tag{4.11}$$

Since $\mathbf{u}_s$ is generated from a binary Markov source, the entropy rate is $H(\mathbf{u}_s) = H^M(p_1, p_2)$, where $H^M(p_1, p_2)$ is defined in (3.4). $\mathbf{u}_r$ is the bit-flipped version of $\mathbf{u}_s$, hence the conditional entropy $H(\mathbf{u}_r|\mathbf{u}_s)$ is

$$H(\mathbf{u}_r|\mathbf{u}_s) = H_b(p_e). \tag{4.12}$$

The joint entropy rate of $\mathbf{u_s}$ and $\mathbf{u}_r$ is

$$H(\mathbf{u}_s, \mathbf{u}_r) = H(\mathbf{u}_s) + H(\mathbf{u}_r|\mathbf{u}_s) = H^M(p_1, p_2) + H_b(p_e). \tag{4.13}$$

For the relay R, $\mathbf{u}_r$ can be regarded as the output of a HMM [127], where $\mathbf{u}_s$ is the sequence of the states, as shown in Fig. 4.4. It is noticed that $H(\mathbf{u}_r)$ represents the entropy rate of this HMM. However, deriving explicit expression for $H(\mathbf{u}_r)$ may not be possible [128]. Instead, making approximation for the entropy rate of HMM using some numerical methods have been studied in [128–130]. According to the results presented in [129], $H(\mathbf{u}_r)$ can be expressed as a function of the transition probability p_1, p_2 and the bit-flipping probability p_e, i.e., $H(\mathbf{u}_r) = \Psi_1(p_1, p_2, p_e)$. For the approximation of $H(\mathbf{u}_r)$, please refer to the Appendix. After obtaining $H(\mathbf{u}_r)$, the conditional entropy $H(\mathbf{u}_s|\mathbf{u}_r)$ can be expressed as

$$\begin{aligned} H(\mathbf{u}_s|\mathbf{u}_r) &= H(\mathbf{u}_s, \mathbf{u}_r) - H(\mathbf{u}_r) \\ &= H^M(p_1, p_2) + H_b(p_e) - \Psi_1(p_1, p_2, p_e) \\ &= \Psi_2(p_1, p_2, p_e). \end{aligned} \tag{4.14}$$

Now the achievable compression rate region defined by (4.8) is obtained, which is shown in Fig. 4.5. It can be seen from the figure that the entire region for the rate pair (R_s, R_r) can be divided into 4 parts, and the probability that (R_s, R_r) falls into Part i is denoted as P_i, $i = 1, 2, 3, 4$. As long as (R_s, R_r) falls into Part 3, $\mathbf{u}_s$ and $\mathbf{u}_r$ can be successfully recovered. However, in the proposed one-way relay system, the objective of D is only to retrieve $\mathbf{u}_s$, which is sent from S. On the other hand, the data sequence $\mathbf{u}_r$ sent from R does not need to be successfully recovered at D. Therefore, if $R_s \geq H(\mathbf{u}_s)$,

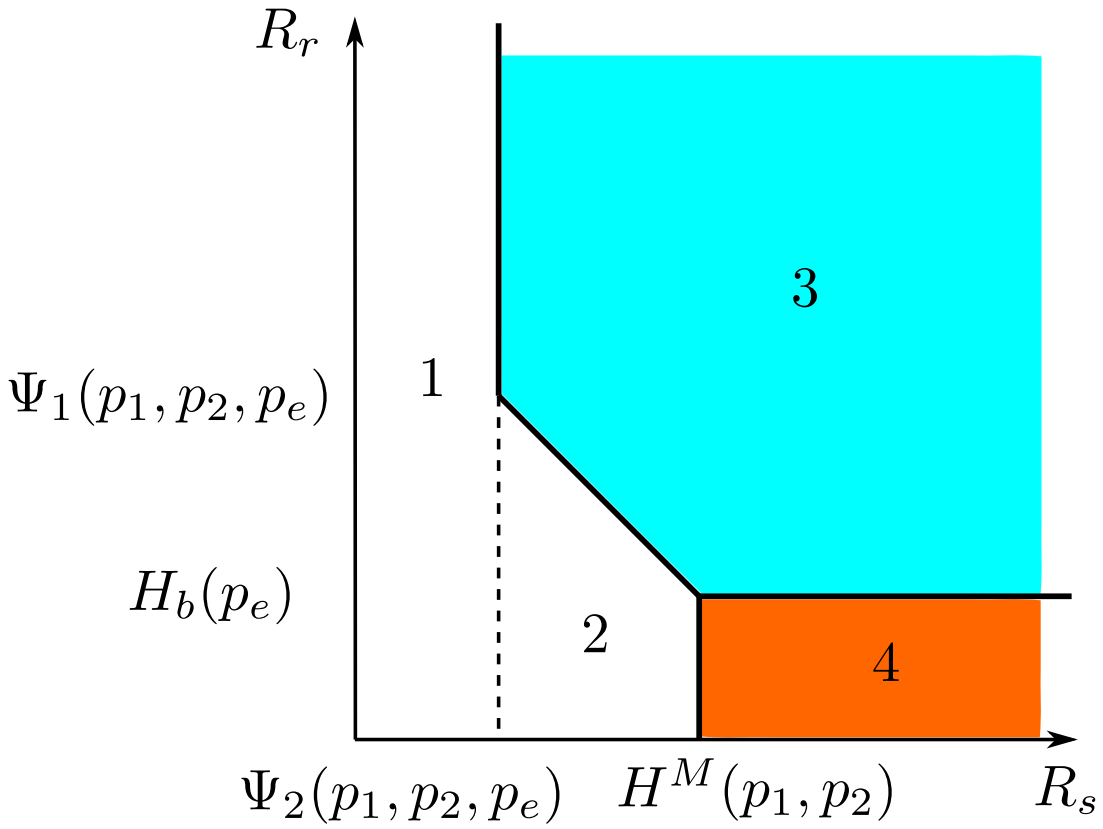

Figure 4.5: The achievable compression rate region for the proposed system, assuming p_e is constant.

an arbitrary value of R_r is satisfactory, which indicates Part 4 should also be included in the achievable rate region [99]. Hence, the achievable rate region of the proposed system is represented by Part 3 and Part 4, as shown in Fig. 4.5. According to the figure, this achievable rate region can be expressed as

$$\begin{cases} R_s \geq \Psi_2(p_1, p_2, p_e) \text{ and } R_s + R_r \geq H^M(p_1, p_2) + H_b(p_e), & \text{if } R_r \geq H_b(pe); \\ R_s \geq H^M(p_1, p_2), & \text{if } 0 \leq R_r < H_b(p_e). \end{cases} \tag{4.15}$$

It should be emphasized here that, in the system considered in this section, source coding for compression is performed neither at S or R. Instead, the correlation knowledge between $\mathbf{u}_s$ and $\mathbf{u}_r$ is exploited at D to enhance the error correction capability of the system.

4.2.3 Performance Limits in AWGN channels

Since we assume p_e is constant, according to Shannon's separation theorem, if the total information transmission rate over independent channels L_{sd} and L_{rd} satisfy [88]

$$\begin{cases} R_s R_{c,s} & \leq & C_{sd}, \\ R_r R_{c,r} & \leq & C_{rd}, \end{cases} \tag{4.16}$$

the error probability after decoding can be made arbitrarily small, where $R_{c,sd}$ and $R_{c,rd}$ are the rates of the channel encoders ENC_s and ENC_r, respectively. C_{sd} and C_{rd} are expressed as

$$\begin{cases} C_{sd} & = & \frac{1}{2}\log_2(1 + 2\Gamma_{sd}), \\ C_{rd} & = & \frac{1}{2}\log_2(1 + 2\Gamma_{rd}), \end{cases} \tag{4.17}$$

which represents the channel capacity of L_{sd} and L_{rd} with one-dimensional transmission, respectively. Then the performance limits of the proposed system can be obtained by combining (4.15) and (4.16), if p_e is constant.

4.2.4 Outage Probability in Rayleigh Fading Channels

If L_{sd} and L_{rd} both suffer from block Rayleigh fading, the instantaneous SNR of L_{sd} and L_{rd} are denoted as γ_{sd} and γ_{rd}, respectively. γ_{sd} is defined as

$$\gamma_{sd} = \frac{|h_{sd}|^2 G_{ij} E_{s,sd}}{2\sigma^2}, \tag{4.18}$$

where $E_{s,sd}$ represents the per-symbol signal power of L_{sd}. Similar definition can be applied to γ_{rd}. Since the channel encoders ENC_s and ENC_r are assumed to be close-limit achieving, according to (4.16) and (4.17), the relationship between the threshold instantaneous SNR of L_{ij} and its corresponding rate R_i is given by

$$R_i = \Phi_i(\gamma_{ij}) = \frac{1}{2R_{c,ij}}\log_2(1 + 2\gamma_{ij}), \tag{4.19}$$

with its inverse function

$$\gamma_{ij} = \Phi_i^{-1}(R_i) = \frac{2^{2R_i R_{c,ij}} - 1}{2}, \tag{4.20}$$

where $i = \{s, r\}$, and $j = d$.

As shown in Fig. 4.5, if rate pair (R_s, R_r) falls into Part 3 or Part 4, then $\mathbf{u}_s$ can be successfully decoded at D. Hence, the outage event happens when (R_s, R_r) falls into Part 1 and Part 2, and the outage probability of the proposed system is defined as

$$P_{out} = P_1 + P_2, \tag{4.21}$$

where

$$\begin{aligned} P_1 &= \Pr\{0 \le R_s \le \Psi_2(p_1, p_2, p_e), R_r \ge 0\} \\ &= \Pr\{\Phi_s^{-1}(0) \le \gamma_{sd} \le \Phi_s^{-1}[\Psi_2(p_1, p_2, p_e)], \gamma_{rd} \ge \Phi_r^{-1}(0)\}, \end{aligned} \tag{4.22}$$

and

$$\begin{aligned} P_2 &= \Pr\{\Psi_2(p_1, p_2, p_e) \le R_s \le H^M(p_1, p_2), R_s + R_r \le H^M(p_1, p_2) + H_b(p_e)\} \\ &= \Pr\{\Phi_s^{-1}[\Psi_2(p_1, p_2, p_e)] \le \gamma_{sd} \le \Phi_s^{-1}[H^M(p_1, p_2)], \\ &\quad \Phi_r^{-1}(0) \le \gamma_{rd} \le \Phi_r^{-1}[H^M(p_1, p_2) + H_b(p_e) - \Phi_s(\gamma_{sd})]\}. \end{aligned} \tag{4.23}$$

Since L_{sd} and L_{rd} suffer from statistically independent block Rayleigh fading, the joint pdf of γ_{sd} and γ_{rd} can be expressed as $p(\gamma_{sd}, \gamma_{rd}) = p(\gamma_{sd})p(\gamma_{rd})$, with

$$p(\gamma_{ij}) = \frac{1}{\Gamma_{ij}} \exp(-\frac{\gamma_{ij}}{\Gamma_{ij}}),\ ij \in \{sd, rd\}, \tag{4.24}$$

where $\Gamma_{ij} = G_{ij}E_{s,ij}/2\sigma^2$ denotes the average SNR of L_{ij}. Based on (4.24), the probabilities P_1 and P_2 can be further derived as

$$\begin{aligned} P_1 &= \int_{\Phi_s^{-1}(0)}^{\Phi_s^{-1}[\Psi_2(p_1,p_2,p_e)]} \int_{\Phi_r^{-1}(0)}^{\Phi_r^{-1}(\infty)} p(\gamma_{sd}, \gamma_{rd}) d\gamma_{rd} d\gamma_{sd} \\ &= \int_{\Phi_s^{-1}(0)}^{\Phi_s^{-1}[\Psi_2(p_1,p_2,p_e)]} \frac{1}{\Gamma_{sd}} \exp(-\frac{\gamma_{sd}}{\Gamma_{sd}}) d\gamma_{sd} \\ &= 1 - \exp\left[-\frac{\Phi_s^{-1}[\Psi_2(p_1, p_2, p_e)]}{\Gamma_{sd}}\right], \end{aligned} \tag{4.25}$$

and

$$\begin{aligned} P_2 &= \int_{\Phi_s^{-1}[\Psi_2(p_1,p_2,p_e)]}^{\Phi_s^{-1}[H^M(p_1,p_2)]} \int_{\Phi_r^{-1}(0)}^{\Phi_r^{-1}[H^M(p_1,p_2)+H_b(p_e)-\Phi_s(\gamma_{sd})]} p(\gamma_{sd}, \gamma_{rd}) d\gamma_{sd} d\gamma_{rd} \\ &= \int_{\Phi_s^{-1}[\Psi_2(p_1,p_2,p_e)]}^{\Phi_s^{-1}[H^M(p_1,p_2)]} p(\gamma_{sd}) \cdot \left[-\exp(-\frac{\gamma_{rd}}{\Gamma_{rd}})\right]_{\Phi_r^{-1}(0)}^{\Phi_r^{-1}[H^M(p_1,p_2)+H_b(p_e)-\Phi_s(\gamma_{sd})]} d\gamma_{sd} \\ &= \frac{1}{\Gamma_{sd}} \int_{\Phi_s^{-1}[\Psi_2(p_1,p_2,p_e)]}^{\Phi_s^{-1}[H^M(p_1,p_2)]} \exp(-\frac{\gamma_{sd}}{\Gamma_{sd}}) \left[1 - \exp\left(-\frac{\Phi_r^{-1}[H^M(p_1, p_2) + H_b(p_e) - \Phi_s(\gamma_{sd})]}{\Gamma_{rd}}\right)\right] d\gamma_{sd} \\ &= \frac{1}{\Gamma_{sd}} \int_{\Phi_s^{-1}[\Psi_2(p_1,p_2,p_e)]}^{\Phi_s^{-1}[H^M(p_1,p_2)]} \\ &\qquad \left[\exp(-\frac{\gamma_{sd}}{\Gamma_{sd}}) - \exp\left(-\frac{\gamma_{sd}}{\Gamma_{sd}} - \frac{\Phi_r^{-1}[H^M(p_1, p_2) + H_b(p_e) - \Phi_s(\gamma_{sd})]}{\Gamma_{rd}}\right)\right] d\gamma_{sd}. \end{aligned} \tag{4.26}$$

It can be found from (4.26) that, the derivation for the explicit expression of P_2 may not be possible. Hence, we use a numerical method to calculated the value of P_2.

4.2.5 Asymptotic Analysis

In The Case $p_e = 0$

If $\mathbf{u}_s$ and $\mathbf{u}_r$ are fully correlated ($p_e = 0$), it is easily to identify $\Psi_1(p_1, p_2, p_e) = H^M(p_1, p_2)$ and $\Psi_2(p_1, p_2, p_e) = 0$. In this case, the integral range of γ_{sd} in (4.25) is from 0 to 0, and the value of P_1 always equals to 0. Hence, the outage probability is determined by P_2 only.

When $\Gamma_{sd} \to \infty$, Γ_{rd} also approaches ∞. According to (3.14), P_2 can be further approximated as

$$\begin{aligned}
P_2 &= \frac{1}{\Gamma_{sd}} \int_0^{\frac{2^{2R_{c,sd}H^M(p_1,p_2)}-1}{2}} \\
&\qquad \left[\exp(-\frac{\gamma_{sd}}{\Gamma_{sd}}) - \exp\left(-\frac{\gamma_{sd}}{\Gamma_{sd}} - \frac{2^{2R_{c,rd}[H^M(p_1,p_2)+H(p_e)-\Phi_s(\gamma_{sd})]}-1}{2\Gamma_{rd}}\right)\right] d\gamma_{sd} \\
&\approx \frac{1}{\Gamma_{sd}} \int_0^{\frac{2^{2R_{c,sd}H^M(p_1,p_2)}-1}{2}} \\
&\qquad \left[(1 - \frac{\gamma_{sd}}{\Gamma_{sd}}) - \left(1 - \frac{\gamma_{sd}}{\Gamma_{sd}} - \frac{2^{2R_{c,rd}[H^M(p_1,p_2)+H(p_e)-\Phi_s(\gamma_{sd})]}-1}{2\Gamma_{rd}}\right)\right] d\gamma_{sd} \\
&= \frac{1}{\Gamma_{sd}} \int_0^{\frac{2^{2R_{c,sd}H^M(p_1,p_2)}-1}{2}} \left[-\frac{1}{2\Gamma_{rd}} + \frac{2^{2R_{c,rd}H^M(p_1,p_2)}}{2^{1+\frac{R_{c,rd}}{R_{c,sd}}}(1+2\gamma_{sd})\Gamma_{rd}}\right] d\gamma_{sd} \\
&= \frac{1}{\Gamma_{sd}} \left[-\frac{\gamma_{sd}}{2\Gamma_{rd}} + \frac{2^{2R_{c,rd}H^M(p_1,p_2)}\ln(1+2\gamma_{sd})}{2^{2+\frac{R_{c,rd}}{R_{c,sd}}}\Gamma_{rd}}\right]_0^{\frac{2^{2R_{c,sd}H^M(p_1,p_2)}-1}{2}} \\
&= \frac{1}{\Gamma_{sd}\Gamma_{rd}} \left[-\frac{2^{2R_{c,sd}H^M(p_1,p_2)}-1}{4} + \frac{2^{2R_{c,rd}H^M(p_1,p_2)}\ln(2^{2R_{c,sd}H^M(p_1,p_2)})}{2^{2+\frac{R_{c,rd}}{R_{c,sd}}}}\right].
\end{aligned} \tag{4.27}$$

It can be seen from (4.27) that, as $\Gamma_{sd} \to \infty$ and $\Gamma_{rd} \to \infty$, p_2 is inversely proportional to the product of Γ_{sd} and Γ_{rd}. Hence, the outage probability exhibits the $2nd$ order diversity.

In The Case $p_e \neq 0$

In the case $\mathbf{u}_s$ and $\mathbf{u}_r$ are not fully correlated ($p_e \neq 0$), as $\Gamma_{sd} \to \infty$, $P_2 \to 0$ according to (4.26). Therefore the outage probability is mainly determined by P_1. According to (3.14), P_1 can be approximated as

$$\begin{aligned}
P_1 &= 1 - \exp\left[-\frac{2^{2\Psi_2(p_1,p_2,p_e)R_{c,sd}}-1}{2\Gamma_{sd}}\right] \\
&\approx \frac{2^{2\Psi_2(p_1,p_2,p_e)R_{c,sd}}-1}{2\Gamma_{sd}}.
\end{aligned} \tag{4.28}$$

It can be concluded that as $\Gamma_{sd} \to \infty$, P_1 is inversely proportional to Γ_{sd}, which indicates the outage probability can not achieve any diversity gain.

It should be emphasized here that, the asymptotic tendency is influenced by the memory structure of $\mathbf{u}_s$, however, no diversity gain can be achieved with the change of source memory, as can be seen from (4.27) and (4.28).

4.3 Practical Code Design

In the theoretical analysis, we assumed both ENC_s and ENC_r have close-limit performance. Furthermore, the extracting method is not specified and the error probability between $\mathbf{u}_s$ and $\mathbf{u}_r$ is assumed to be constant. In this section, we propose a practical coding/decoding scheme that exploits the source-relay correlation and source memory.

4.3.1 Coding Structure

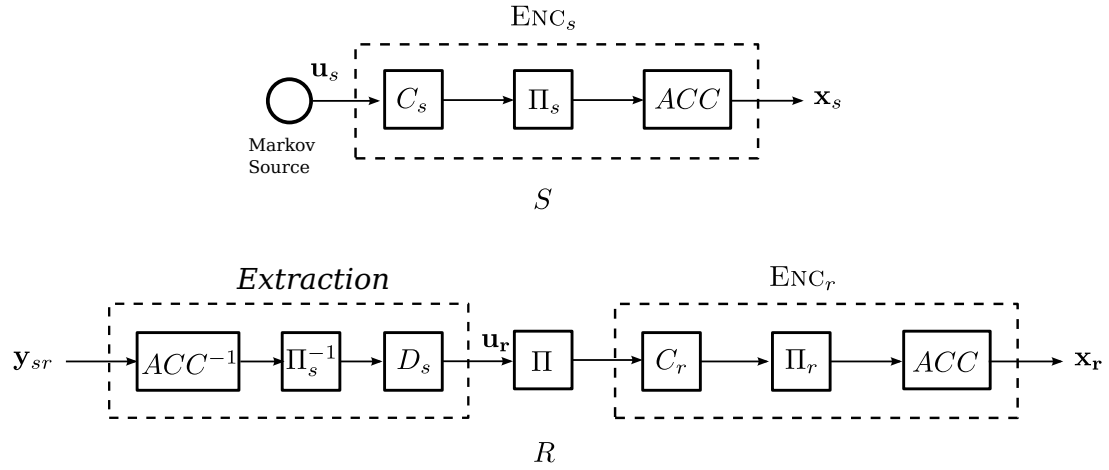

Figure 4.6: Code structure for source and relay.

The block diagrams of the proposed coding structure for the source and relay nodes are shown in Fig. 4.6. At the source node S, SCCC which consists of a RSC code C_s followed by a interleaver Π_s and a doped ACC with a doping rate Q_s are used for ENC_s.

At the relay node R, the decoding process is invoked only once (i.e., no iterative processing at the relay) to obtain $\mathbf{u}_r$, which is used for *extracting*. Errors may occur between $\mathbf{u_s}$ and $\mathbf{u_r}$, as shown in Fig. 4.7. Apparently, if iterative decoding is performed at the relay node, the error probability between $\mathbf{u}$ and $\mathbf{u}_r$ can be further reduced. However, by performing extracting at the relay node, relay complexity can be significantly reduced without causing any significant performance degradation by the proposed algorithm, as detailed in Subsection 4.3.2. ENC_r has the same coding structure with ENC_s, except that the doping rate for the ACC is Q_r.

4.3.2 Distributed Joint Source-Channel Decoding Strategy

The block diagram of the proposed DJSC decoder for one-way relay system exploiting the source-relay correlation and the source memory structure is illustrated in Fig. 4.8. The BCJR algorithm is used for MAP-decoding of CC and ACC. Here, D_s and D_r denotes the decoder of C_s and C_r, respectively. In order to exploit the knowledge of the memory

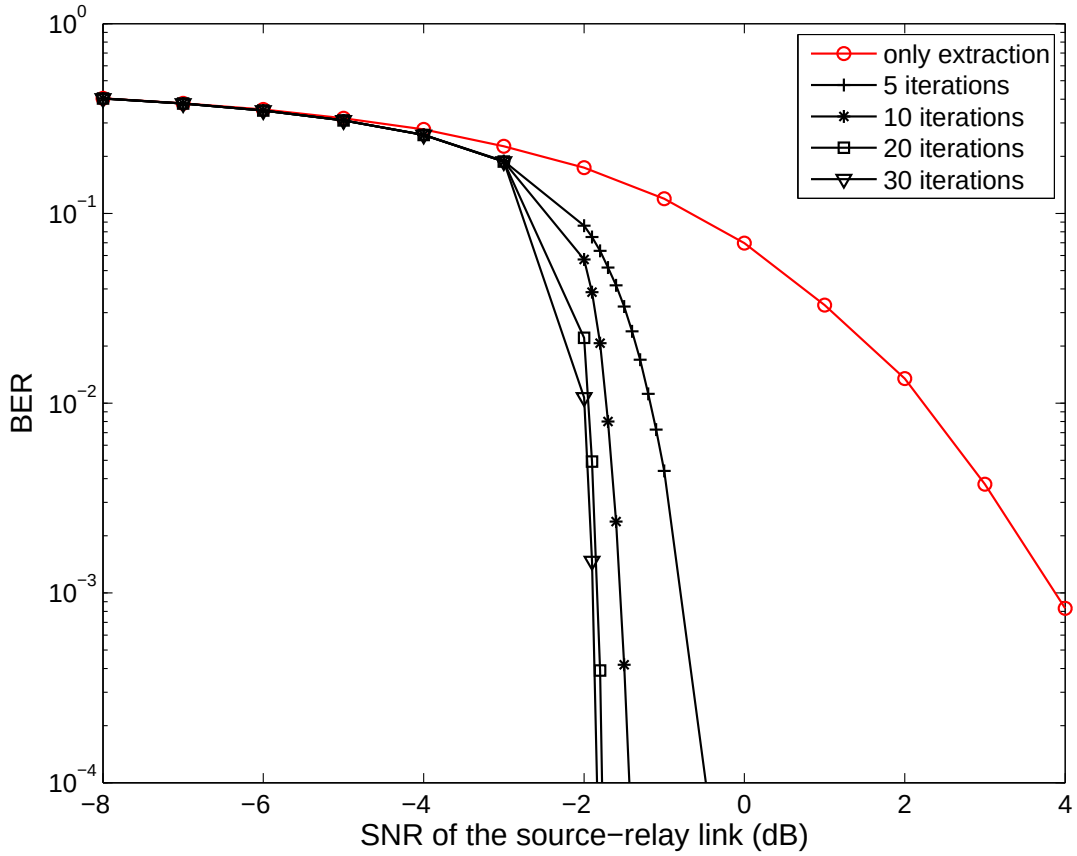

Figure 4.7: BER of the source-relay link over AWGN channel versus Γ_{sr}. The doping rate at the source node is $Q_s = 1$.

structure of the Markov source, the outer code C_s is combined with the Markov source and treated as a single constituent code, and the modified version of the BCJR algorithm proposed in **Chapter 3** is used to jointly perform source and channel decoding at D_s. However, D_r can not exploit the source memory due to the additional interleaver Π, as shown in Fig. 4.6.

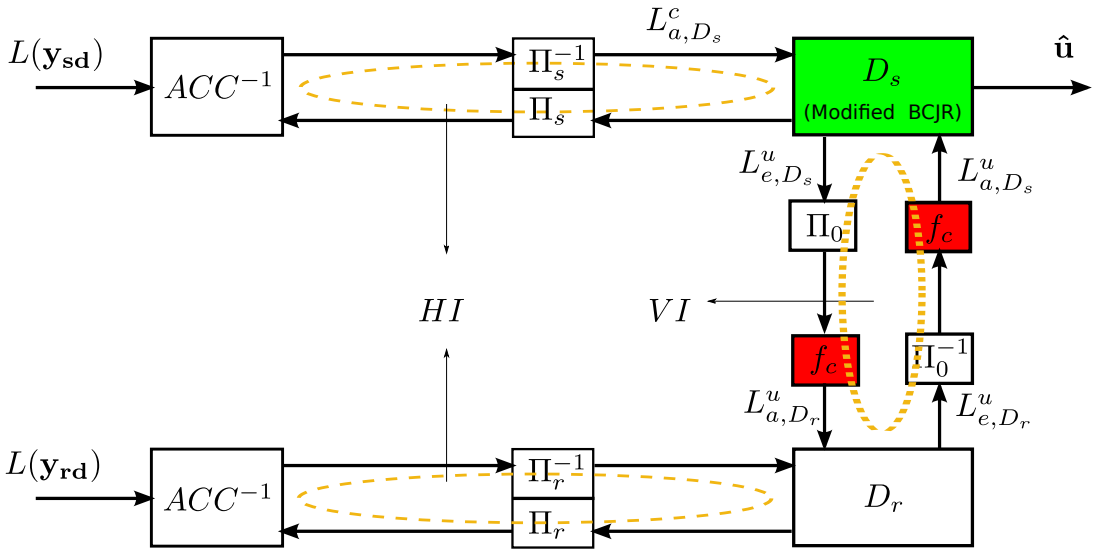

Figure 4.8: The proposed DJSC decoder for single relay system exploiting the source-relay correlation and the source memory structure. ACC^{-1} denotes the de-accumulator. D_s and D_r denotes the decoder of C_s and C_r, respectively.

At the destination node, the received signals from the source and the relay are first converted to LLR sequences $L(\mathbf{y}_{sd})$ and $L(\mathbf{y}_{rd})$, respectively, and then decoded via two horizontal iterations (HIs), as shown in Fig. 4.8. The extrinsic LLRs generated from D_s and D_r in the two HIs are further exchanged by several vertical iterations (VI) through a LLR updating function f_c, of which the role is detailed in the next subsection. This process is performed iteratively and after enough iterations, hard decision is made based on the *a posteriori* LLRs obtained from D_s.

LLR Updating Function

First of all, the value p_e (error probability occurring in the source-relay link L_{sr}) is estimated at the destination using the *a posteriori* LLRs of the uncoded bits, L^u_{p,D_s} and L^u_{p,D_r} from the decoders D_s and D_r, as

$$\hat{p_e} = \frac{1}{N}\sum_{n=1}^{N} \frac{\exp(L^u_{p,D_s}) + \exp(L^u_{p,D_r})}{[1+\exp(L^u_{p,D_s})]\cdot[1+\exp(L^u_{p,D_r})]}, \tag{4.29}$$

where N indicates the number of the *a posteriori* LLR pairs from the two decoders with sufficient reliability; only the LLRs with their absolute values larger than a given threshold T can be used for calculating $\hat{p_e}$ [88].

After obtaining the estimated error probability using (4.29), the probability of $\mathbf{u}_s$ can be updated from $\mathbf{u}_r$ as

$$\begin{cases} \Pr(u_{s,t}=0) &= (1-\hat{p_e})\cdot\Pr(u_{r,t}=0) + \hat{p_e}\cdot\Pr(u_{r,t}=1), \\ \Pr(u_{s,t}=1) &= (1-\hat{p_e})\cdot\Pr(u_{r,t}=1) + \hat{p_e}\cdot\Pr(u_{r,t}=0), \end{cases} \tag{4.30}$$

where $u_{s,t}$ and $u_{r,t}$ denote the t-th elements of $\mathbf{u}_s$ and $\mathbf{u}_r$, respectively. This leads to the LLR updating function [88] for $\mathbf{u}_s$:

$$L(u_{s,t}) = \ln \frac{\Pr(u_{s,t}=0)}{\Pr(u_{s,t}=1)} = \ln \frac{(1-\hat{p_e}) \cdot \exp[L(u_{r,t})] + \hat{p_e}}{(1-\hat{p_e}) + \hat{p_e} \cdot \exp[L(u_{r,t})]}. \tag{4.31}$$

Similarly, the LLR updating function for $\mathbf{u}_r$ can be expressed as:

$$L(u_{r,t}) = \ln \frac{\Pr(u_{r,t}=0)}{\Pr(u_{r,t}=1)} = \ln \frac{(1-\hat{p_e}) \cdot \exp[L(u_{s,t})] + \hat{p_e}}{(1-\hat{p_e}) + \hat{p_e} \cdot \exp[L(u_{s,t})]}. \tag{4.32}$$

In summary, the general form of the LLR updating function f_c, as shown in Fig. 4.8, is given as

$$f_c(x, \hat{p_e}) = \ln \frac{(1-\hat{p_e}) \cdot \exp(x) + \hat{p_e}}{(1-\hat{p_e}) + \hat{p_e} \cdot \exp(x)}, \tag{4.33}$$

where x denotes the input LLRs. The output of f_c is the updated LLRs by exploiting $\hat{p_e}$ as the source-relay correlation. The *VI* operations of the proposed decoder can be expressed as

$$\mathbf{L}^u_{a,D_s} = f_c[\Pi^{-1}(\mathbf{L}^u_{e,D_r}), \hat{p_e}], \tag{4.34}$$

$$\mathbf{L}^u_{a,D_r} = f_c[\Pi(\mathbf{L}^u_{e,D_s}), \hat{p_e}], \tag{4.35}$$

where $\Pi(\cdot)$ and $\Pi^{-1}(\cdot)$ denote interleaving and de-interleaving functions corresponding to Π, respectively. $\mathbf{L}^u_{a,D_s}$ and $\mathbf{L}^u_{e,D_s}$ denote the *a priori* LLRs fed into, and extrinsic LLRs generated by D_s, respectively, both for the uncoded bits. Similar definitions apply to $\mathbf{L}^u_{a,D_r}$ and $\mathbf{L}^u_{e,D_r}$ for D_r.

4.4 3D EXIT Chart Analysis

In this section, we present results of three-dimensional (3D) EXIT chart [120, 121, 131] analysis conducted to identify the impact of the memory structure of the Markov source and the source-relay correlation on the joint decoder. The analysis focuses on the decoder D_s since the main aim is to successfully retrieve the information estimates $\hat{\mathbf{u}}_s$. As shown in Fig. 4.8, the decoder D_s exploits two *a priori* LLRs: $\mathbf{L}^c_{a,D_s}$ and the updated version of $\mathbf{L}^u_{e,D_r}$, $\mathbf{L}^u_{a,D_s}$. Therefore, the EXIT function of D_s can be characterized as

$$I^c_{e,D_s} = T^c_{D_s}(I^c_{a,D_s}, I^u_{e,D_r}, p_e), \tag{4.36}$$

where I^c_{e,D_s} denotes the mutual information between the extrinsic LLRs, L^c_{e,D_s} generated from D_s, and the coded bits of D_s. I^c_{e,D_s} can be obtained by the histogram measurement [121]. Similar definitions can be applied to I^c_{a,D_s} and I^u_{e,D_r}.

First of all, we assume that the source-relay correlation is not exploited and only focus on the exploitation of source memory. In this case, $I^u_{e,D_r} = 0$ and the EXIT analysis of D_s can be simplified to two-dimensional. The EXIT curves with the standard and modified BCJR algorithms are illustrated in Fig. 4.9. The code used in the analysis is a half rate memory-1 RSC with the generator polynomials $(G_r, G) = (3, 2)_8$. It can be observed from Fig. 4.9 that, compared to the standard BCJR algorithm, the EXIT curves obtained by using the modified BCJR algorithm are lifted up over the entire a

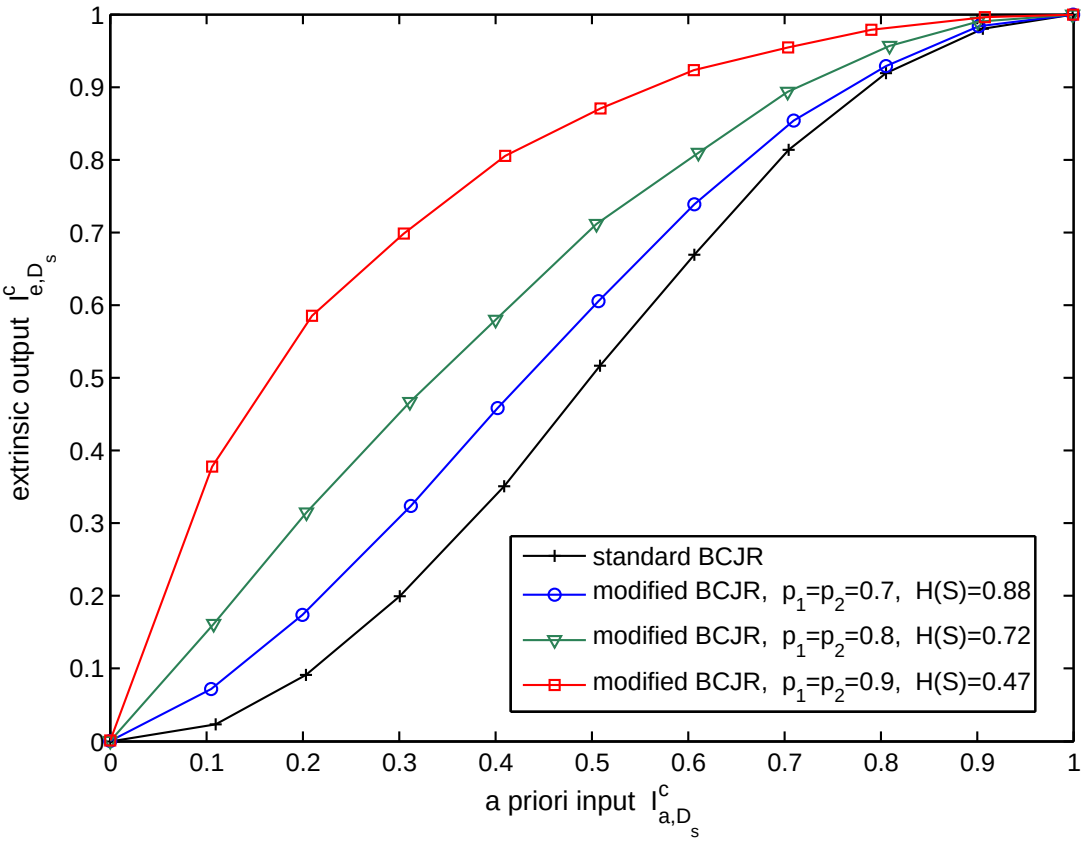

Figure 4.9: Extrinsic information transfer characteristic of D_s, with standard BCJR and with modified BCJR. The source-relay correlation is not considered. Generator polynomials of C_s is $(G_r, G) = (3, 2)_8$.

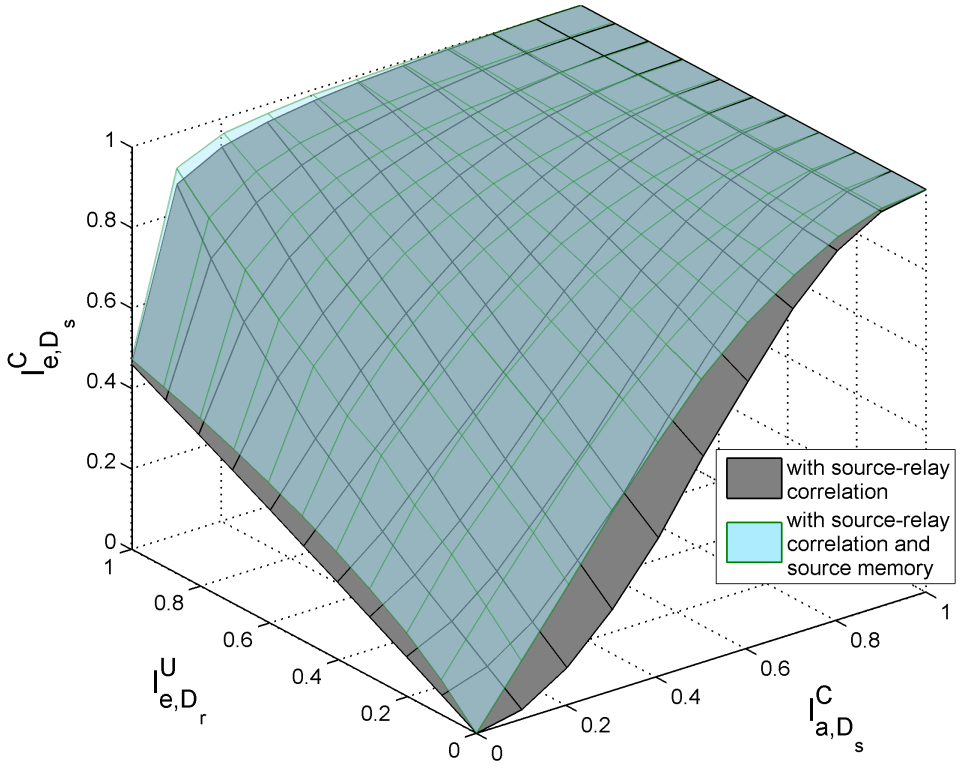

(a) $p_e = 0.01$

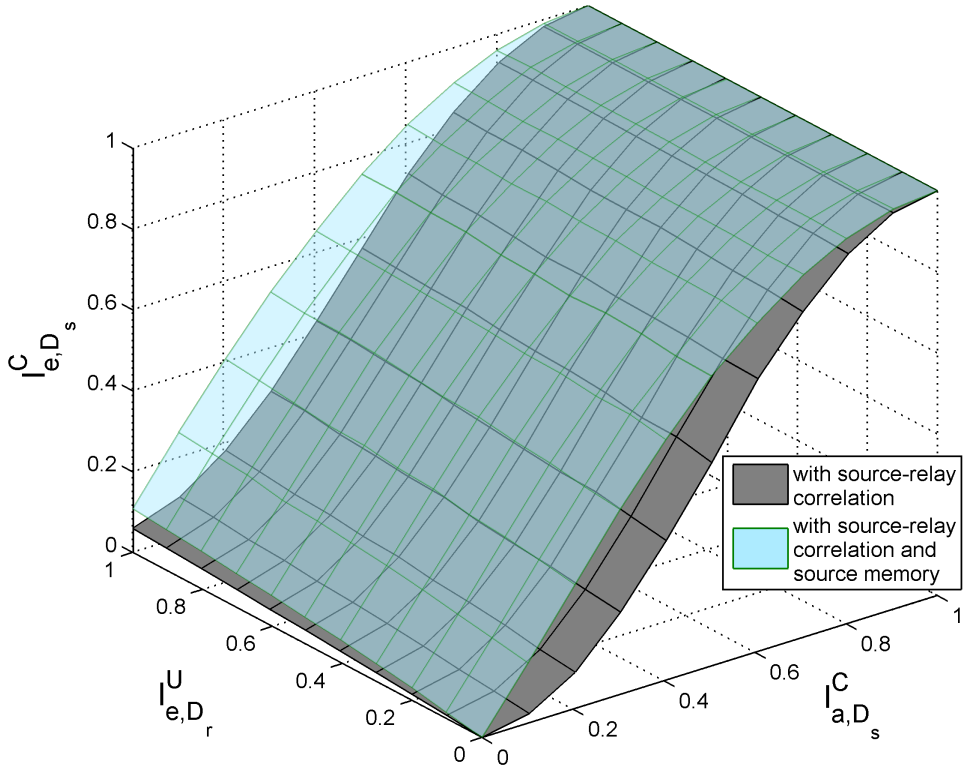

(b) $p_e = 0.3$

Figure 4.10: The EXIT planes of decoder D_s with different p_e values. For Markov source, $p_1 = p_2 = 0.8$, $H(S) = 0.72$.

priori input region, indicating that larger extrinsic mutual information can be obtained. It is also worth noticing that the contribution of the source memory represented by the increase in extrinsic mutual information becomes larger as the entropy of Markov source decreases.

Next we conduct 3D EXIT chart analysis for D_s to evaluate the impact of the source-relay correlation, where the source memory is not exploited. The corresponding EXIT planes of D_s, shown in gray, are illustrated in Fig. 4.10. Two different scenarios, a relatively strong source-relay correlation (corresponding to small p_e value) and a relatively weak source-relay correlation (corresponding to large p_e value) are considered. It can be seen from Fig. 4.10(a) that with a strong source-relay correlation, the extrinsic information I^u_{e,D_r} provided by D_r, has a significant effect on $T^c_{D_s}(\cdot)$. On the contrary, when the source-relay correlation is weak, I^u_{e,D_r} has a negligible influence on $T^c_{D_s}(\cdot)$, as shown in Fig. 4.10(b).

For the proposed DJSC decoding scheme, both the source memory (temporal) and the source-relay (spatial) correlations are exploited in the iterative decoding process. The impact of the source memory and the source-relay correlations on D_s, represented by the 3D EXIT planes, shown in light-blue, is presented in Fig. 4.10. We can observe that higher extrinsic mutual information can be achieved (EXIT planes are lifted up) by exploiting the source memory and the source-relay correlations simultaneously, which will help decoder D_s to perfectly retrieve the source information sequence even at a low SNR scenario.

It can be seen from Fig. 4.10 that the EXIT planes of D_s changes with the value of p_e. Moreover, as shown in Fig. 4.8, there are two HIs and one VI in our proposed DJSC decoding technique. Hence, code optimization which involves the optimization of these iteration loops is a challenging topic. In this section, the EXIT chart analysis is only used to demonstrate the convergence behavior of the proposed DJSC technique, and code optimization based on EXIT chart analysis is out of the scope of this section. Instead, the practical code parameters used for simulations are empirically chosen.

4.5 Numerical Results

In this section, we present the results of simulations conducted to evaluate the convergence property, the BER performance in AWGN channels and the FER performance in block Rayleigh fading channels of the proposed DJSC technique. The encoder used at the source and relay nodes, C_s and C_r, respectively, are both memory-1 half rate RSC with generator polynomials $(G_r, G) = (3, 2)_8$. Five VIs took place after every HI, with the aim of exchanging extrinsic information to exploit the source-relay correlation. The whole process was repeated 50 times. All the three relay location scenarios were evaluated, with respect to the SNR of the source-destination link. The doping rates were set at $Q_s = Q_r = 2$ for location A, while $Q_s = 1,\ Q_r = 16$ for both the location B and C.

4.5.1 Convergence Behavior

The convergence behavior with the proposed DJSC decoder at the relay location A with $\Gamma_{sd} = -3.5$ dB is illustrated in Fig. 4.11. As described in Subsection 4.3.2, the decoding algorithms for D_s and D_r are not the same, and thus the upper and lower HIs are evaluated separately. It can be observed from Fig. 4.11(b) that the EXIT planes of D_r and ACC decoder finally intersect with each other at about $I^c_{e,D_r} = 0.52$, which corresponds to $I^u_{e,D_r} = 0.59$. This observation indicates that D_r can provide D_s with $I^u_{e,D_r} = 0.59$

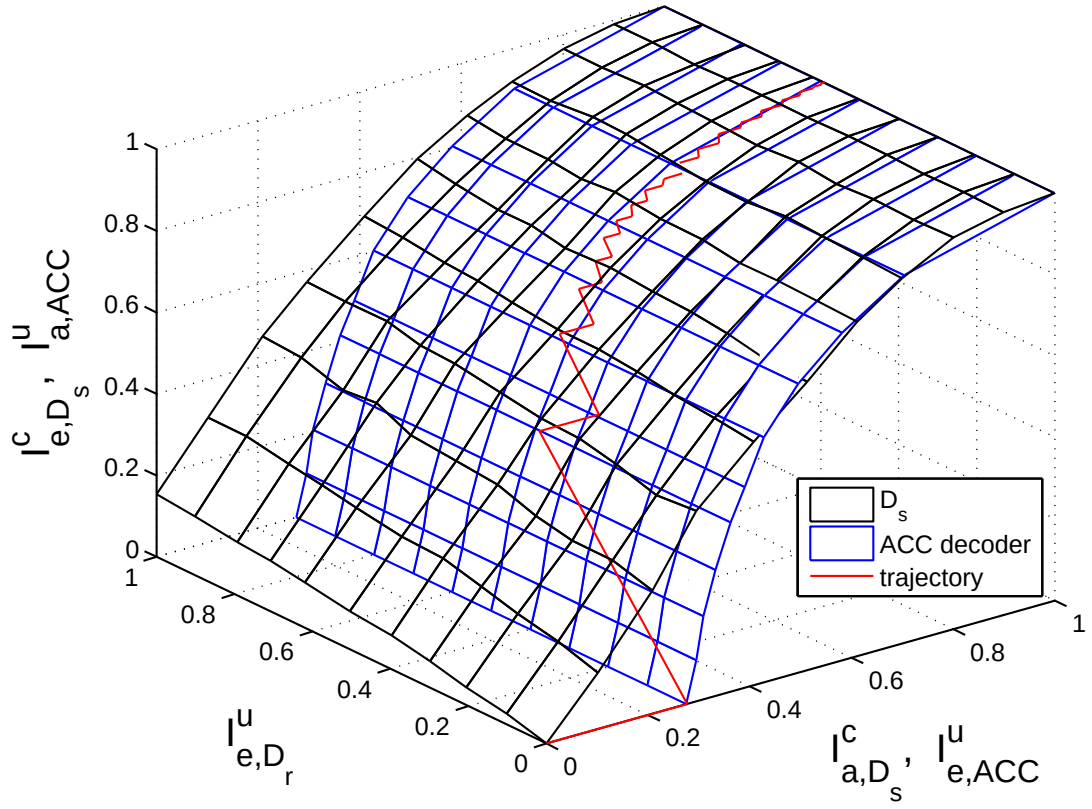

(a) Upper *HI* with f_c function

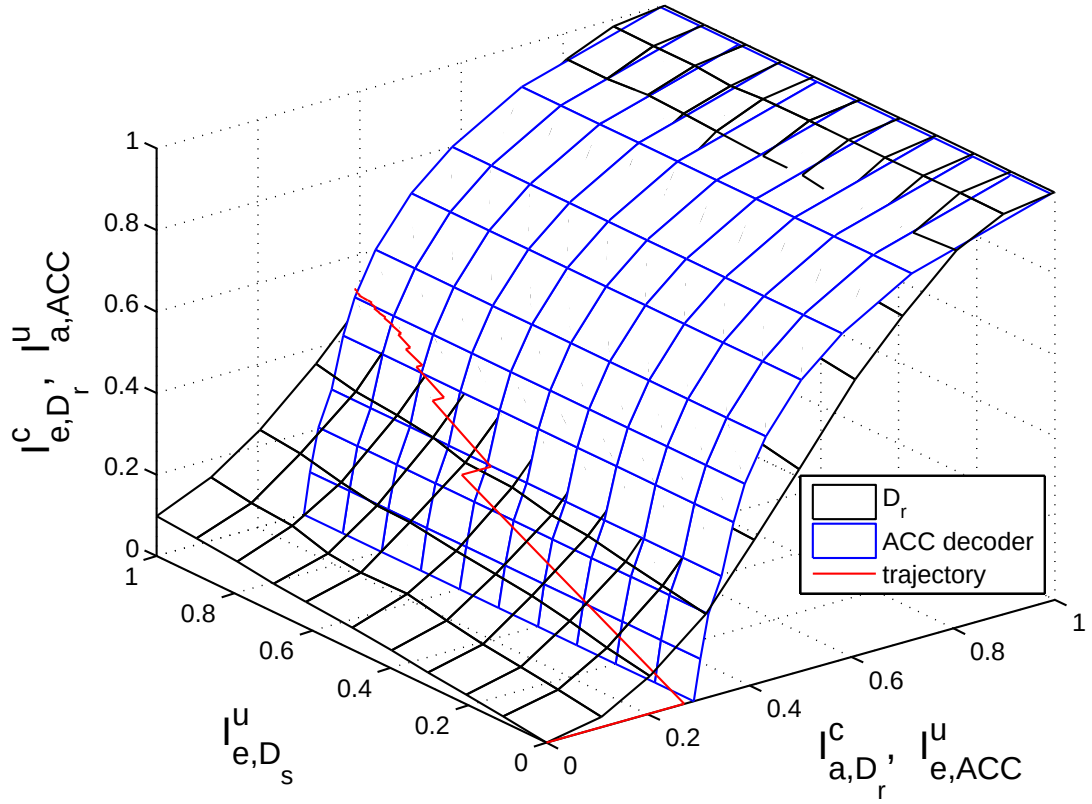

(b) Lower *HI* with f_c function

Figure 4.11: The 3D EXIT chart analysis for the proposed DJSC decoder in relay location A, $\Gamma_{sd} = -3.5$ dB.

a priori mutual information via the *VI*. Fig. 4.11(a) shows that when $I^u_{e,D_r} = 0$, the convergence tunnel is closed, but it is slightly open at $I^u_{e,D_r} = 0.59$. Therefore, through extrinsic information exchange between D_s and D_r, the trajectory of the upper *HI* can sneak through the convergence tunnel and finally reach the convergence point while the trajectory of the lower *HI* gets stuck. It should be noted here that since $\hat{p_e}$ is estimated and updated during every iteration, the trajectory of the upper *HI* does not match exactly with the EXIT planes of D_s and the ACC decoder, especially at the first several iterations. Similar phenomena is observed for the trajectory of the lower *HI*.

4.5.2 Contribution of the Source-Relay Correlation

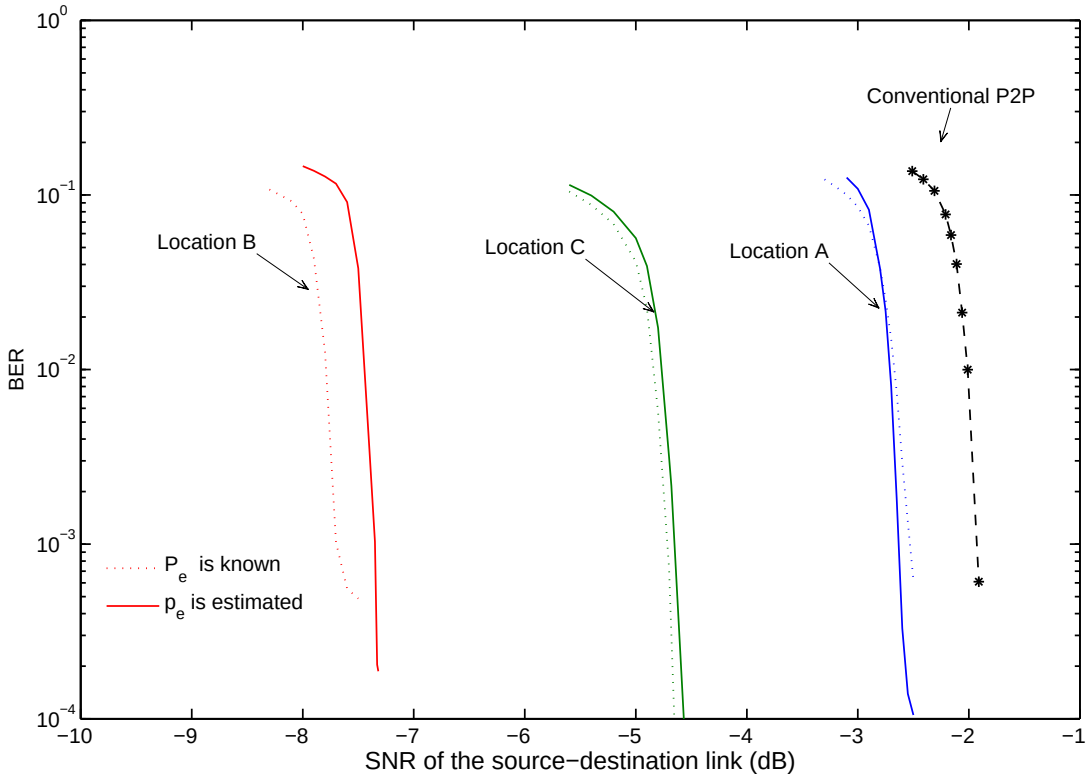

Figure 4.12: The BER performance of the proposed DJSC decoder for relay systems versus Γ_{sd} in AWGN channels. Three different relay location scenarios are considered. The memory structure of Markov source is not considered.

The performance gains obtained by exploiting only the source-relay correlations largely rely on the quality of the source-relay link (which can be characterized by p_e), as described in the previous subsection. Fig. 4.12 shows the BER performance of the proposed technique when p_e is known and unknown at the decoder, while the memory structure of Markov source is not taken into account. The threshold T on LLRs for estimating $\hat{p_e}$ [88] is set at 1. It can be observed that for relay locations A and C, the BER performance of the proposed decoder is almost the same whether p_e is known or unknown at the decoder. However, for relay location B, convergence threshold is -7.7 dB and -7.4 dB when p_e is known and unknown at the decoder, respectively, which results in a performance degradation of 0.3 dB. It can also be seen from Fig. 4.12 that, the performance gains obtained

by exploiting only source-relay correlation (p_e is assumed to be unknown at the decoder) for the locations A, B and C, over the conventional P2P communication system where *relaying is not involved*, are 0.6 dB, 5.4 dB and 2.6 dB, respectively. Among these three different relay location scenarios, it is found that the quality of the source-relay link with the location A is the worst and that with the location B is the best, if Γ_{sd} is the same. This is consistent with the simulation results.

4.5.3 BER Performance in AWGN channels

In this subsection, we evaluate the BER performance of the proposed DJSC technique. The information sequences are generated from Markov sources with different state transition probabilities. The block length is 10000 bits, and 1000 different blocks were transmitted for the sake of keeping reasonable accuracy. The threshold for estimating $\hat{p_e}$ [88] is set at $T = 1$.

In the theoretical analysis, we assumed P_e is constant. However, in the BER simulations, p_e is determined by both the quality of L_{sr} (the value of Γ_{sr}) and the *extracting method* used at R. According to Subsection 4.3.1, p_e varies with Γ_{sr}. Therefore, deriving the exact limits of the proposed system may not be possible. Instead, lower bound of the limits can be obtained by assuming $p_e = 0$. In this case, the achievable rate region in (4.15) becomes

$$\begin{cases} R_s & \geq & 0, \\ R_r & \geq & 0, \\ R_s + R_r & \geq & H^M(p_1, p_2). \end{cases} \tag{4.37}$$

By combining (4.16) and (4.37), we can obtain the lower bound of the limits, which are shown in Table 4.1. It should be mentioned that in the three relay locations considered, $p_e \neq 0$. Especially, in relay location C, the quality of L_{sr} is the worst where $p_e \gg 0$, and therefore big gaps between the lower bound of the limits and the corresponding BER performance are expected.

Table 4.1: Lower bound of the performance limits of the proposed technique in AWGN channels.

Markov Source Parameters			Relay locations		
p_1	p_2	$H(S)$	A (dB)	B (dB)	C (dB)
0.5	0.5	1	-6.84	-9.43	-24.27
0.7	0.7	0.88	-7.48	-10.08	-25.01
0.8	0.8	0.72	-8.47	-11.1	-26.13
0.9	0.9	0.47	-10.54	-13.2	-28.4

The proposed DJSC technique exploits both source-relay correlation and the memory structure of Markov source simultaneously during the iterative decoding process, thus more performance gains should be achieved. The BER performance of the proposed DJSC technique for relay location A is shown in Fig. 4.13. As a reference, the BER curve of the technique that only exploit the source-relay correlation is also provided, which is labeled as "w/o Markov source". It can be observed that by exploiting the memory structure of Markov source, the proposed DJSC technique can achieve 0.3 dB, 1.2 dB and 2.2 dB performance gains over "w/o Markov source" for $p_1 = p_2 = 0.7, 0.8$ and 0.9, respectively.

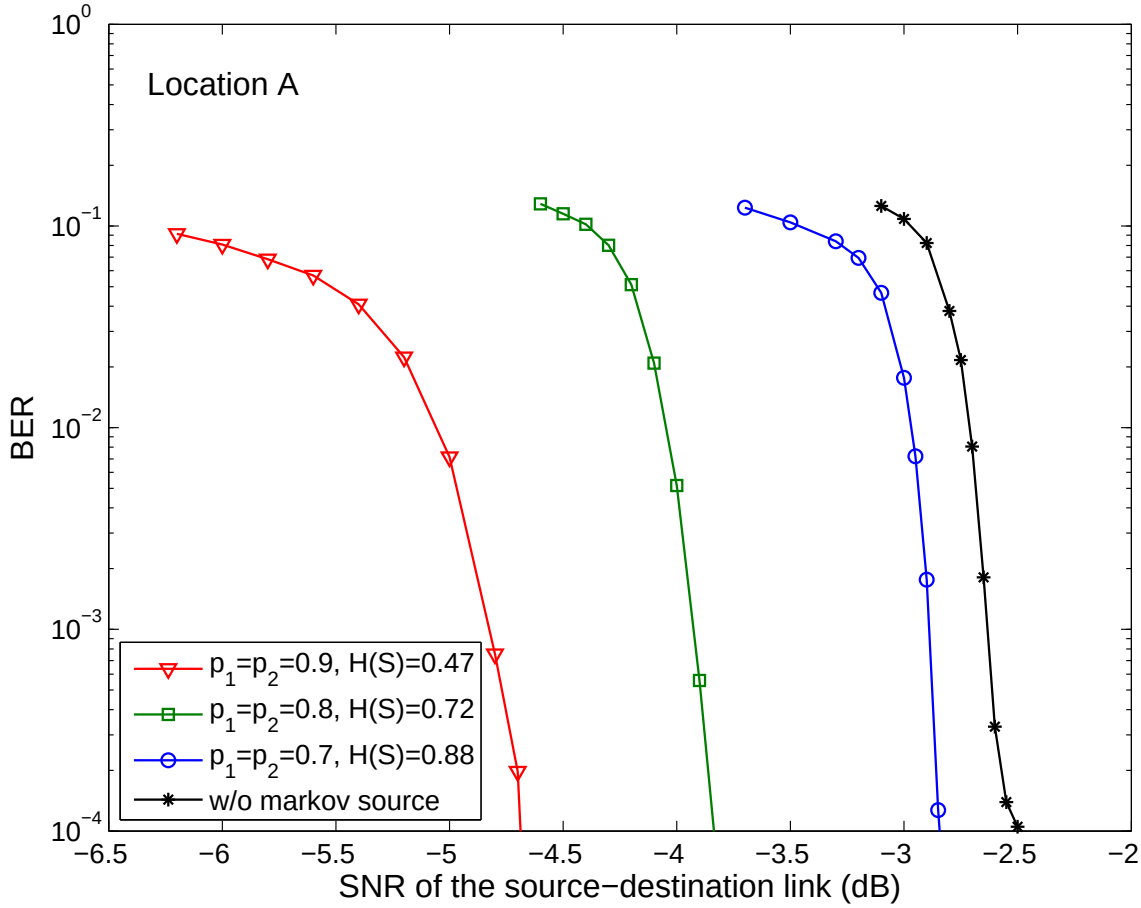

Figure 4.13: The BER performance of the proposed DJSC decoder for relay location A versus Γ_{sd} in AWGN channels. Three different Markov sources are considered.

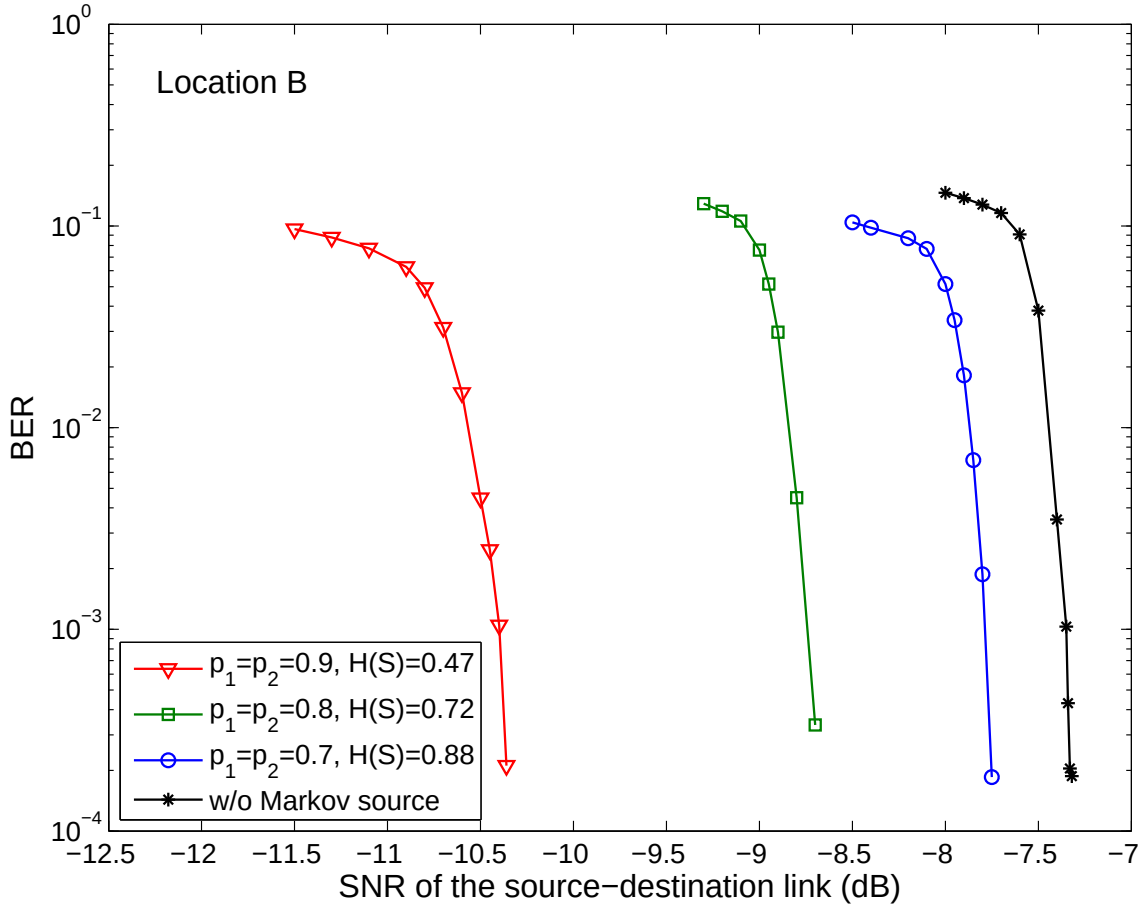

Figure 4.14: The BER performance of the proposed DJSC decoder for relay location B versus Γ_{sd} in AWGN channels. Three different Markov sources are considered.

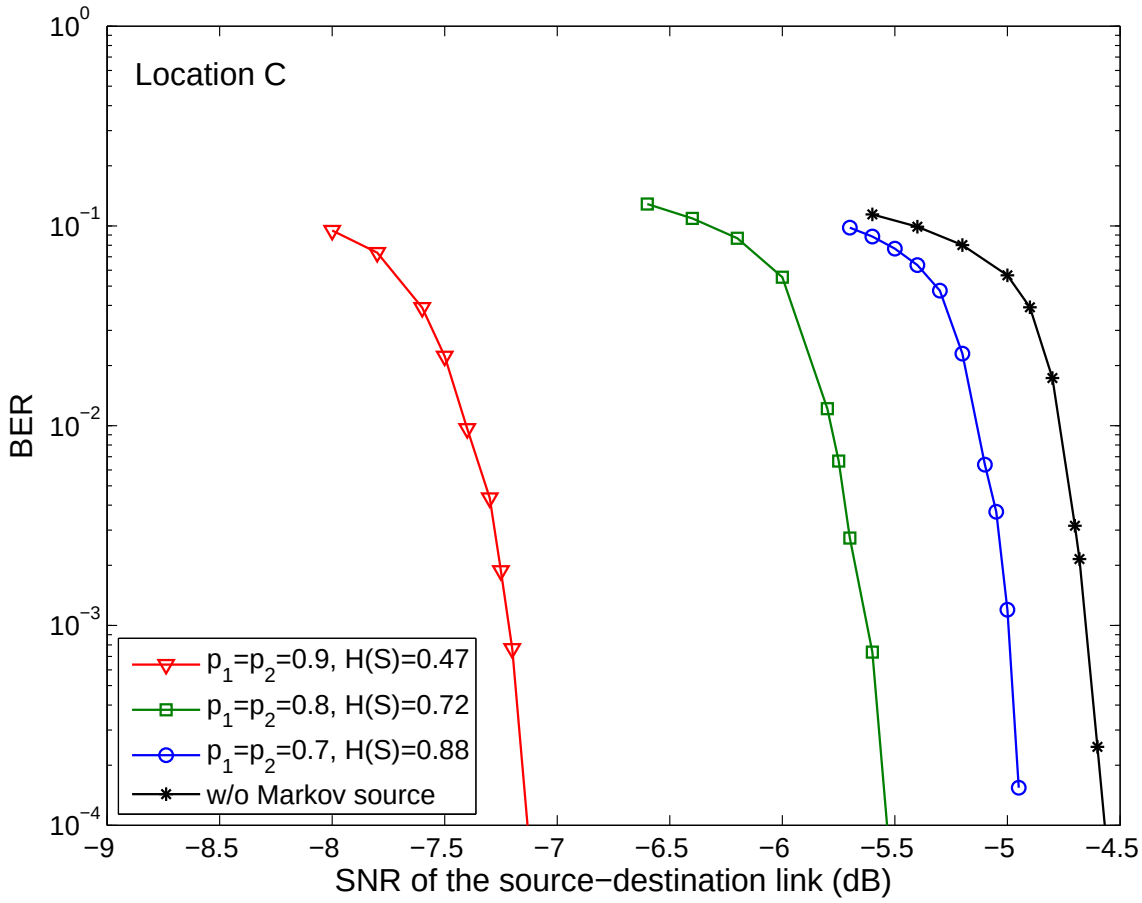

Figure 4.15: The BER performance of the proposed DJSC decoder for relay location C versus Γ_{sd} in AWGN channels. Three different Markov sources are considered.

The BER performance of the proposed DJSC technique for the relay locations B and C are presented in Figs. 4.14 and 4.15, respectively. The performance gains achieved by the proposed DJSC technique are summarized in Table. 4.2. It is found that by exploiting the memory structure of Markov source, considerable gains can also be achieved for the relay locations B and C.

Table 4.2: BER performance gains (dB) of the proposed DJSC technique over the technique that only exploits source-relay correlation.

Markov Source Parameters			Relay locations		
p_1	p_2	$H(S)$	A	B	C
0.7	0.7	0.88	0.3 dB	0.45 dB	0.45 dB
0.8	0.8	0.72	1.2 dB	1.4 dB	0.9 dB
0.9	0.9	0.47	2.2 dB	3.05 dB	2.6 dB

4.5.4 Application to Image Transmission

The proposed technique was applied to image transmission to verify the effectiveness of the proposed DJSC technique. The results with the conventional P2P, the proposed DJSC technique that only exploits source-relay correlation (DJSC/SR) and that only exploits the source memory (DJSC/SM) are also provided for comparison. Two cases were tested: (A) binary (black and white) image and (B) Grayscale image with 8-digits pixel representations. In (A), each pixel of the image has only two possible values (0 or 1). Binary images are widely used in simple devices, such as laser printers, fax machines, and bilevel computer displays. It is quite straightforward that the binary image can be modeled as Markov source. For a binary image with 256×256 pixels, shown in Fig. 4.16(a) as an example, the average state transition probabilities are found to be $p_1 = 0.9538$ and $p_2 = 0.9480$ through measurement. The image data is encoded column-by-column. Figs. 4.16(b-e) show the estimates of the image obtained as the result of decoding at $\Gamma_{sd} = -10$ dB with the conventional P2P technique, DJSC/SR, DJSC/SM and DJSC, respectively. As can be seen from Fig. 4.16, with the conventional P2P transmission, the estimated image quality is the worst containing 43.8% pixel errors (see the figure caption), since neither source-relay correlation nor source memory is exploited. With DJSC/SR and DJSC/SM, the estimated images contain 19.4% and 8.1% pixel errors, respectively. The proposed DJSC that exploits both source-relay correlation and source memory achieves perfect recovery of the image, with 0% pixel error.

Grayscale images are widely used in some special applications, such as medical imaging, remote sensing and video monitoring. An example of a grayscale image with 256×256 pixels is shown in Fig. 4.17(a), which is used in the simulation for (B). There are 8 bit planes in this image: the first bit plane contains the set of the most significant bits of each pixel, and the $8th$ contains the least significant bits, where each bit plane is a binary image. The image data is encoded plane-by-plane and column-by-column within each plane, therefore the grayscale image can also be modeled as Markov source. The average state transition probabilities are found to be $p_1 = 0.7167$ and $p_2 = 0.6741$ through measurement. Figs. 4.17(b-e) show the estimates of the image, obtained as the result of decoding, at $\Gamma_{sd} = -7.5$ dB with the conventional P2P, DJSC/SR, DJSC/SM and DJSC, respectively. It can be observed that the performance with DJSC/SR (50.27% pixel errors) and

(a)

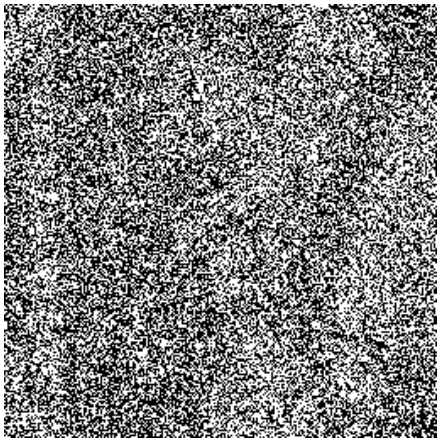

(b)

(c)

(d)

(e)

Figure 4.16: Image transmission for a binary image with $p_1 = 0.9538$ and $p_2 = 0.9480$ at $\Gamma_{sd} = -10$ dB, the relay location is B, (a) original transmitted image, (b) conventional P2P (43.8% pixel errors), (c) DJSC/SR (19.4% pixel errors), (d) DJSC/SM (8.1% pixel errors), (e) DJSC (0% pixel errors).

(a)

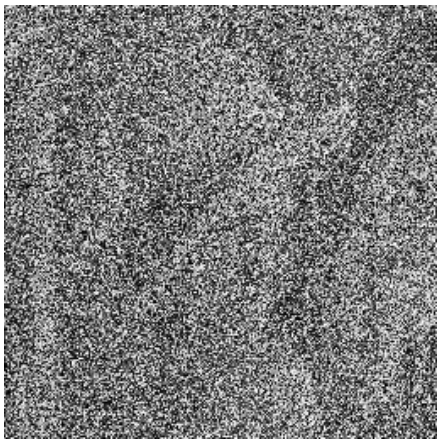

(b)

(c)

(d)

(e)

Figure 4.17: Image transmission for a gray image with $p_1 = 0.7167$ and $p_2 = 0.6741$ at $\Gamma_{sd} = -7.5$ dB, the relay location is B, (a) original transmitted image, (b) conventional P2P (98.1% pixel errors), (c) DJSC/SR (50.27% pixel errors), (d) DJSC/SM (96.9% pixel errors), (e) DJSC (0% pixel errors).

DJSC/SM (96.9% pixel errors) are much better than that with conventional P2P (98.1% pixel errors). However, by exploiting the source-relay correlation and the source memory simultaneously, the proposed DJSC achieves perfect recovery of the image, with 0% pixel error.

4.5.5 FER Performance in Rayleigh Fading Channels

The numerical results of the theoretical outage probability calculation and the FER performance of the proposed DJSC technique for relay locations A, B and C are shown in Fig. 4.18, 4.19 and 4.20, respectively. The frame length is set at 2000 bits, and in total $100,000$ different frames were transmitted from the source node to the destination node over block Rayleigh fading channels. The theoretical outage curve of P2P transmission is also provided in these figures for comparison. It should be emphasized here that the theoretical outage curves for the proposed DJSC technique is obtained by assuming $p_e = 0$, due to the reason presented in Subsection 4.5.3, and therefore, they are lower bound of the outage probability, while in simulations, links L_{sr}, L_{sd} and L_{rd} all suffer from Rayleigh fading. Moreover, instead of using static threshold for $\hat{p_e}$ estimation, we use an adaptive threshold algorithm proposed in [132] to improve the accuracy of estimation and hence the FER performance in block Rayleigh fading channels.

It is found from these figures that, the theoretical outage probability decreases as the time-domain correlation of the Markov source becomes stronger for all the three relay location scenarios, since the memory structure of the Markov source can be exploited at the destination node. Compared with P2P transmission, $2nd$ order diversity can be observed in the theoretical outage curves, because the source-relay correlation is exploited at the destination node with the assumption $p_e = 0$. However, the theoretical outage curves with different Markov sources are parallel to each other, which indicates that no diversity gain can be achieve by exploiting the memory structure of the Markov sources (the improvement is only a parallel shift of the outage curve). The FER curves exhibits the same tendency as their corresponding theoretical outage curves, however, there are still large gaps between them because the theoretical outage curves are just lower bound obtained by assuming $p_e = 0$. In all the three relay location scenarios, the gaps between FER curves and their corresponding theoretical outage curves in location C are the largest, which is because of the same reason that described in Subsection 4.5.3.

4.6 Summary

In this chapter, we have investigated the problem of transmitting binary Markov source in a one-way relay system, where the ErF relay strategy is adopted. The relay does not aim to completely eliminate the errors in the source-relay link. Instead, the relay only extracts and forwards the source information sequence to the destination, even though the extracted information sequence may contain some errors. The error probability of the source-relay link is regarded as source-relay correlation. We aim at exploiting the source-relay correlation and the memory structure of Markov source at the destination node.

In the theoretical analyses, the achievable compression rate region of the system was first determined, according to the Slepian-Wolf theorem, by assuming the source-relay correlation is constant. Lower bound of the performance limits in AWGN channels and the

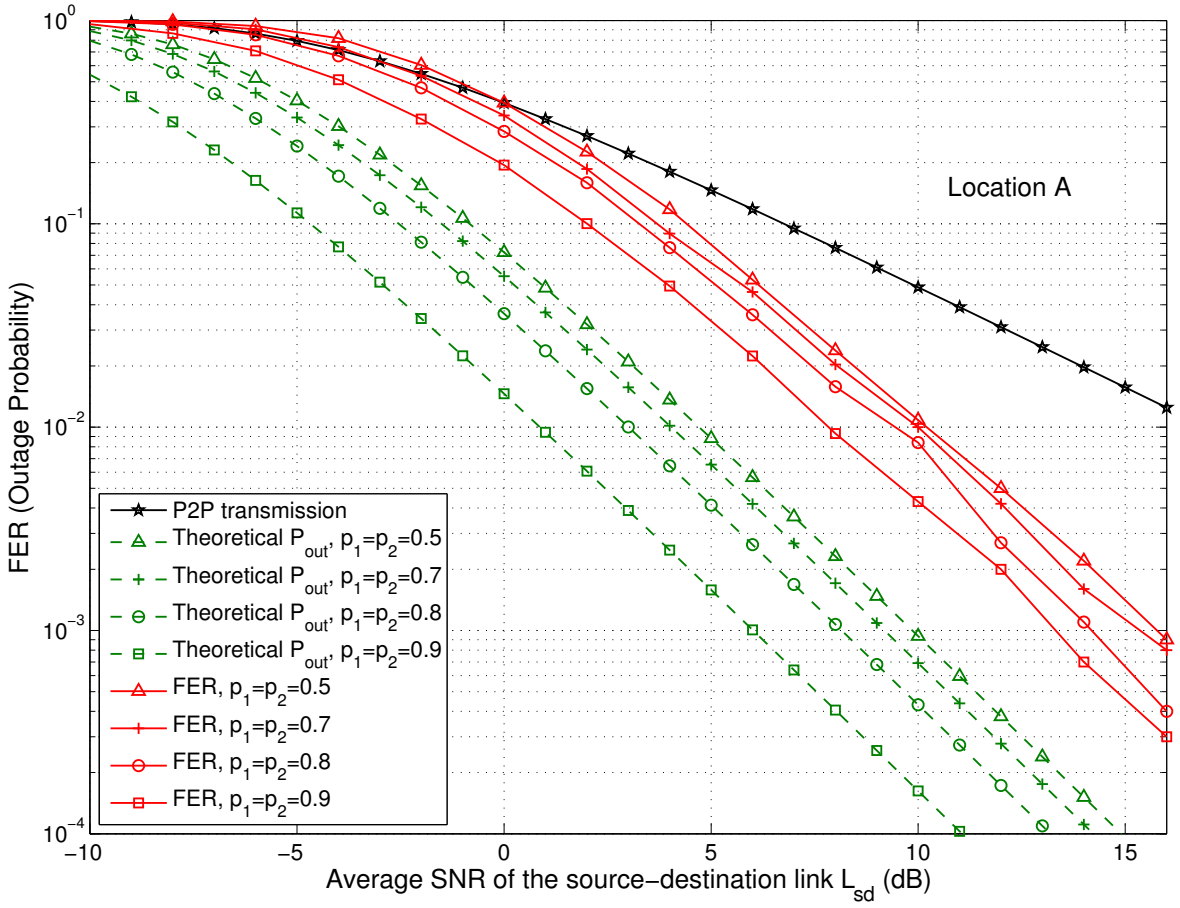

Figure 4.18: FER performance of the proposed DJSC technique for relay location A, with respect to Γ_{sd}, where all the links suffer form Rayleigh fading. Three different Markov sources are considered. Dotted lines are lower bounds of outage probability, which are obtained by assuming $p_e = 0$.

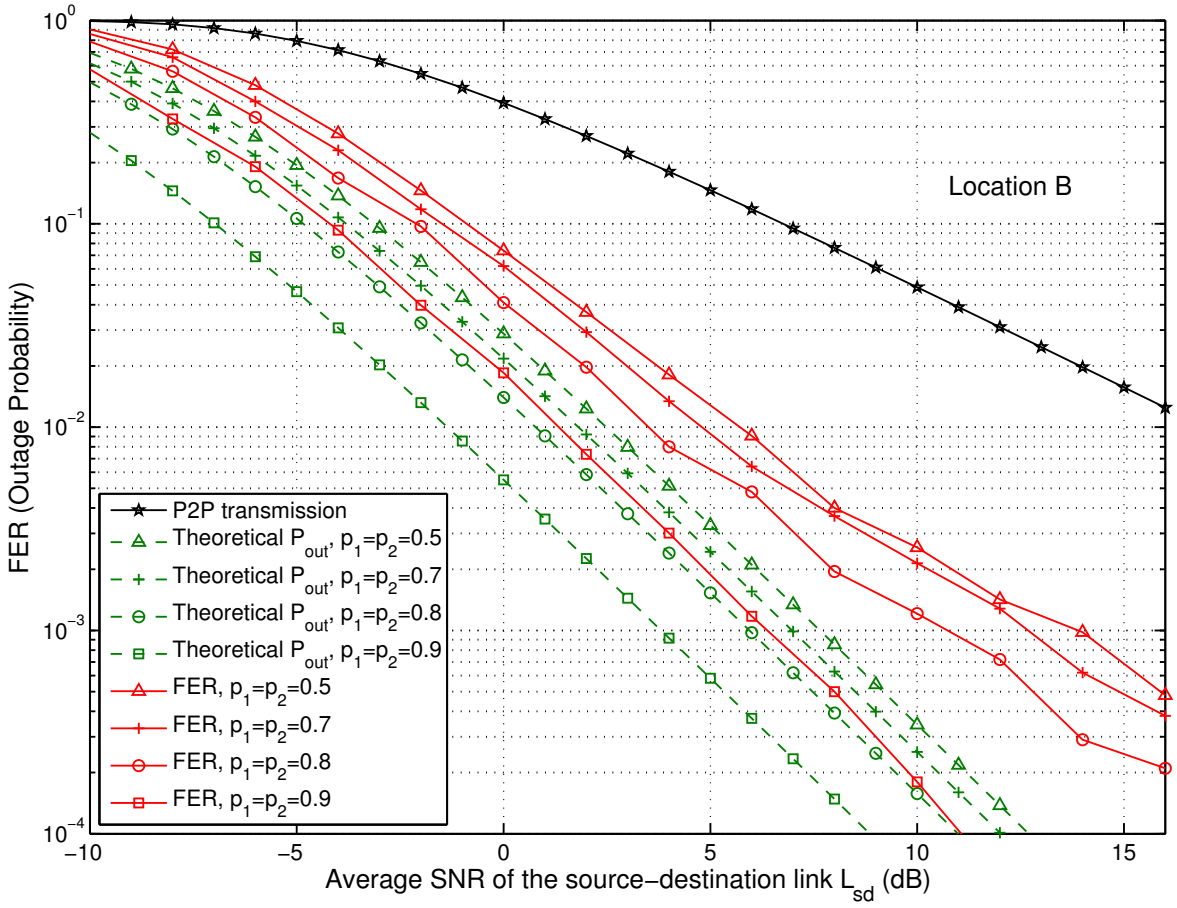

Figure 4.19: FER performance of the proposed DJSC technique for relay location B, with respect to Γ_{sd}, where all the links suffer form Rayleigh fading. Three different Markov sources are considered. Dotted lines are lower bounds of outage probability, which are obtained by assuming $p_e = 0$.

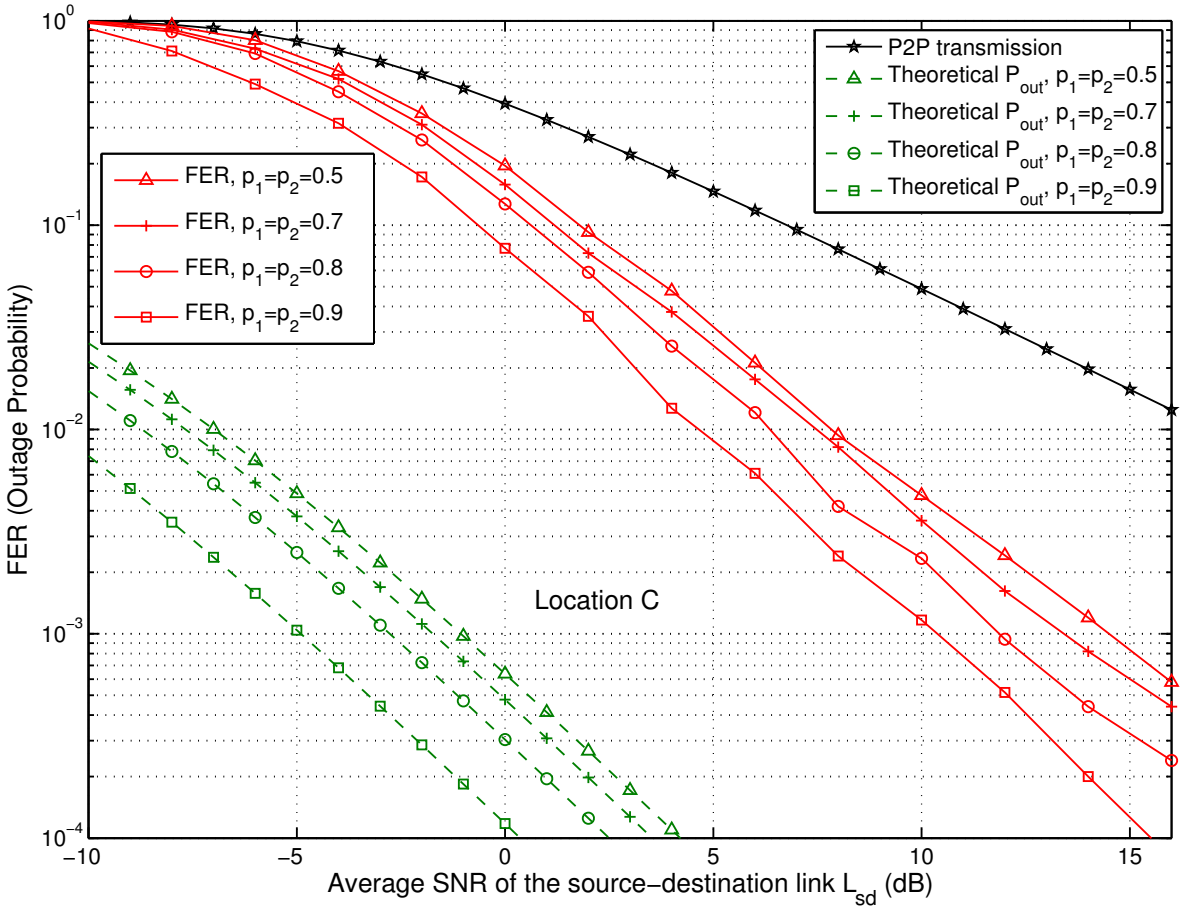

Figure 4.20: FER performance of the proposed DJSC technique for relay location C, with respect to Γ_{sd}, where all the links suffer form Rayleigh fading. Three different Markov sources are considered. Dotted lines are lower bounds of outage probability, which are obtained by assuming $p_e = 0$.

outage probability in Rayleigh fading channels were then derived based on the achievable compression rate region. The most important finding of asymptotic analysis is that with the help of memory structure of Markov source, the outage probability of the system will be reduced, but diversity order stays the same. Moreover, only if the information transmitted from the source and relay nodes are fully correlated, $2nd$ order diversity can be achieved. Otherwise, it converges to no diversity as the average SNR of the source-destination link increases.

We also proposed a new DJSC decoding scheme for the problem considered. In our proposed technique, the LLR updating function is adopted to estimate and exploit the source-relay correlation. Furthermore, the JSC technique proposed in **Chapter 3** is employed to exploit the memory structure of the Markov source. The convergence property of the proposed DJSC decoding technique was evaluated through 3D EXIT chart analysis.

A series of simulations was conducted to evaluate the effectiveness of the proposed DJSC decoding technique and the results obtained from the theoretical analyses. In the simulations, three different relay location scenarios were considered. In location A, the source and relay nodes keep the same distance to the destination node. In location B and C, the relay node is located closer to the source node and closer to the destination node, respectively. The BER and FER performance results showed that the proposed DJSC technique achieves considerable gains over the techniques that only exploit the source-relay correlation.

Chapter 5

Correlated Sources Transmission in Orthogonal Multiple Access Relay Channel

In this chapter, the problem of transmitting two correlated binary sources over orthogonal MARC, where two source nodes are communicating with a common destination node with the assistance of a single relay node, is investigated.

First of all, the system model assumed in this chapter is briefly introduced. The achievable compression rate region of this system is then derived based on the theorem for source coding with side information. The performance limits in AWGN channels and the outage probability in block Rayleigh fading channels are derived based on the achievable rate region. The impact of source correlation and the quality of the relay-destination link on the performance of the system is investigated through asymptotic analysis. Furthermore, we propose a practical coding/decoding scheme for the system considered, where a novel JSCN decoding technique is proposed to fully exploit the correlation between the sources, as well as the benefit of network coding. Finally, the effectiveness of the proposed JSCN decoding technique and the accuracy of the theoretical analysis are verified through a series of computer simulations.

5.1 System Model

The abstract model for two correlated sources transmission over MARC is shown in Fig. 5.1(a). The information sequence emitted from the two source nodes S_1 and S_2 are correlated. It is assumed that S_1 and S_2 can not communicate with each other. Instead, the relay node is used to help the two sources to improve the probability of successful signal reception of the information sequences sent from the sources at the destination, by performing network coding. Both the source correlation and benefit of network coding can be exploited at the destination node.

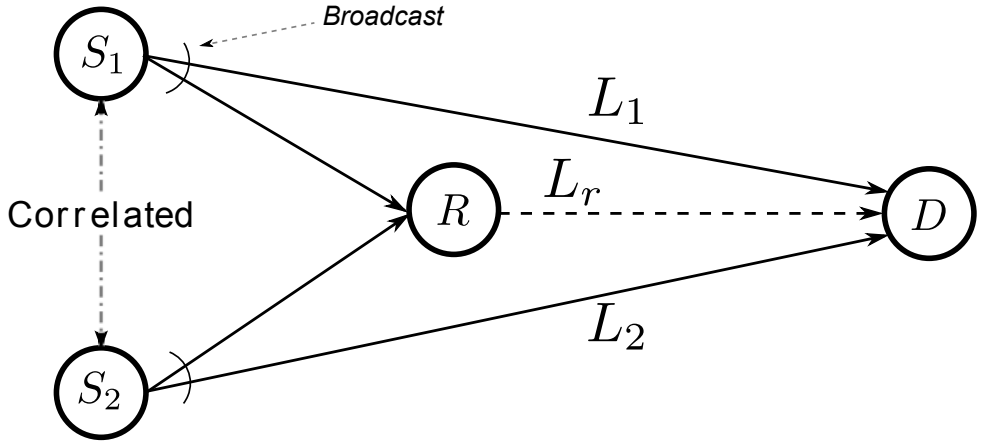

(a) The abstract MARC model considered in this chapter. The source nodes S_1 and S_2 communicate with a common destination node D with the help of a single relay node R.

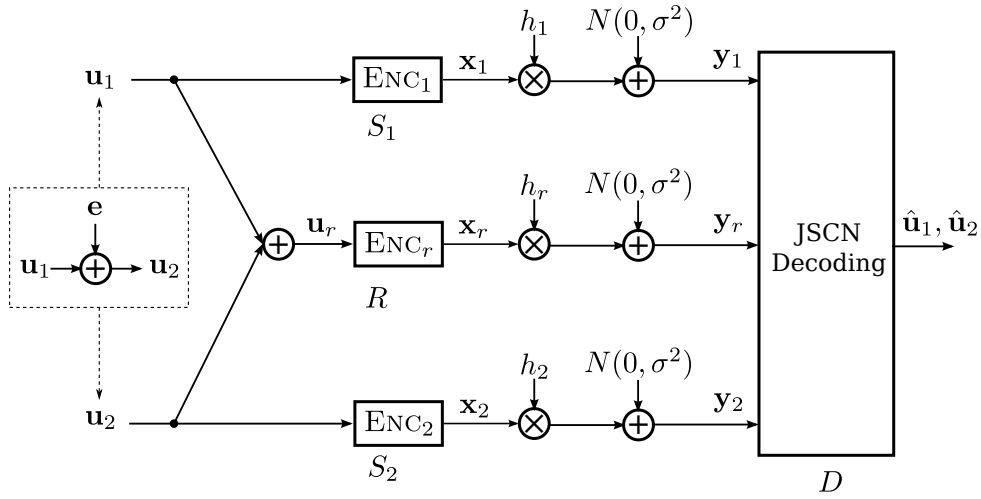

(b) The diagram of the simplified system model, assuming the source-relay links are error free. Enc_1, Enc_2 and Enc_r are channel codes for S_1, S_2 and S_r, respectively.

Figure 5.1: System model for two correlated source transmission in MARC.

5.1.1 Problem Simplification

We assume the source-relay links are error free and therefore the relay can always successfully retrieve the data sequences sent from the two source nodes.[1] The system model can be simplified with this assumption, as shown in Fig. 5.1(b). The binary data sequences $\mathbf{u}_1$ and $\mathbf{u}_2$, emitted from the two source nodes S_1 and S_2, respectively, are correlated with each other. The correlation between the sources can be described using the bit-flipping model [133] as follows. $\mathbf{u}_1$ is generated from an i.i.d. binary source with equiprobability, i.e., $\Pr(u_1^k = 0) = \Pr(u_1^k = 1) = 0.5$, where u_1^k denotes the k-th symbol of $\mathbf{u}_1$. $\mathbf{u}_2$ is then defined as $u_2^k = u_1^k \oplus e^k$ and $\Pr(e^k = 1) = 1 - \Pr(e^k = 0) = p$, where $\oplus$ denotes modulo-2 addition and p is the bit-flipping probability. The source correlation can be characterized by the bit-flipping probability p, and it is assumed that p in known to the destination node. Moreover, the transmissions from the two sources are assumed to be orthogonal due to time division transmission [134]. Consequently, three different time slots are assigned to the two source and relay nodes, since the relay is assumed to work in half-duplex mode.

At the two source nodes, the data sequence $\mathbf{u}_1$ and $\mathbf{u}_2$ are first independently encoded by the channel encoders ENC_1 and ENC_2, and then modulated by BPSK to obtain the modulated sequences $\mathbf{x}_1$ and $\mathbf{x}_2$, respectively. Then, at their dedicated time slots, each source node forwards the BPSK-modulated sequence, $\mathbf{x}_1$ or $\mathbf{x}_2$, to the relay node R and the destination node D. R performs XOR operation on the perfectly recovered sequences $\mathbf{u}_1$ and $\mathbf{u}_2$ as $\mathbf{u}_r = \mathbf{u}_1 \oplus \mathbf{u}_2$. The XORed sequence, $\mathbf{u}_r$, is encoded by the channel encoder ENC_r and then modulated by BPSK to generate the signal sequence $\mathbf{x}_r$ to be transmitted.

After receiving signals from S_1, S_2 and R, joint decoding that exploits both the source correlation and benefit of network coding is performed at D to retrieve $\mathbf{u}_1$ and $\mathbf{u}_2$. This will be detailed in Subsection 5.3.2.

5.1.2 Channel Model

For notational simplicity, the link between S_1 and D is referred to as L_1. Similar definitions are applied to the links from S_2 and R to D by L_2 and L_r, respectively, as shown in Fig. 5.1(a). In this subsection, the source-destination and relay-destination links are assumed to suffer from AWGN and frequency non-selective block Rayleigh fading. The received signal sequence at the destination can be expressed as

$$\mathbf{y}_i = h_i \cdot \mathbf{x}_i + \mathbf{n}_i, \tag{5.1}$$

where $i = 1, 2, r$ corresponds to source nodes S_1, S_2 and relay node R, respectively. $\mathbf{n}_i$ and h_i represent zero mean, variance σ^2 i.i.d. complex Gaussian noise vector and the complex block Rayleigh fading channel gain of L_i, respectively.

We assume that the two source nodes both have the same distance to the destination. Therefore, the average SNRs of both L_1 and L_2 are the same, i.e., $\Gamma_1 = \Gamma_2 = \Gamma$. The relay node can be located with the same distance to the destination as the sources, or closer to the destination. In this chapter, we consider two different cases of the relay location, as shown in Fig. 5.2. In *Case 1*, the relay and two source nodes have identical distance to the destination node. In *Case 2*, the relay node is closer to the destination node than

[1] Alternatively, the relay may perform detection and decoding over received signals to obtain estimates of the source information, respectively, however, in this case, the source-relay links are assumed to be error free after decoding.

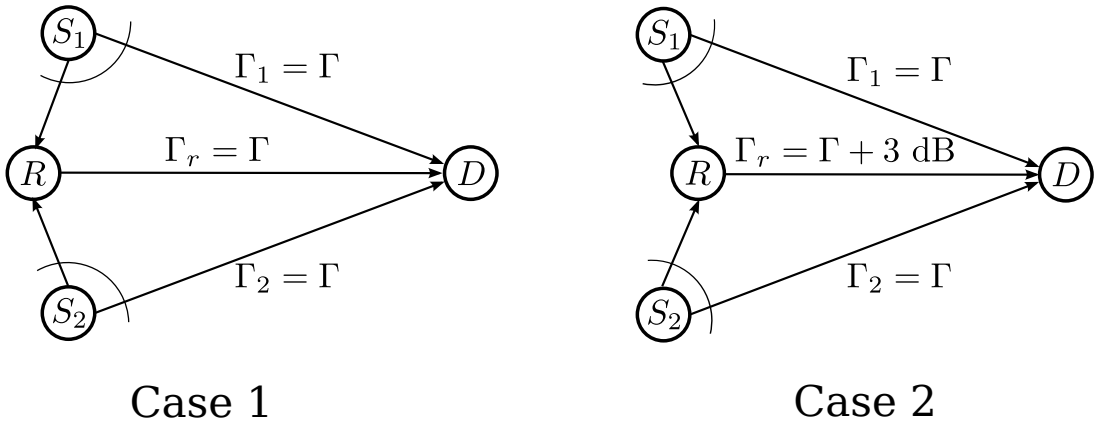

Figure 5.2: Two cases considered for the proposed MARC system . In case 1, the relay and two source nodes keep the same distance to the destination node and thus the SNR of the three links are the same. In case 2, the SNR of the relay-destination link is increased by 3 dB.

the two source nodes. Due to the geometric gain [99], the average SNR of the L_r is larger than that with L_1 and L_2. Here, we assume the average SNR of the relay-destination link is 3 dB larger than Γ. Hence $\Gamma_r = \Gamma$ for *Case 1*, and $\Gamma_r = \Gamma + 3$ dB for *Case 2*.

5.2 Theoretical Analysis

5.2.1 Theorem for Lossless Source Coding with Side Information

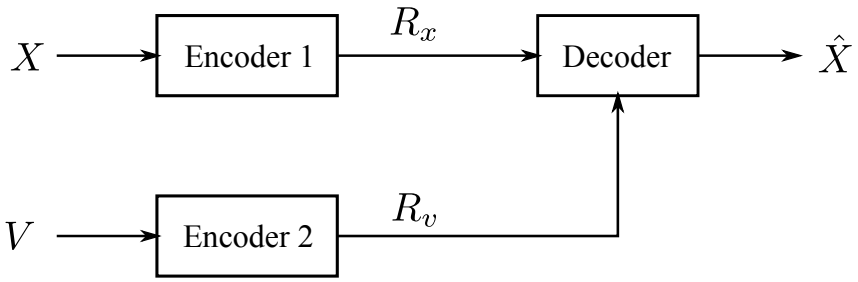

Figure 5.3: An example of source coding with side information.

Let $\{X_i, V_i\}_{i=1}^{\infty}$ be a sequence of i.i.d. discrete random pairs with $(X_i, V_i) \sim p(x, v)$. X and V are separately encoded at rate R_x and R_v, respectively. The encoded sequences are jointly decoded at the decoder, however, only X is to be recovered, which is the main difference with the Slepian-Wolf theorem. Therefore, V that is statistically dependent on X is used as side information at the decoder. This problem is referred to as lossless source coding with side information, which is depicted in Fig. 5.3. The achievable rate pair (R_x, R_v) is specified by the following theorem [114, 135].

Theorem 5.1 (Lossless Source Coding with Side Information) *For a sequence* $\{X_i, V_i\}_{i=1}^{\infty}$ *of discrete random pairs* (X_i, V_i) *drawing i.i.d.* $\sim p(x, v)$*, where* $X_i \in \mathscr{X}$ *and*

$V_i \in \mathscr{V}$. *Then for any rate pair that satisfies*

$$\begin{cases} R_x & \geq & H(X|\hat{V}), \\ R_v & \geq & I(V;\hat{V}). \end{cases} \tag{5.2}$$

for some joint probability mass function $p(x,v)p(\hat{v}|v)$*, there exists an integer* n *and mappings*

$$\begin{array}{rrcl} f_1: & \mathscr{X}^n & \rightarrow & I = \{1, 2, \cdots, 2^{nR_x}\}, \\ f_2: & \mathscr{V}^n & \rightarrow & J = \{1, 2, \cdots, 2^{nR_v}\}, \\ g: & I \times J & \rightarrow & \mathscr{X}^n \times \mathscr{Y}^n, \end{array} \tag{5.3}$$

such that

$$\Pr\{g(f_1(X_1, \cdot, X_n), f_2(Y_1, \cdots, Y_n)) \neq (X_i, \cdots, X_n, Y_1, \cdots, Y_n)\} \leq \varepsilon. \tag{5.4}$$

The random variable $\hat{V}$ can be regarded as the estimate of V at the decoder. According to this theorem, we can use $R_2 = I(V;\hat{V})$ bits per symbol to describe an approximate version of V. Then X can be described at the rate of $H(X|\hat{V})$ bits per symbol in the presence of side information $\hat{V}$ at the decoder. Moreover, as long as the rate pair satisfies (5.2), the error probability after decoding can be made arbitrarily small.

5.2.2 Achievable Compression Rate Region

Due to the XOR operation at the relay node, the achievable compression rate for $\mathbf{u}_1$ and $\mathbf{u}_2$ may not only be determined by the Slepian-Wolf theorem. However, in MARC considered in our system, the destination only aims to recover the data sequence $\mathbf{u}_1$ and $\mathbf{u}_2$, which are sent from source node S_1 and S_2, respectively (we are not interested in the sequence transmitted from the relay, but we only use it). The data sequence $\mathbf{u}_r$ sent from the relay can be regarded as additional redundancy and are used to enhance the performance of the system. Therefore, the theorem for lossless source coding with side information can be used for determining the achievable compression rate region for MARC with correlated sources.

In the theorem for lossless source coding with side information [114, 135], only one source is considered. It can be extended to two sources scenario [136] or even arbitrary number of sources scenario [135, Theorem 10.4]. Therefore, according to the theorem for lossless source coding with side information, the achievable compression rate region of the MARC model described in Section 5.1 is given by

$$\begin{cases} R_1 & \geq & H(\mathbf{u}_1|\mathbf{u}_2, \hat{\mathbf{u}}_r), \\ R_2 & \geq & H(\mathbf{u}_2|\mathbf{u}_1, \hat{\mathbf{u}}_r), \\ R_1 + R_2 & \geq & H(\mathbf{u}_1, \mathbf{u}_2|\hat{\mathbf{u}}_r), \\ R_r & \geq & I(\mathbf{u}_r; \hat{\mathbf{u}}_r), \end{cases} \tag{5.5}$$

where R_1, R_2 and R_r are the compression rates for $\mathbf{u}_1$, $\mathbf{u}_2$ and $\mathbf{u}_r$, respectively. $\hat{\mathbf{u}}_r$ is the estimate of $\mathbf{u}_r$ at the final output. Since the destination node does not aim to successfully decode $\mathbf{u}_r$, $\hat{\mathbf{u}}_r$ may contain some errors. The relationship between $\mathbf{u}_r$ and $\hat{\mathbf{u}}_r$ can also be expressed as a bit-flipping model with error probability $\alpha, \alpha \in [0, 0.5]$.

Derivation of $I(\mathbf{u}_r;\hat{\mathbf{u}}_r)$, $H(\mathbf{u}_1|\mathbf{u}_2,\hat{\mathbf{u}}_r)$, $H(\mathbf{u}_2|\mathbf{u}_1,\hat{\mathbf{u}}_r)$, and $H(\mathbf{u}_1,\mathbf{u}_2|\hat{\mathbf{u}}_r)$

As described in Section. 5.1, the appearance probabilities of $\mathbf{u}_1$ and $\mathbf{u}_2$ are equiprobable, which means $\Pr(u_1^k=0)=\Pr(u_2^k=0)=\frac{1}{2}$, then we have $H(\mathbf{u}_1)=H(\mathbf{u}_2)=1$. Furthermore, $\mathbf{u}_1$ and $\mathbf{u}_2$ are correlated and the correlation is modeled as bit-flipping with probability p, which leads to

$$H(\mathbf{u}_1)=H(\mathbf{u}_2)=1, \tag{5.6}$$
$$H(\mathbf{u}_1|\mathbf{u}_2)=H(\mathbf{u}_2|\mathbf{u}_1)=H_b(p) \tag{5.7}$$
$$H(\mathbf{u}_1,\mathbf{u}_2)=1+H_b(p). \tag{5.8}$$

The information sent from the relay node is $\mathbf{u}_r=\mathbf{u}_1\oplus\mathbf{u}_2$, hence $\Pr(u_r^k=1)=1-\Pr(u_r^k=0)=p$. The estimate of $\mathbf{u}_r$ obtained at the destination node after decoding, $\hat{\mathbf{u}}_r$, is a bit-flipped version of $\mathbf{u}_r$ with probability α, and therefore $\Pr(\hat{u}_r^k=1)=1-\Pr(\hat{u}_r^k)=\alpha+p-2\alpha p$.

The mutual information between $\mathbf{u}_r$ and $\hat{\mathbf{u}}_r$ can be expressed as

$$\begin{aligned} I(\mathbf{u}_r;\hat{\mathbf{u}}_r) &= H(\hat{\mathbf{u}}_r)-H(\hat{\mathbf{u}}_r|\mathbf{u}_r) \\ &= H_b(\alpha+p-2\alpha p)-H_b(\alpha). \end{aligned} \tag{5.9}$$

According to the chain rule for entropy, the joint entropy of $\mathbf{u}_1$, $\mathbf{u}_2$, $\mathbf{u}_r$ and $\hat{\mathbf{u}}_r$ can be expressed as

$$H(\mathbf{u}_1,\mathbf{u}_2,\mathbf{u}_r,\hat{\mathbf{u}}_r)=H(\mathbf{u}_1)+H(\mathbf{u}_2|\mathbf{u}_1)+H(\mathbf{u}_r|\mathbf{u}_1,\mathbf{u}_2)+H(\hat{\mathbf{u}}_r|\mathbf{u}_1,\mathbf{u}_2,\mathbf{u}_r), \tag{5.10}$$

where $H(\mathbf{u}_r|\mathbf{u}_1,\mathbf{u}_2)=0$, and $H(\hat{\mathbf{u}}_r|\mathbf{u}_1,\mathbf{u}_2,\mathbf{u}_r)=H(\hat{\mathbf{u}}_r|\mathbf{u}_r)$. $H(\mathbf{u}_1,\mathbf{u}_2,\mathbf{u}_r,\hat{\mathbf{u}}_r)$ can also be expressed in another way, as

$$H(\mathbf{u}_1,\mathbf{u}_2,\mathbf{u}_r,\hat{\mathbf{u}}_r)=H(\hat{\mathbf{u}}_r)+H(\mathbf{u}_1,\mathbf{u}_2|\hat{\mathbf{u}}_r)+H(\mathbf{u}_r|\mathbf{u}_1,\mathbf{u}_2,\hat{\mathbf{u}}_r), \tag{5.11}$$

where $H(\mathbf{u}_r|\mathbf{u}_1,\mathbf{u}_2,\hat{\mathbf{u}}_r)=0$.

By combining (5.10) and (5.11), we can get

$$\begin{aligned} H(\mathbf{u}_1,\mathbf{u}_2|\hat{\mathbf{u}}_r) &= H(\mathbf{u}_1)+H(\mathbf{u}_2|\mathbf{u}_1)-[H(\hat{\mathbf{u}}_r)-H(\hat{\mathbf{u}}_r|\mathbf{u}_r)] \\ &= 1+H_b(p)-I(\mathbf{u}_r;\hat{\mathbf{u}}_r). \end{aligned} \tag{5.12}$$

$H(\mathbf{u}_1,\mathbf{u}_2|\hat{\mathbf{u}}_r)$ can be further expressed as

$$\begin{aligned} H(\mathbf{u}_1,\mathbf{u}_2|\hat{\mathbf{u}}_r) &= H(\mathbf{u}_1|\hat{\mathbf{u}}_r)+H(\mathbf{u}_2|\mathbf{u}_1,\hat{\mathbf{u}}_r) \\ &= H(\mathbf{u}_2|\hat{\mathbf{u}}_r)+H(\mathbf{u}_1|\mathbf{u}_2,\hat{\mathbf{u}}_r). \end{aligned} \tag{5.13}$$

Given the fact that both $\mathbf{u}_1$ and $\mathbf{u}_2$ are independent of $\hat{\mathbf{u}}_r$ and $H(\mathbf{u}_1|\hat{\mathbf{u}}_r)=H(\mathbf{u}_2|\hat{\mathbf{u}}_r)=1$, we have

$$H(\mathbf{u}_1|\mathbf{u}_2,\hat{\mathbf{u}}_r)=H(\mathbf{u}_2|\mathbf{u}_1,\hat{\mathbf{u}}_r)=H_b(p)-I(\mathbf{u}_r;\hat{\mathbf{u}}_r). \tag{5.14}$$

Combining all the results above, now we have

$$\begin{cases} H(\mathbf{u}_2|\mathbf{u}_1,\hat{\mathbf{u}}_r)=H_b(p)-I(\mathbf{u}_r;\hat{\mathbf{u}}_r), \\ H(\mathbf{u}_1|\mathbf{u}_2,\hat{\mathbf{u}}_r)=H_b(p)-I(\mathbf{u}_r;\hat{\mathbf{u}}_r), \\ H(\mathbf{u}_1,\mathbf{u}_2|\hat{\mathbf{u}}_r)=1+H_b(p)-I(\mathbf{u}_r;\hat{\mathbf{u}}_r), \\ I(\mathbf{u}_r;\hat{\mathbf{u}}_r)=H_b(\alpha+p-2\alpha p)-H_b(\alpha). \end{cases} \tag{5.15}$$

Illustration of the Achievable Compression Rate Region

According to (5.15), the achievable compression rate region is determined by the source correlation p and the error probability α. For a given p value, the achievable compression rate region is determined only by α. First we focus on the achievable compression rate region of R_1 and R_2. If $\alpha = 0.5$, the estimate $\hat{\mathbf{u}}_r$ of $\mathbf{u}_r$ after decoding does not contain any information of $\mathbf{u}_r$ and hence can not be utilized in the joint decoding process. In this case, the achievable compression rate region for R_1 and R_2 is $R_1 \geq H_b(p)$, $R_2 \geq H_b(p)$ and $R_1 + R_2 \geq 1 + H_b(p)$, which is the region surrounded by a polygon as shown in Fig. 5.4. It can be seen that the region is the same as that determined by the Slepian-Wolf theorem for two correlated sources. If $\alpha = 0$, $\mathbf{u}_r$ can be successfully decoded at the destination. Hence, the achievable compression rate region for R_1 and R_2 becomes $R_1 \geq 0$, $R_2 \geq 0$ and $R_1 + R_2 \geq 1$, as depicted in Fig 5.4. In this case, the achievable compression rate region for R_1 and R_2 is the largest. If $0 < \alpha < 0.5$, the achievable compression rate region for R_1 and R_2 is between these two extreme cases, which is also shown in the same figure.

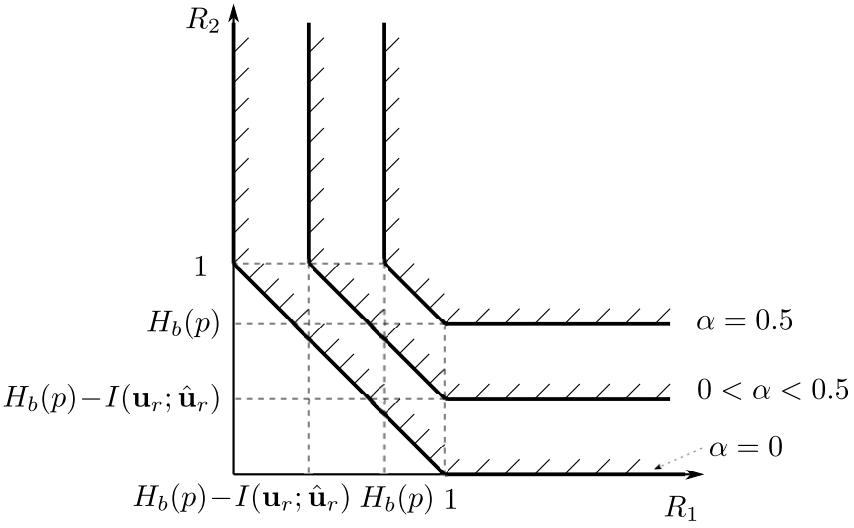

Figure 5.4: The achievable compression rate region for R_1 and R_2. α is the error probability between $\mathbf{u}_r$ and $\hat{\mathbf{u}}_r$.

The error probability α between $\mathbf{u}_r$ and $\hat{\mathbf{u}}_r$, is determined by the quality of L_r. Since we assume the channel encoders ENC_1, ENC_2 and ENC_r are close-limit achieving, obviously, the minimum compression rate for R_r is $R_{r,min} = I(\mathbf{u}_r; \hat{\mathbf{u}}_r)$. Taking R_r into the account, the achievable compression rate region for the proposed system can be determined, which is the 3-dimensional (3D) space surrounded by the polyhedron, as shown in Fig. 5.5.

It should be emphasized that, source coding for compression is performed at neither S_1, S_2 nor R. Instead, the correlation knowledge among $\mathbf{u}_1$, $\mathbf{u}_2$ and $\mathbf{u}_r$ are exploited at the destination to enhance the error correction capability of the system.

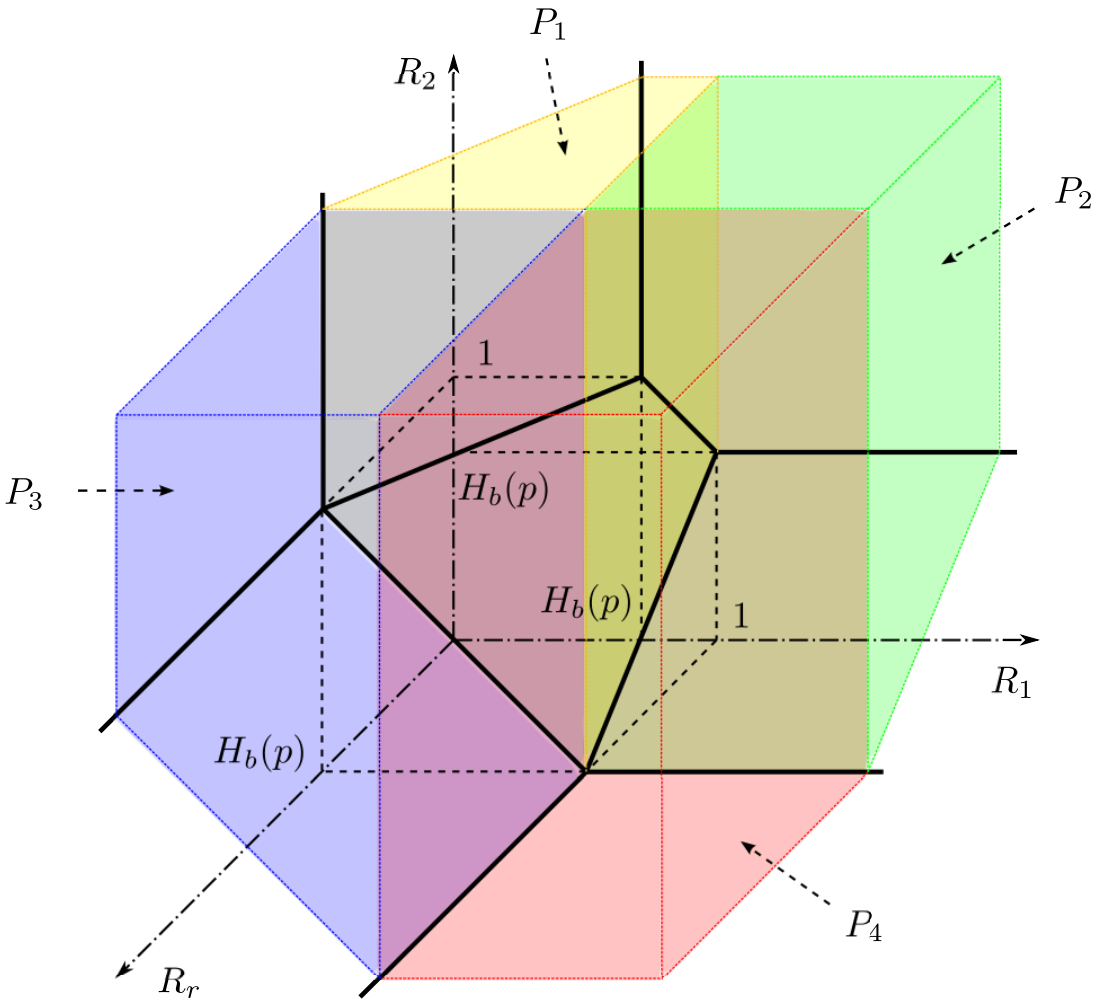

Figure 5.5: The achievable compression rate region for the proposed system.

5.2.3 Performance Limits in AWGN Channels

According to Shannon's separation theorem, if the *total* information transmission rates over independent channels satisfy [88]

$$\begin{cases} R_1 R_{c1} & \leq & C_1, \\ R_2 R_{c2} & \leq & C_2, \\ R_r R_{cr} & \leq & C_r, \end{cases} \tag{5.16}$$

message error probability can be infinitesimally reduced, where R_{c1}, R_{c2} and R_{cr} are the rates of the channel encoders ENC_1, ENC_2 and ENC_r, respectively. C_1, C_2 and C_r are the channel capacity of the links L_1, L_2 and L_r, respectively. In AWGN channels with one-dimensional modulation, the channel capacity is defined as

$$C_i = \frac{1}{2}\log_2(1 + 2\Gamma_i), \tag{5.17}$$

where $i = 1, 2, r$ corresponds to source nodes S_1, S_2 and relay node R, respectively. Γ_i denote the SNR of L_i.

Case 1

The instantaneous SNR of the source-relay and relay-destination links are the same in the relay location *Case 1*, i.e., $\Gamma_1 = \Gamma_2 = \Gamma_r$. In this case, obviously $R_1 = R_2 = R_r = R$. Then the compression rate R is determined by

$$\begin{cases} R \geq \frac{1}{2}[1 + H(\alpha) + H(p) - H(\alpha + p - 2\alpha p)] = f_1(\alpha, p), \\ R \geq H(\alpha + p - 2\alpha p) - H(\alpha) = f_2(\alpha, p), \end{cases} \tag{5.18}$$

where $f_1(\alpha, p)$ and $f_2(\alpha, p)$ correspond to the compression rates for the two source nodes and the relay node, respectively.

The minimum compression rate R_{min} is achieved on the intersection of $f_1(\alpha, p)$ and $f_2(\alpha, p)$, as shown in Fig. 5.6. It can be observed that for a certain p value, as α increases, less bits are needed to describe $\mathbf{u}_r$ while more bits are needed for describing $\mathbf{u}_1$ and $\mathbf{u}_2$. It can also be seen from this figure that if $H(p) \leq 0.5$, R_{min} is only determined by $f_1(\alpha, p)$. By combining (5.16) and (5.18), we can obtain the performance limit of our system in AWGN channels for *Case 1*.

Case 2

In the relay location *Case 2*, the instantaneous SNR of the relay-destination link is increased by 3 dB, i.e., $\Gamma_r = \Gamma_1 + 3$ dB. In this case, the relationship between R_1, R_2 and R_r can not be explicitly identified. However, the performance limit of our system can be calculated by combining (5.5), (5.15) and (5.16).

5.2.4 Outage Probability in Rayleigh Fading Channels

According to [99], the outage probability of the proposed system can be derived once the achievable compression rate region is determined. The instantaneous SNR of L_i is denoted by $\gamma_i = |h_i|^2 E_{s,i}/2\sigma^2$, where $E_{s,i}$ represents the per-symbol signal power of L_i and

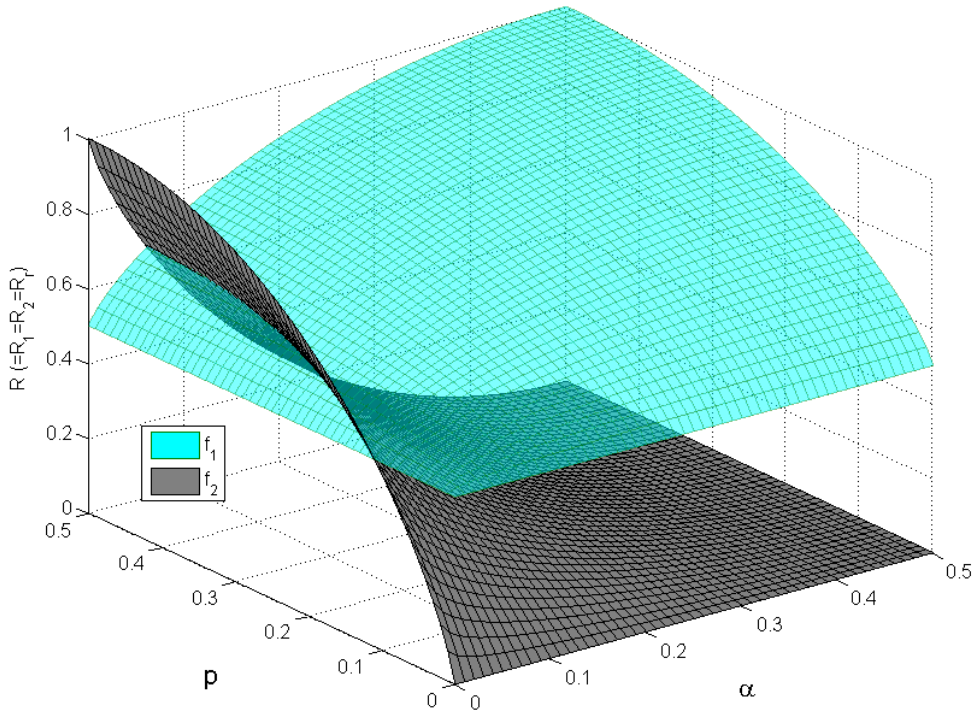

Figure 5.6: The minimum compression rate for our system in *case 1*. p denotes the bit-flipping probability between the two sources. α denotes the error probability between $\mathbf{u}_r$ and $\hat{\mathbf{u}}_r$.

$i = 1, 2, r$ corresponds to S_1, S_2 and D, respectively. Since the channel codes used for the transmission over L_1, L_2 and L_r are assumed to be close-limit achieving, corresponding to their rates, according to (5.16) and (5.17), the relationship between the threshold instantaneous SNR of L_i and its corresponding rate R_i is given by

$$R_i = \Phi_i(\gamma_i) = \frac{1}{2R_{ci}} \log_2(1 + 2\gamma_i), \tag{5.19}$$

with its reverse function

$$\gamma_i = \Phi_i^{-1}(R_i) = \frac{2^{2R_i R_{ci}} - 1}{2}. \tag{5.20}$$

As shown in Fig. 5.5, the entire rate region for the proposed system can be divided into 4 parts, with P_j, $j = 1, 2, 3, 4$, representing the probability that the rate combination (R_1, R_2, R_r) falls into Part j. As mentioned in Subsection 5.2.2, α is determined by the quality of L_r and the minimum value for R_r is $R_{r,min} = I(\mathbf{u}_r; \hat{\mathbf{u}}_r)$. If the instantaneous SNR of L_r, γ_r, falls under a certain threshold, then $\hat{\mathbf{u}}_r \neq \mathbf{u}_r$ at D after decoding. In this case, $R_{r,min}$ ranges from 0 to $H_b(p)$ and the achievable rate region is represented by P_1 and P_2. On the contrary, if γ_r is above this certain threshold, then $\hat{\mathbf{u}}_r = \mathbf{u}_r$ at D after decoding. In this case, $R_{r,min} = H(p)$ and the achievable rate region is represented by P_3 and P_4.

If (R_1, R_2, R_r) falls into the achievable rate region, $\mathbf{u}_1$ and $\mathbf{u}_2$ can be successfully decoded at D. Hence, the outage event happens when (R_1, R_2, R_r) falls outside the achievable rate region, and the outage probability of the proposed system is expressed as

$$P_{out} = 1 - P_1 - P_2 - P_3 - P_4, \tag{5.21}$$

where

$$\begin{aligned} P_1 &= \Pr\{0 \leq R_r \leq H_b(p), H_b(p) - I(\mathbf{u}_r; \hat{\mathbf{u}}_r) \leq R_1 \leq 1, R_1 + R_2 \geq 1 + H_b(p) - I(\mathbf{u}_r; \hat{\mathbf{u}}_r)\} \\ &= \Pr\{\Phi_r^{-1}(0) \leq \gamma_r \leq \Phi_r^{-1}[H_b(p)], \Phi_1^{-1}[H_b(p) - \Phi_r(\gamma_r)] \leq \gamma_1 \leq \Phi_1^{-1}(1), \\ &\qquad \gamma_2 \geq \Phi_2^{-1}[1 + H_b(p) - \Phi_r(\gamma_r) - \Phi_1(\gamma_1)]\}, \end{aligned} \tag{5.22}$$

$$\begin{aligned} P_2 &= \Pr\{0 \leq R_r \leq H_b(p), R_1 \geq 1, R_2 \geq H_b(p) - I(\mathbf{u}_r; \hat{\mathbf{u}}_r)\} \\ &= \Pr\{\Phi_r^{-1}(0) \leq \gamma_r \leq \Phi_r^{-1}[H_b(p)], \gamma_1 \geq \Phi_1^{-1}(1), \gamma_2 \geq \Phi_2^{-1}[H_b(p) - \Phi_r(\gamma_r)]\}, \end{aligned} \tag{5.23}$$

$$\begin{aligned} P_3 &= \Pr\{R_r \geq H_b(p), 0 \leq R_1 \leq 1, R_1 + R_2 \geq 1\} \\ &= \Pr\{\gamma_r \geq \Phi_r^{-1}[H_b(p)], \Phi_1^{-1}(0) \leq \gamma_1 \leq \Phi_1^{-1}(1), \gamma_2 \geq \Phi_2^{-1}[1 - \Phi_1(\gamma_1)]\}, \end{aligned} \tag{5.24}$$

and

$$\begin{aligned} P_4 &= \Pr\{R_r \geq H_b(p), R_1 \geq 1, R_2 \geq 0\} \\ &= \Pr\{\gamma_r \geq \Phi_r^{-1}[H_b(p)], \gamma_1 \geq \Phi_1^{-1}(1), \gamma_2 \geq \Phi_2^{-1}(0)\}. \end{aligned} \tag{5.25}$$

Since L_1, L_2 and L_r are suffering from statistically independent block Rayleigh fading, the joint *pdf* of the instantaneous SNRs can be expressed as $p(\gamma_r, \gamma_1, \gamma_2) = p(\gamma_r) \cdot p(\gamma_1) \cdot p(\gamma_2)$, where

$$p(\gamma_i) = \frac{1}{\Gamma_i} \exp(-\frac{\gamma_i}{\Gamma_i}), \ i = 1, 2, r. \tag{5.26}$$

Here $\Gamma_i = E_{s,i}/2\sigma^2$ represents the average SNR of L_i. With (5.26), the probabilities P_1, P_2, P_3 and P_4 can be further expressed as triple integrals, as:

$$\begin{aligned}
P_1 &= \int_{\Phi_r^{-1}(0)}^{\Phi_r^{-1}[H_b(p)]} d\gamma_r \int_{\Phi_1^{-1}[H_b(p)-\Phi_r(\gamma_r)]}^{\Phi_1^{-1}(1)} d\gamma_1 \int_{\Phi_2^{-1}[1+H_b(p)-\Phi_r(\gamma_r)-\Phi_1(\gamma_1)]}^{\Phi_2^{-1}(\infty)} p(\gamma_r)p(\gamma_1)p(\gamma_2)d\gamma_2 \\
&= \int_{\Phi_r^{-1}(0)}^{\Phi_r^{-1}[H_b(p)]} d\gamma_r \int_{\Phi_1^{-1}[H_b(p)-\Phi_r(\gamma_r)]}^{\Phi_1^{-1}(1)} p(\gamma_r)p(\gamma_1) \left[-\exp(-\frac{\gamma_2}{\Gamma_2})\right]_{\Phi_2^{-1}[1+H_b(p)-\Phi_r(\gamma_r)-\Phi_1(\gamma_1)]}^{\Phi_2^{-1}(\infty)} d\gamma_1 \\
&= \frac{1}{\Gamma_r\Gamma_1} \int_0^{\frac{2^{R_{cr}H_b(p)}-1}{2}} d\gamma_r \int_{\frac{2^{2R_{c1}[H_b(p)-\frac{1}{2R_{cr}}\log_2(1+2\gamma_r)]}-1}{2}}^{\frac{1}{2}} \\
&\qquad \exp\left\{-\frac{\gamma_r}{\Gamma_r} - \frac{\gamma_1}{\Gamma_1} - \frac{\Phi_2^{-1}[1+H_b(p)-\Phi_r(\gamma_r)-\Phi_1(\gamma_1)]}{\Gamma_2}\right\} d\gamma_1,
\end{aligned} \tag{5.27}$$

$$\begin{aligned}
P_2 &= \int_{\Phi_r^{-1}(0)}^{\Phi_r^{-1}[H_b(p)]} d\gamma_r \int_{\Phi_1^{-1}(1)}^{\Phi_1^{-1}(\infty)} d\gamma_1 \int_{\Phi_2^{-1}[H_b(p)-\Phi_r(\gamma_r)]}^{\Phi_2^{-1}(\infty)} p(\gamma_r)p(\gamma_1)p(\gamma_2)d\gamma_2 \\
&= \int_{\Phi_r^{-1}(0)}^{\Phi_r^{-1}[H_b(p)]} p(\gamma_r) \left[-\exp(-\frac{\gamma_1}{\Gamma_1})\right]_{\Phi_1^{-1}(1)}^{\Phi_1^{-1}(\infty)} \left[-\exp(\frac{\gamma_2}{\Gamma_2})\right]_{\Phi_2^{-1}[H_b(p)-\Phi_r(\gamma_r)]}^{\Phi_2^{-1}(\infty)} d\gamma_r \\
&= \frac{1}{\Gamma_r}\exp(-\frac{1}{2\Gamma_1}) \int_0^{\frac{2^{2R_{cr}H_b(p)}-1}{2}} \exp\left\{-\frac{\gamma_r}{\Gamma_r} - \frac{2^{2R_{c2}[H_b(p)-\frac{1}{2R_{cr}}\log_2(1+2\gamma_r)]}-1}{2\Gamma_2}\right\} d\gamma_r,
\end{aligned} \tag{5.28}$$

$$\begin{aligned}
P_3 &= \int_{\Phi_r^{-1}[H_b(p)]}^{\Phi_r^{-1}(\infty)} d\gamma_r \int_{\Phi_1^{-1}(0)}^{\Phi_1^{-1}(1)} d\gamma_1 \int_{\Phi_2^{-1}[1-\Phi_1(\gamma_1)]}^{\Phi^{-1}(\infty)} p(\gamma_r)p(\gamma_1)p(\gamma_2)d\gamma_2 \\
&= \int_{\Phi_1^{-1}(0)}^{\Phi_1^{-1}(1)} \left[-\exp(-\frac{\gamma_r}{\Gamma_r})\right]_{\Phi_r^{-1}[H_b(p)]}^{\Phi_r^{-1}(\infty)} \cdot p(\gamma_1) \cdot \left[-\exp(\frac{\gamma_2}{\Gamma_2})\right]_{\Phi_2^{-1}[1-\Phi_1(\gamma_1)]}^{\Phi_2^{-1}(\infty)} d\gamma_1 \\
&= \frac{1}{\Gamma_1}\exp\left[-\frac{2^{2R_{cr}H_b(p)}-1}{2\Gamma_r}\right] \cdot \int_0^{\frac{1}{2}} \exp\left\{-\frac{\gamma_1}{\Gamma_1} - \frac{2^{2R_{c2}[1-\frac{1}{2R_{c1}}\log_2(1+2\gamma_1)]}-1}{2\Gamma_2}\right\} d\gamma_1,
\end{aligned} \tag{5.29}$$

and

$$\begin{aligned}
P_4 &= \int_{\Phi_r^{-1}[H_b(p)]}^{\Phi_r^{-1}(\infty)} d\gamma_r \int_{\Phi_1^{-1}(1)}^{\Phi_1^{-1}(\infty)} d\gamma_1 \int_{\Phi_2^{-1}(0)}^{\Phi_2^{-1}(\infty)} p(\gamma_r)p(\gamma_1)p(\gamma_2)d\gamma_2 \\
&= \left[-\exp(-\frac{\gamma_r}{\Gamma_r})\right]_{\Phi_r^{-1}[H_b(p)]}^{\Phi_r^{-1}(\infty)} \cdot \left[-\exp(-\frac{\gamma_1}{\Gamma_1})\right]_{\Phi_1^{-1}(1)}^{\Phi_1^{-1}(\infty)} \cdot \left[-\exp(-\frac{\gamma_2}{\Gamma_2})\right]_{\Phi_2^{-1}(0)}^{\Phi_2^{-1}(\infty)} \\
&= \exp(-\frac{1}{2\Gamma_1})\exp\left[-\frac{2^{2R_{cr}H_b(p)}-1}{2\Gamma_r}\right].
\end{aligned} \tag{5.30}$$

Except for P_4, the derivation for the explicit expressions of the integrals in (5.27), (5.28) and (5.29) may not be possible. Instead, a numerical method [137] is used to calculate the values of P_1, P_2 and P_3.

5.2.5 Asymptotic Property

In this subsection, we evaluate the outage probability of the proposed system when the two sources are fully correlated ($p = 0$). In this case, we have $H_b(p) = 0$. The integral ranges of γ_r in (5.27) and (5.28) are both from 0 to 0, which means $P_1 = P_2 = 0$. Moreover, we can have

$$\exp\left[-\frac{2^{2R_{cr}H_b(p)}-1}{2\Gamma_r}\right] = 1. \tag{5.31}$$

and the outage probability becomes

$$\begin{aligned} P_{out,p=0} &= 1 - P_1 - P_2 - P_3 - P_4 \\ &= 1 - \exp(-\frac{1}{2\Gamma_1}) \\ -\frac{1}{\Gamma_1}\int_0^{\frac{1}{2}} &\exp\left\{-\frac{\gamma_1}{\Gamma_1} - \frac{2^{2R_{c2}[1-\frac{1}{2R_{c1}}\log_2(1+2\gamma_1)]}-1}{2\Gamma_2}\right\} d\gamma_1. \end{aligned} \tag{5.32}$$

It is found from (5.32) that if the two sources are fully correlated, the outage probability is only determined by the quality of L_1 and L_2.

As mentioned in Subsection 5.1.2, we assume $\Gamma_1 = \Gamma_2$ and Γ_r is Δ dB larger than Γ_1, i.e., $\Gamma_r = \Gamma_1 \cdot 10^{\Delta/10}$. In this subsection, we only considered the case when $\Delta = 0$ (*Case 1*) and that when $\Delta = 3$ (*Case 2*). Next the outage probability of the proposed system is evaluated when Δ approaches infinity. For given Γ_1, when $\Delta \to \infty$, $\frac{1}{\Gamma_r} = \frac{1}{\Gamma_1 \cdot 10^{\Delta/10}} \to 0$. According to (5.27) and (5.28), we have $P_1 = P_2 = 0$. Furthermore, as $\Delta \to \infty$, it is found that

$$\exp\left[-\frac{2^{2R_{cr}H_b(p)}-1}{2\Gamma_r}\right] = \exp\left[-\frac{2^{2R_{cr}H_b(p)}-1}{2(\Gamma_1 \cdot 10^{\Delta/10})}\right] \to 1. \tag{5.33}$$

Obviously, the outage probability of the proposed system when $\Delta \to \infty$ is the same as in the case the two sources are fully correlated, as:

$$P_{out,\Delta\to\infty} = P_{out,p=0}. \tag{5.34}$$

5.3 Practical Code Design

In the theoretical analysis, we did not specify the coding structure for ENC_1, ENC_2 and ENC_r and assume that they all have close-limit performance. In this section, we propose a coding/decoding scheme that exploits the source correlation and the benefit of network coding simultaneously.

5.3.1 Coding Structure

The block diagram of the coding structure of ENC_i, $i = 1, 2, r$ is shown in Fig. 5.7, where SCCC is used. The outer code in SCCC is a non-recursive non-systematic convolutional (NRNSC) code, and the inner code is doped accumulator with doping rate Q_i. The NRNSC codes C_1, C_2 and C_r are all half-rate memory-1 code with generator polynomial $(3, 2)_8$, therefore $R_{c1} = R_{c2} = R_{cr} = 1/2$. It has been shown in [96] that even with this simple SCCC code, still excellent performance can be achieved.

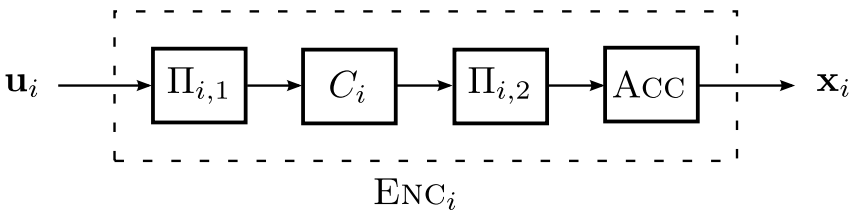

Figure 5.7: Coding structure for ENC$_i$, $i = 1, 2, r$. C_i is convolutional code and ACC denotes doped accumulator.

5.3.2 Joint Source-Channel-Network Decoding Structure

The block diagram of the proposed JSCN decoder for MARC is illustrated in Fig. 5.8. As can be seen from the figure, the joint decoding process is divided into two constituent function, operated iteratively. We refer to these two processes as Local Iteration (LI) and Global Iteration (GI). To perform channel decoding for RSC codes C_1, C_2 and C_r as well as ACC, we perform MAP-decoding using the BCJR algorithm.

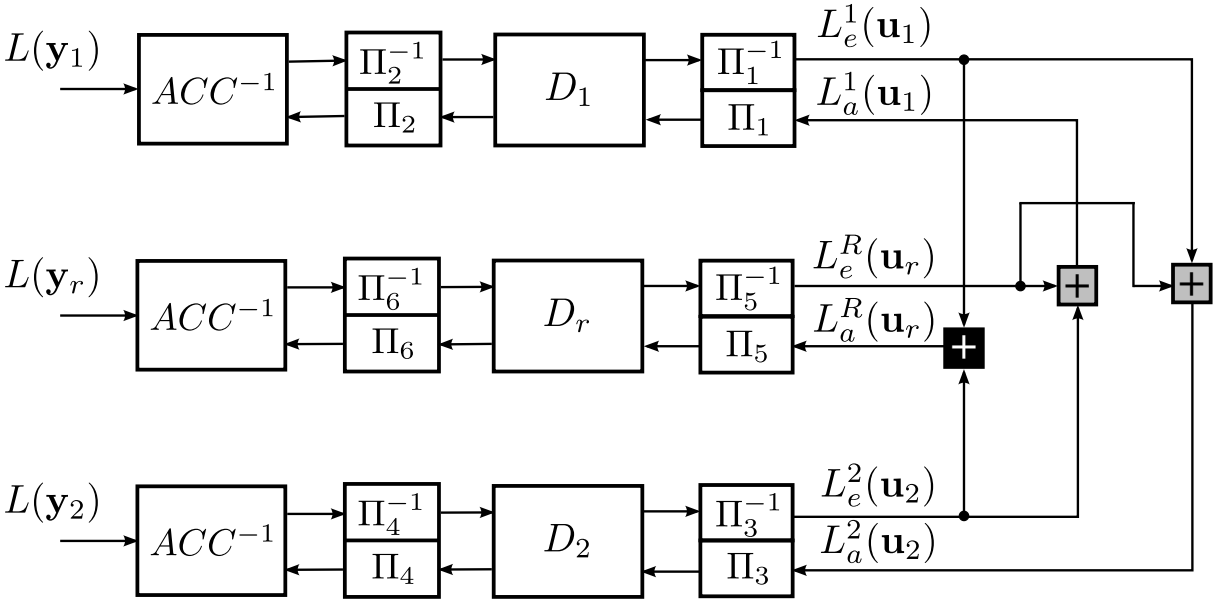

Figure 5.8: The proposed JSCN decoder. D_1, D_2 and D_r denotes the decoders of the NRNSC codes C_1, C_2 and C_r used by S_1, S_2 and R, respectively. ACC^{-1} denotes the decoder for ACC.

The received signals at the destination are first converted into LLRs as

$$L(y_i^k) = \ln \frac{\Pr(y_i^k | x_i^k = +1)}{\Pr(y_i^k | x_i^k = -1)} = \frac{2}{\sigma^2} \Re\{h_i^* \cdot y_i^k\}, \tag{5.35}$$

where $i = 1, 2, r$ denotes S_1, S_2 and R, respectively. y_i^k and x_i^k are the k-th symbol of $\mathbf{y}_i$ and $\mathbf{x}_i$, respectively. h_i^* indicates the complex conjugation of h_i and $\Re\{\cdot\}$ indicates the real part of its arguments. The obtained LLR sequences $L(\mathbf{y}_1)$, $L(\mathbf{y}_2)$ and $L(\mathbf{y}_r)$ are then fed into three independent LIs. In the LI, the extrinsic LLRs are exchanged via the corresponding interleaver/deinterleaver between the SISO decoder ACC^{-1} and SISO decoder D_1, D_2 or D_r used by S_1, S_2 or R, respectively.

After each LI step, the extrinsic LLRs generated from D_1, D_2 and D_r are further exchanged via the GI. As depicted in Fig. 5.1(b), XOR network coding is applied at the relay and the relationship among the data sequences transmitted from the two sources and relay nodes can be expressed as $\mathbf{u}_r = \mathbf{u}_1 \oplus \mathbf{u}_2$. In conventional MARC that does not take into account the source correlation, joint network-channel (JNC) decoding is performed at the destination where the GI can be performed as

$$\begin{aligned} L_a^R(\mathbf{u}_r) &= L_e^1(\mathbf{u}_1) \boxplus L_e^2(\mathbf{u}_2) \\ &= \ln \frac{1+\exp[L_e^1(\mathbf{u}_1)+L_e^2(\mathbf{u}_2)]}{\exp[L_e^1(\mathbf{u}_1)]+\exp[L_e^2(\mathbf{u}_2)]}, \end{aligned} \tag{5.36}$$

with $\boxplus$ denoting the boxplus operation which is equivalent to the XOR operation in the LLR domain [138, 139]. $L_e(\mathbf{u}_1)$ and $L_e(\mathbf{u}_2)$ denote the extrinsic LLRs generated from DEC_1 and DEC_2, respectively, and $L_a^R(\mathbf{u}_r)$ denotes the *a priori* LLRs fed into DEC_r. The *a priori* LLRs fed into DEC_1 and DEC_2, which are denoted as $L_a(\mathbf{u}_1)$ and $L_a(\mathbf{u}_2)$, respectively, can be obtained in the same way.

If the two correlated sources are transmitted to the destination node without the help of the relay node, only the source correlation can be exploited at the destination. In this case, joint source-channel (JSC) decoding can be performed at the destination to exploit the source correlation. D_1 and D_2 can exchange their extrinsic information via the f_c function defined in (4.33).

In our proposed system, the two sources are correlated and XOR network coding is performed at the relay node. In order to take into account the correlation knowledge between $\mathbf{u}_1$ and $\mathbf{u}_2$, as well as with the assistance of network coding, modified versions of the boxplus operation are derived to perform JSCN at the destination, which is detailed in the next subsection. Finally, after sufficient iterations, hard decisions are made based on the output of D_1 and D_2 to get the estimate of $\mathbf{u}_1$ and $\mathbf{u}_2$, respectively.

5.3.3 Modified Versions of Boxplus Operation

Modified Boxplus Operation for Relay Node

Since the correlation between $\mathbf{u}_1$ and $\mathbf{u}_2$ is modeled by the bit-flipping model, it is quite straightforward to obtain the following equations, according to [88, 133]:

$$\begin{aligned} \Pr(u_r^k=0) &= \Pr(u_1^k=0, u_2^k=0) + \Pr(u_1^k=1, u_2^k=1) \\ &= \Pr(u_1^k=0)\cdot\Pr(u_2^k=0)\cdot(1-p) + \Pr(u_1^k=1)\cdot\Pr(u_2^k=1)\cdot(1-p), \end{aligned} \tag{5.37}$$

$$\begin{aligned} \Pr(u_r^k=1) &= \Pr(u_1^k=0, u_2^k=1) + \Pr(u_1^k=1, u_2^k=0) \\ &= \Pr(u_1^k=0)\cdot\Pr(u_2^k=1)\cdot p + \Pr(u_1^k=1)\cdot\Pr(u_2^k=0)\cdot p, \end{aligned} \tag{5.38}$$

where u_1^k, u_2^k and u_r^k denote the k-th symbol of $\mathbf{u}_1$, $\mathbf{u}_2$ and $\mathbf{u}_r$, respectively. With (5.37) and (5.38), the LLR for u_r^k can be obtained as

$$\begin{aligned} L(u_r^k) = L(u_1^k) \boxplus_r L(u_2^k) &= \ln \frac{\Pr(u_r^k=0)}{\Pr(u_r^k=1)} \\ &= \ln \frac{1-p}{p} + \ln \frac{1+\exp[L(u_1^k)+L(u_2^k)]}{\exp[L(u_1^k)]+\exp[L(u_2^k)]}, \end{aligned} \tag{5.39}$$

where $\boxplus_r$ denotes the modified version of the boxplus operation for updating the LLR values of $\mathbf{u}_r$, based on the LLR values of $\mathbf{u}_1$ and $\mathbf{u}_2$, which corresponds to the black square in Fig. 5.8. It can be observed from (5.39) that the correlation between $\mathbf{u}_1$ and $\mathbf{u}_2$ has now been exploited.

Modified Boxplus Operation for Source Node

Since the LLR updating rules for the source node is different from that of the relay node, let us demonstrate the derivation process for the LLR updating function for the signal transmitted from S_1. In the same way as $\boxplus_r$ was derived, we can obtain the following equations:

$$\begin{aligned}\Pr(u_1^k=0) &= \Pr(u_r^k=0,u_2^k=0)+\Pr(u_r^k=1,u_2^k=1)\\ &= \Pr(u_r^k=0)\cdot\Pr(u_2^k=0)\cdot(1-p)+\Pr(u_r^k=1)\cdot\Pr(u_2^k=1)\cdot p,\end{aligned} \tag{5.40}$$

$$\begin{aligned}\Pr(u_1^k=1) &= \Pr(u_r^k=0,u_2^k=1)+\Pr(u_r^k=1,u_2^k=0)\\ &= \Pr(u_r^k=0)\cdot\Pr(u_2^k=1)\cdot(1-p)+\Pr(u_r^k=1)\cdot\Pr(u_2^k=0)\cdot p,\end{aligned} \tag{5.41}$$

where u_1^k, u_2^k and u_r^k denotes the k-th symbol of $\mathbf{u}_1$, $\mathbf{u}_2$ and $\mathbf{u}_r$, respectively. It can be obtained from (5.40) and (5.41) that the LLR updating function for u_1^k is

$$\begin{aligned}L(u_1^k) &= L(u_r^k)\boxplus_s L(u_2^k)=\ln\frac{\Pr(u_1^k=0)}{\Pr(u_1^k=1)}\\ &= \ln\frac{p+(1-p)\cdot\exp[L(u_r^k)+L(u_2^k)]}{(1-p)\cdot\exp[L(u_r^k)]+p\cdot\exp[L(u_2^k)]},\end{aligned} \tag{5.42}$$

where $\boxplus_s$ denotes the modified version of boxplus operation for updating the LLR values of $\mathbf{u}_1$, which corresponds to the gray square in Fig. 5.8. The LLR updating function for S_2 can be derived in the same way.

In summary, the GI operation of the proposed decoder, as shown in Fig. 5.8, can be expressed as:

$$\begin{cases} L_a(\mathbf{u}_r)=L_e(\mathbf{u}_1)\boxplus_r L_e(\mathbf{u}_2),\\ L_a(\mathbf{u}_1)=L_e(\mathbf{u}_r)\boxplus_s L_e(\mathbf{u}_2),\\ L_a(\mathbf{u}_2)=L_e(\mathbf{u}_r)\boxplus_s L_e(\mathbf{u}_1).\end{cases} \tag{5.43}$$

By performing GI operations with the modified boxplus functions, the extrinsic LLRs are updated, which take into account both the impact of the source correlation and XOR network coding at the relay.

Extreme Cases Consideration

Note that in the case $p = 0.5$, indicating that the two sources being uncorrelated, the modified boxplus operations, $\boxplus_r$ and $\boxplus_s$, are both equivalent to the original boxplus operation $\boxplus$. Furthermore, if the relay node does not help in the decoding process, which is corresponding to the case $L_e^R(\mathbf{u}_r)=0$, the modified boxplus operation $\boxplus_s$ is equivalent to the original f_c function defined in (4.33).

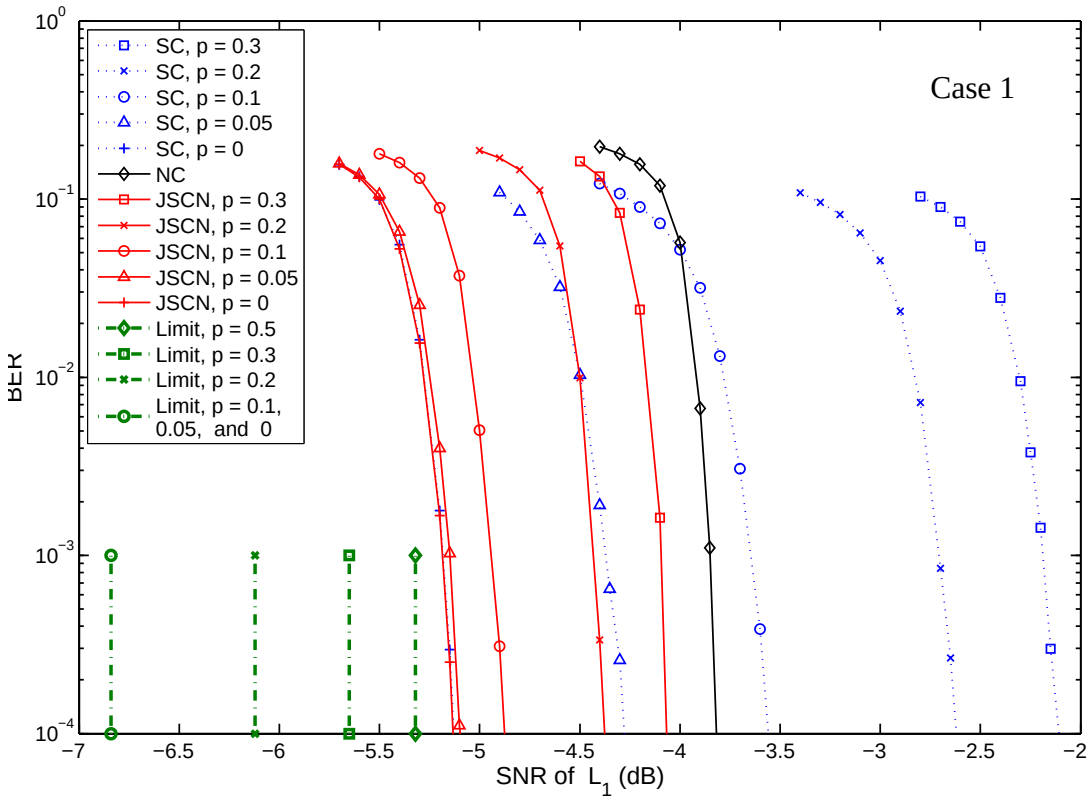

Figure 5.9: BER performance of the proposed JSCN technique for MARC with correlated sources in Case 1, with respect to the SNR of L_1. Different source correlation are considered.

5.4 Numerical Results

5.4.1 BER Performance in AWGN Channels

In this subsection, we evaluate the BER performance of the proposed technique in AWGN channels. Note that the BER performance is averaged over S_1 and S_2. In our simulations, the doping rates were set as $Q_1 = Q_2 = Q_R = 1$. We performed GI after every LI, and the whole process was repeated 20 times.

The frame length is set at $10,000$ bits, and 1000 different frames were transmitted from each source node. To demonstrate the performance gains achieved by the exploitation of correlation between the two sources, the BER curve of conventional XOR network coding based MARC that does not exploit source correlation is also provided, which is denoted by "NC". In this conventional MARC, the original boxplus operation of (5.36) is used for extrinsic information exchange during the joint channel-network decoding process. As a reference, the BER performance of the system that does not utilize network coding (without relay node) but only exploits the source correlation by using the f_c function defined in (4.33) is also provided in the same figure, which is denoted as "SC".

The BER performance of the proposed system in *Case 1* is depicted in Fig. 5.9. It can be observed that the BER performance of our JSCN coding scheme provides significant gain over both "SC" and "NC". It should be emphasized here that as the source correlation becomes larger, the gain over "NC" increases while the gain over "SC" decreases. However, even with a relative small p value ($p = 0.05$), still considerable gains can be achieved

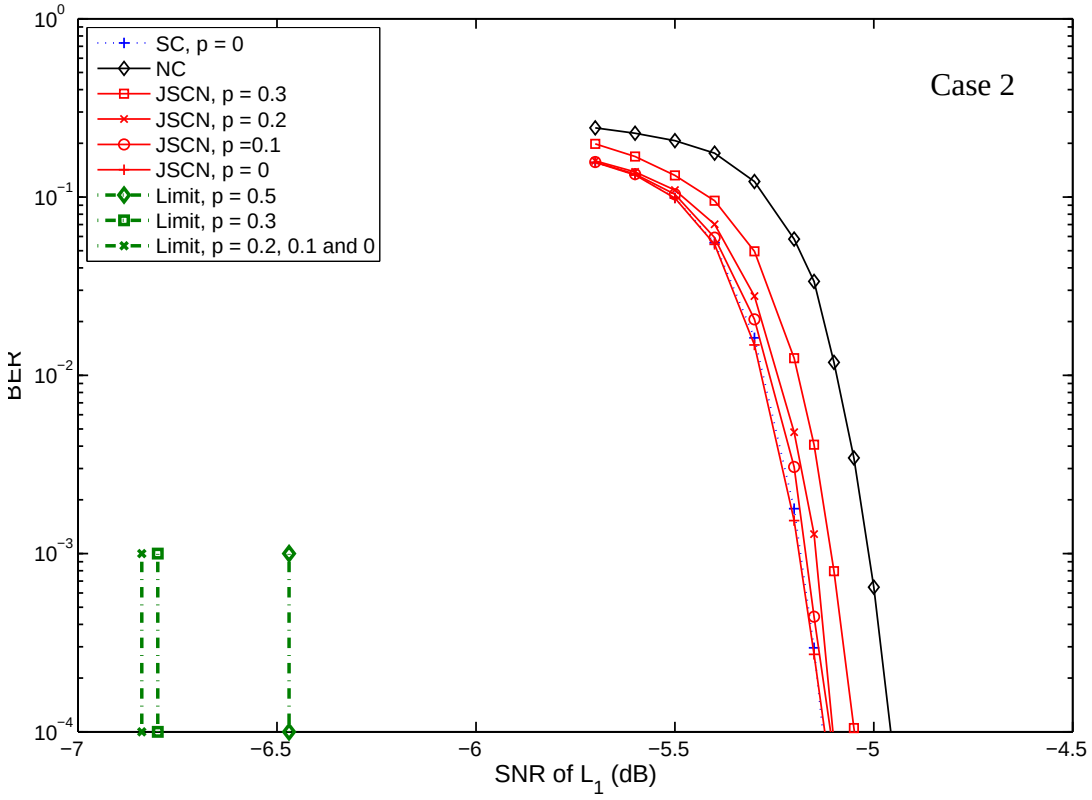

Figure 5.10: BER performance of the proposed JSCN technique for MARC with correlated sources in Case 2, with respect to the SNR of L_1. Different source correlation are considered.

over "SC". If the two sources are fully correlated ($p = 0$), the BER performance of the proposed JSCN technique and that of "SC" are the same. Because in this case, the modified boxplus operation $\boxplus_s$ used in JSCN and the f_c function used in "SC" become equivalent, as described in Subsection 5.3.3.

Fig. 5.10 shows the BER performance of the proposed system in *Case 2*. As can be seen from the figure, if $p = 0$, the BER performance of the proposed system is the same as that in *Case 1*. This is because the modified boxplus operation $\boxplus_s$ becomes equivalent to the f_c function used in "SC" if $p = 0$, which means $\boxplus_s$ does not take any help from the relay node. For $p = 0.3, 0.2$ and 0.1, the performance are quite close to that with $p = 0$.

The performance limits of our system in AWGN channels with some different source correlations (different p value) are summarized in Table 5.1, for both *Case 1* and *Case 2*. It should be noted here that the limits for $p = 0.1, 0.05$ and 0 in *Case 1* are the same (-6.84 dB). This is because the limit is dominated by the source-destination links for $p \leq 0.1$, as shown in Fig. 5.6. Similar phenomena can be observed in *Case 2*, and hence in this case the limits for $p = 0.2, 0.1, 0.05$ and 0 are the same. The performance gains over "NC" and "SC", as well as the gaps to the theoretical limits with our proposed technique in both *Case 1* and *Case 2* are also summarized in Table 5.1, at BER $= 10^{-4}$. Note that the gaps between the theoretical limits and the BER performance of our proposed JSCN technique are roughly $1-2$ dB. This is because we are not using very close-limit achieving codes for per-link transmission in this subsection. As shown in [96, 140], however, proper tuning of the doping rates Q_1, Q_2 and Q_r may result in even smaller gap to the limit.

Table 5.1: Performance Gains and Gaps to the Theoretical Limits for the Proposed JSCN Coding Scheme, at the BER level of 10^{-4}.

		p	Limits (dB)	Gains (dB)		Gaps (dB)
				over NC	over SC	
Case 1	NC	0.5	-5.32	-	-	1.5
	JSCN	0.3	-5.65	0.25	1.96	1.58
		0.2	-6.12	0.55	1.75	1.75
		0.1	-6.84	1.06	1.32	1.96
		0.05	-6.84	1.17	0.81	1.75
		0	-6.84	1.31	0	1.71
Case 2	NC	0.5	-6.47	-	-	1.52
	JSCN	0.3	-6.80	0.1	2.94	1.75
		0.2	-6.84	0.15	2.48	1.74
		0.1	-6.84	0.16	1.55	1.73
		0	-6.84	0.18	0	1.71

5.4.2 FER Performance in Rayleigh Fading Channels

In this subsection, the numerical results of the theoretical outage probability calculation and the FER performance of the proposed JSCN technique obtained through simulations are presented. The frame length is set at 2000 bits, and 100, 000 different frames were transmitted from each source node.

Fig. 5.11 demonstrates the theoretical outage curves and the FER performance of the proposed system in *Case 1*, with different source correlations. It is found that, as the source correlation becomes stronger, the theoretical outage probability decreases, since the source correlation can be exploited at the destination. Similarly, we can observe that the larger the source correlation, the larger the FER performance improvement by using the proposed JSCN technique. For the given p value, there is around $1-2$ dB gap between the FER curve obtained through simulations and the theoretical outage curve. This is because the channel codes used for the three links L_1, L_2 and L_r can not achieve very close limit performance, as indicated in Subsection 5.4.1. The theoretical outage curve of the P2P transmission, of which decay corresponds to no-diversity, are also provided in the same figure.

The theoretical outage curves and the FER performance of the proposed system in *Case 2* are illustrated in Fig. 5.12. The FER and theoretical outage curves exhibit the same decay as the $2nd$ order diversity. The gaps between the FER simulation results and their corresponding theoretical outage curves are around $1 - 2$ dB. Note that if $p = 0$, the theoretical outage curve in *Case 2* is the same as that obtained in *Case 1*, which is consistent to the mathematical proof presented in Subsection 5.2.5. Furthermore, the FER curve for $p = 0$ in *Case 2* is almost the same as that obtained in *Case 1*, which also agrees with the results shown in Subsection 5.4.1.

The outage probability analysis of two correlated sources transmission without network coding in block Rayleigh fading channels is presented in [99], where it is shown that the $2nd$ order diversity can be achieved only if the two sources are correlated, and the decay asymptotically converges into no-diversity if the two sources are not fully correlated. However, It can be seen from Figs. 5.11 and 5.12 that the $2nd$ order diversity can be

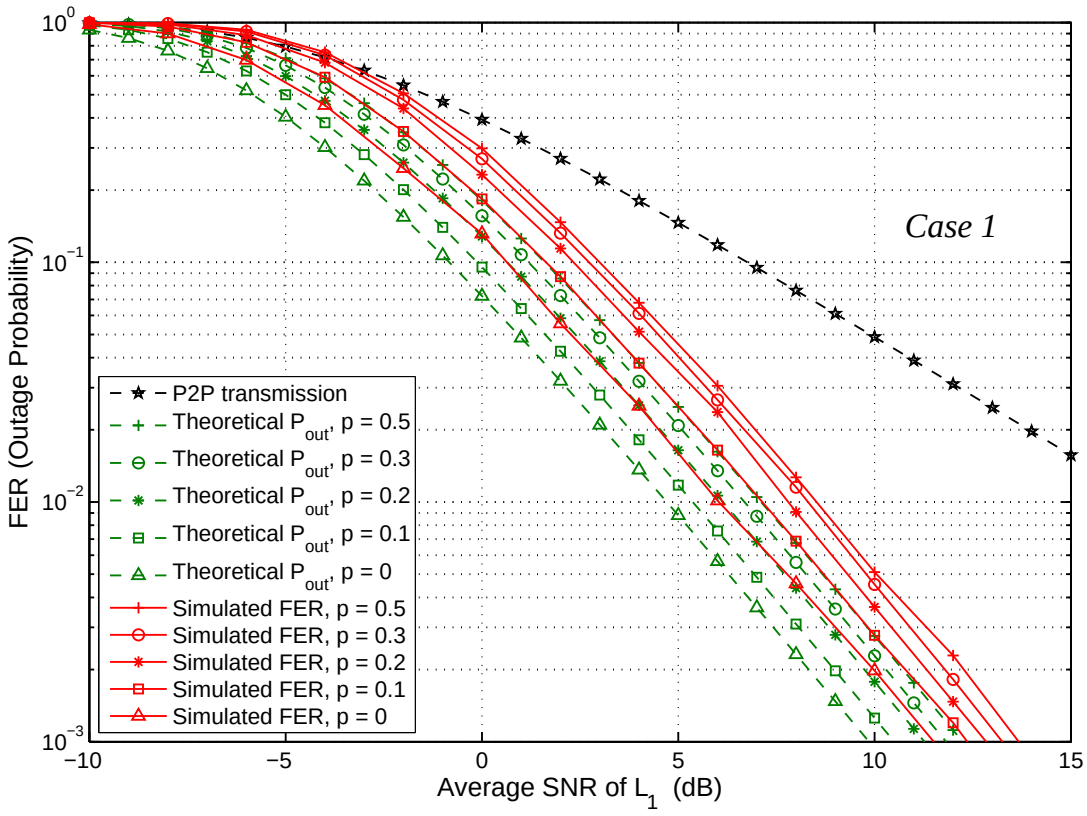

Figure 5.11: FER performance of the proposed JSCN technique for MARC with correlated sources in *Case 1*, with respect to the average SNR of L_1. Different source correlation are considered.

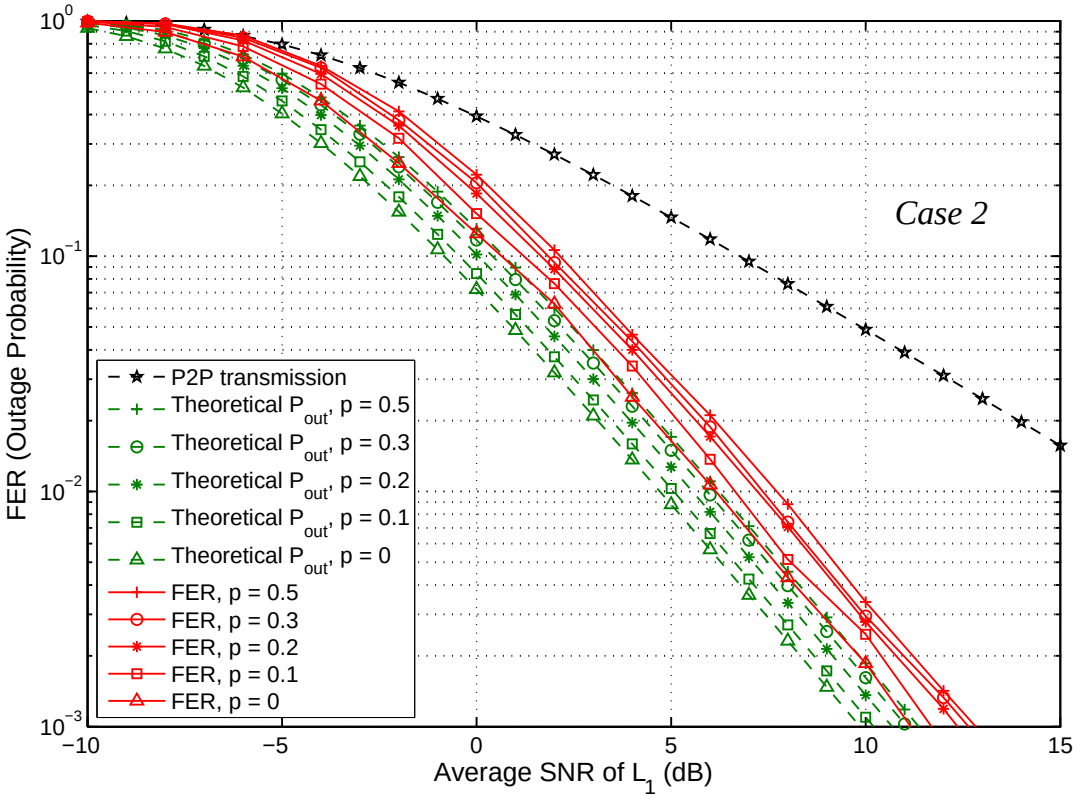

Figure 5.12: FER performance of the proposed JSCN technique for MARC with correlated sources in *Case 2*, with respect to the average SNR of L_1. Different source correlation are considered.

always achieved, regardless of the p value.

It can also be observed from Figs. 5.11 and 5.12 that, as the quality of the L_r is improved (Δ increases), the theoretical outage probability with $p \in (0, 0.5]$ converges into the theoretical outage probability with $p = 0$, which is consistent to the asymptotic tendency analysis provided in Subsection 5.2.5. It is expected that if the quality of L_r is good enough, the difference in theoretical outage curves due to different p values becomes very minor. Similar tendency can be observed in the FER performance curves obtained through simulations.

5.5 Summary

The problem of transmitting two correlated sources over orthogonal MARC has been intensively investigated in this chapter, where the correlation between the two sources is exploited at the destination node.

The achievable compression rate region has been studied according to the theorem for source coding with side information. It is found that the compression rate region has a three-dimensional structure, which is specified by the space surrounded by the polyhedron. The theoretical limits for the BER performance and the outage probability of our system in AWGN channels and Rayleigh fading channels, respectively, have been calculated based on the achievable compression rate region. The asymptotic analysis shows that, the outage probability is only determined by the quality of source-destination links if the two sources are fully correlated. Moreover, if the two sources are not fully correlated, the outage probability asymptotically converges into that obtained by assuming the two sources are fully correlated, as the average SNR of the relay-destination link increases.

We then proposed a practical coding/decoding scheme for the problem considered. In order to fully exploit the source correlation while still exploiting the benefit of XOR network coding, an iterative JSCN decoding technique, which involves modified versions of the boxplus operation, was proposed for extrinsic information exchange at the destination.

A series of simulations based on some practical channel codes was conducted to verify the effectiveness of the proposed JSCN decoding technique and the results obtained from theoretical analyses. In the simulations, the two source nodes are located at the same distance to the destination node. Two different cases about the relay location were considered; in *Case 1* the relay has the same distance to the destination node, and in *Case 2* the relay is located closer to the destination node. The BER and FER performance results show that the proposed JSCN technique achieves considerable gains over conventional MARC where the source correlation knowledge is not exploited. However, since the quality of the relay-destination link in *Case 2* is better than that in *Case 1*, the gains in *Case 2* is less than that achieved in *Case 1*. It is also found that the $2nd$ order diversity can always be achieved, regardless of the strength of the source correlation. The simulation results and the theoretical limit analysis are consistent with each other.

Besides XOR network coding, some other network cooperative strategies can also be used at the relay node, such as superposition coding [141,142]. Even though we know that there are a lot of pros-and-cons comparisons/discussions of those techniques [143–145], we are not intended to be involved in such investigations, because the superiority/inferiority is at large depending on the viewpoints.

Chapter 6

Conclusions and Outlook

6.1 Conclusions

In this dissertation, we have investigated cooperative wireless communications by focusing on exploiting the multi-dimensional correlation among multiple sources. The objective of this research is to create theoretical bases and to develop practical coding/decoding framework that best utilize the correlation knowledge among the distributed multiple sources. In particular, we focused on three representative problems in cooperative wireless communications to illustrate the impact of source correlation on the system performance and how the correlation knowledge among the distributed multiple sources can be best utilized. For each problem, the research is comprised of the following phases:

1. Information theoretical limits analysis.
2. Practical code design and decoding algorithm development that exploits the correlation knowledge.
3. Performance evaluation of the proposed techniques through simulations.
4. Accuracy verification of the theoretical limits obtained in (1).

The first problem we considered was binary Markov source transmission in conventional P2P communication systems. The design concepts and the algorithms are the basis for solving similar problem that may arising in cooperative wireless communications. The achievable compression rate region was determined by the source coding theorem, which should be larger than the entropy of the Markov source. Then the performance limits in AWGN channels and the outage probability in block Rayleigh fading channels were derived. A new JSC decoding scheme based on SCCC was proposed to fully exploit the source memory. A modified version of BCJR algorithm was derived to perform joint decoding of the Markov source and the outer code. To further approach the performance limits, coding doping is employed for inner code. Furthermore, the code parameters, including generator polynomials of the outer and inner codes, and the doping rate of the inner code, were optimized based on EXIT chart analysis.

We then applied the results obtained from the first problem to the second problem that we investigated, which is binary Markov source transmission in a one-way relay system. The relay does not aim to complete eliminate the errors occurring in the source-relay link. Instead, ErF relaying strategy is used for reducing the computational complexity

of the relay. The error probability of the source-relay link is regarded as source-relay correlation. Therefore, there are two dimensional correlation, one is the Markov source memory and the other is the source-relay correlation. The achievable compression rate region of this system was derived based on the Slepian-Wolf theorem. The lower bound of the performance limits in AWGN channels and the outage probability in block Rayleigh fading channels were derived based on the achievable compression rate region, by assuming no error occurs in the source-relay link. We proposed a DJSC decoding scheme to exploit the source-relay correlation and the source memory simultaneously. The JSC technique proposed in the first problem is used to exploit the source memory, while the LLR updating function is used to estimate and exploit the source-relay correlation. The convergence property of the proposed DJSC technique was evaluated through 3D EXIT chart analysis.

The third problem we investigated was correlated source transmission over MARC, where two source nodes are communicating with a common destination with the help of a single relay node. The source-relay link was assumed to be error free and XOR network coding was employed at the relay. The achievable compression rate region of this system was derived based on the theorem for lossless source coding with side information. The performance limits in AWGN channels and the outage probability in block Rayleigh fading channels were derived based on the achievable compression rate region. A JSCN decoding scheme was then proposed to fully exploit the correlation between the two sources, while still maintain the benefit of network coding.

In the three problems, the effectiveness of the proposed JSC, DJSC and JSCN techniques in terms of the BER performance in AWGN channels and the FER performance in block Rayleigh fading channels were verified through a series of simulations. It has been found from the simulation results that, the theoretical limits are consistent with the BER and FER performance. The impacts of source correlation on the performance of the corresponding systems were investigated through asymptotic tendency analysis, and further verified through simulation results. By exploiting source correlations, the outage probability of the three systems can be reduced significantly (FER performance are improved). However, by exploiting the memory structure of Markov source, no diversity gain can be achieved in the first and second problems. In the second problem, if the information sent from the source and relay are fully correlated, $2nd$ order diversity can be achieved; otherwise, the outage probability asymptotically converges into no diversity. In the third problem, $2nd$ order diversity can always be achieved because of the network coding, however no additional diversity gain can be achieved by exploiting the correlation between the two sources.

The three problems considered in this thesis are quite simple, however, with the aim of seeking for the mathematical strictness of the derivations. It is expected that the results obtained in this research can be extended to more complicate forms of cooperative wireless communications.

6.2 Future Work

To apply the results obtained from the investigation of the three problems to more general cooperative wireless communications, there are several issues left as future work, which are listed as follow.

- In the problem of Markov source transmission in P2P communications, the code op-

timization was performed by manually examining the EXIT curve matching of the outer and inner codes, yielding in sub-optimality of the code. Therefore, employing more sophisticated optimization techniques, such as EXIT-constrained Switching Algorithm (EBSA) [146], to obtain the best code parameters for this problem should be an interesting extension. Moreover, in the problems of Markov source transmission in one-way relay system and correlated sources transmission over MARC, the code parameters were chose empirically in this thesis. The code parameters optimization in those two problems is also left as future study.

- In the problem of Markov source transmission in one-way relay system, only lower bound of the theoretical limits were derived, where the error probability occurring in the source-relay link was assumed to be 0, when deriving the theoretical limits. However, in practice, the error probability varies with the quality of the source-relay link. Tighter bound of the theoretical limits can be derived, if the relationship between the error probability and the SNR of the source-relay link can be explicitly defined.

- In the problem of correlated sources transmission over MARC, the source-relay links are assumed to be error free. However, in practical applications, errors may happen in the source-relay links. A technique that takes into account the errors happening in the source-relay links is presented in [133]. The results presented in [133] can straightforwardly be extended to the rate region analysis, as well as the outage calculation. However, it requires multiple integrals with respect to the pdf of multiple link's variations. This is also left as future work.

- Extension to full-duplex relay and non-orthogonal channels scenarios is an interesting and challenging topic. With full-duplex relay and non-orthogonal channels, the channels are not independent and the channel capacity is specified by the multiple Access Channel (MAC) capacity region [114]. Derivation of the theoretical limits in this scenario is still an open research problem to be solved.

- In this thesis, we only consider the lossless source coding problem. Thus an interesting research direction would be the extension to lossy source coding. Wyner and Ziv have defined the rate-distortion function for lossy source coding with side information [18], which can be used for deriving the theoretical limits at a given distortion level. However, based on the network information theory, the rate-distortion function for more then two sources is still an open question.

- Another interesting extension is to consider more general network topologies and other relay strategies. Based on different network topologies and cooperative strategies, optimal resource allocation policies can be derived under the performance limits criteria and rate-distortion constraints to achieve significant performance gains.

Appendix A

Approximation for the Entropy Rate of a Hidden Markov Process

Let $X = \{X_k\}_{k=1}^{\infty}$ be a first-order stationary binary Markov process, with the state transition probability $\pi_{ab} = \Pr\{X_{k+1=b}|X_k = a\},\ a, b \in \{0, 1\}$. The state transition matrix of X can be expressed as

$$A = \begin{bmatrix} 1-\pi_{01} & \pi_{01} \\ \pi_{10} & 1-\pi_{10} \end{bmatrix}, \quad 0 \leq \pi_{01}, \pi_{10} \leq 1. \tag{A.1}$$

Define a random process $Z = \{Z_k\}_{k=1}^{\infty}$ with $Z_k = X_k \oplus E_k$, where $\oplus$ is modulus-2 addition, and E_k is generated from a Bernoulli process which is independent of X_K and satisfies $\Pr\{E_k = 1\} = \epsilon$. Therefore, $\{Z_k\}_{k=1}^{\infty}$ can be regarded as the observation of $\{X_k\}_{k=1}^{\infty}$ through a binary symmetric channel.

For the sake of simplicity, we only consider symmetric Markov process, i.e., $\pi_{01} = \pi_{10} = \pi$. Since the entropy rate of X is symmetric on π, we assume that $0 \leq \pi \leq 0.5$ without loss of generality. Define the log-likelihood process as

$$l_k = \log \frac{\Pr\{X_{k+1} = 1|Z_1^k\}}{\Pr\{X_{k+1} = 0|Z_1^k\}}, \tag{A.2}$$

where Z_1^k denotes the sub-sequence of Z from the time index 1 to k. It has been proved that l_k can be derived by the standard forward recursions as

$$l_k = (2Z_k - 1) \log \frac{1-\epsilon}{\epsilon} + f(l_{k-1}), \tag{A.3}$$

where $f(x) = \log \frac{e^x(1-\pi)+\pi}{e^x\pi+(1-\pi)}$. Then the entropy rate of Z can be expressed as

$$H(Z) = H(\pi, \epsilon) = \lim_{k\to\infty} H(Z_{k+1}|Z_1^k) = E\left[H_b\left(\frac{e^{l_k}}{1+e^{l_k}} * \pi * \epsilon\right)\right], \tag{A.4}$$

with $H_b(x) = -x\log_2(x) - (1-x)\log_2(1-x)$ and $*$ denoting binary convolution defined by $p * q = (1-p)q + p(1-q)$.

A derivation of the approximated entropy rate, which is based on approximating the stationary distribution of l_k, has been proposed in [129]. Consider a finite-state Markov process with M states evolving according to

$$Y_k = Q\left[r_k \log \frac{1-\epsilon}{\epsilon} + s_k f(Y_{k-1})\right], \tag{A.5}$$

where r_k and s_k are i.i.d. sequences independent of Y, with the property $\Pr\{r_k = -1\} = 1 - \Pr\{r_k = 1\} = \epsilon$ and $\Pr\{s_k = -1\} = 1 - \Pr\{s_k = 1\} = \pi$, respectively. Q denotes a M-level uniform quantizer defined in the interval $\left[-\log\frac{(1-\pi)(1-\epsilon)}{\pi\epsilon}, \log\frac{(1-\pi)(1-\epsilon)}{\pi\epsilon}\right]$. The approximation algorithm is summarized in Algorithm 1.

Algorithm 1 Entropy rate approximation algorithm

Input:

The transition probability of Markov chain, π.

The observation error probability, ϵ.

A uniform quantizer Q defined in the interval $\left[-\log\frac{(1-\pi)(1-\epsilon)}{\pi\epsilon}, \log\frac{(1-\pi)(1-\epsilon)}{\pi\epsilon}\right]$ with M levels. The quantization levels are $q_1, q_2, \cdots, q_M$.

Output: The estimate of the entropy rate, $\hat{H}$.

1: Construct a $M \times M$ stochastic matrix P_M, of which the elements are defined as

$$P_M(i,j) = \begin{cases} (1-\pi)(1-\epsilon), & \text{if} \quad q_j = Q\left(\log\frac{1-\epsilon}{\epsilon} + f(q_i)\right), \\ (1-\pi)\epsilon, & \text{if} \quad q_j = Q\left(-\log\frac{1-\epsilon}{\epsilon} + f(q_i)\right), \\ \pi(1-\epsilon), & \text{if} \quad q_j = Q\left(\log\frac{1-\epsilon}{\epsilon} - f(q_i)\right), \\ \pi\epsilon, & \text{if} \quad q_j = Q\left(-\log\frac{1-\epsilon}{\epsilon} - f(q_i)\right), \\ 0, & \text{otherwise}, \end{cases} \qquad 1 \le i, j \le M. \tag{A.6}$$

2: Compute stationary distribution of P_M, i.e., find a M-dimensional row vector that satisfies $a_M \cdot P_M = a_M$.

3: Calculate the estimate of the entropy rate by

$$\hat{H} = \sum_{i=1}^{M} a_M(i) \cdot H_b\left(\frac{e^{q_i}}{1+e^{q_i}} * \pi * \epsilon\right). \tag{A.7}$$

4: **return** $\hat{H}$.

Using Algorithm 1, we can numerically estimate the entropy rate of a hidden Markov process, which is shown in Fig. A.1. It can be seen from the figure that the entropy rate is a function of the transition probability π and observation error probability ϵ. Note that increasing M can make the estimate of entropy rate more accurate, and M is set as 1000 in our simulations.

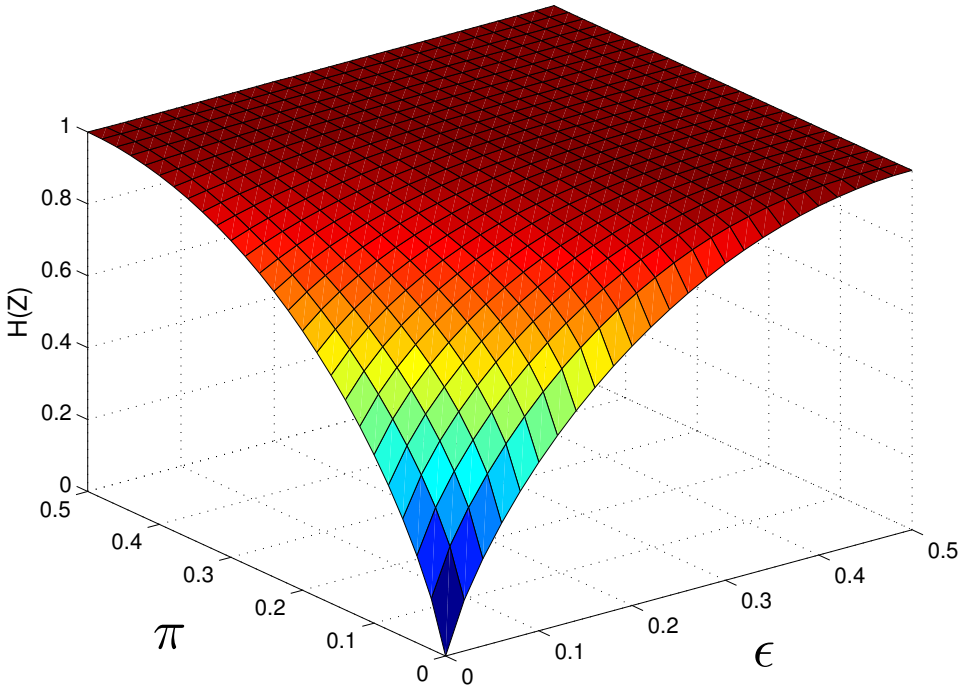

Figure A.1: The entropy rate a hidden Markov process as a function of the transition probability π and the observation error probability ϵ.

Bibliography

[1] M. Abrar, X. Gui, A. Punchihewa, S. Khan, and M. Iqbal, "Cooperative diversity versus antenna diversity in wireless communication systems," in *New Trends in Information Science and Service Science (NISS), 2010 4th International Conference on*, 2010, pp. 260–263.

[2] Y. Li, "Distributed coding for cooperative wireless networks: An overview and recent advances," *IEEE Communications Magazine*, vol. 47, no. 8, pp. 71–77, 2009.

[3] J. Mietzner, R. Schober, L. Lampe, W. H. Gerstacker, and P. A. Hoeher, "Multiple-antenna techniques for wireless communications - a comprehensive literature survey," *IEEE Communications Surveys & Tutorials*, vol. 11, no. 2, pp. 87–105, 2009.

[4] Y. Zhang, H.-H. Chen, and M. Guizani, *Cooperative wireless communications*. Auerbach Publications, 2009.

[5] K. R. Liu, A. K. Sadek, W. Su, and A. Kwasinski, *Cooperative communications and networking*. Cambridge University Press, 2009.

[6] P. Liu, Z. Tao, Z. Lin, E. Erkip, and S. S. Panwar, "Cooperative wireless communications: a cross-layer approach," *IEEE Wireless Communications Magazine*, vol. 13, no. 4, pp. 84–92, 2006.

[7] Q. Li, R. Q. Hu, Y. Qian, and G. Wu, "Cooperative communications for wireless networks: techniques and applications in LTE-advanced systems," *IEEE Wireless Communications Magazine*, vol. 19, no. 2, pp. 22–29, 2012.

[8] E. C. van der Meulen, "Three-terminal communication channels," *Advanced Applied Probability*, vol. 3, pp. 120–154, 1971.

[9] T. M. Cover and A. E. Gamal, "Capacity theorems for the relay channel," *IEEE Transactions on Information Theory*, vol. 25, no. 5, pp. 572–584, 1979.

[10] Y.-W. W. P. Hong, W.-J. Huang, F.-H. Chiu, and C.-C. C. J. Kuo, "Cooperative communications in resource-constrained wireless networks," *IEEE Signal Processing Magazine*, vol. 24, no. 3, pp. 47–57, 2007.

[11] G. Kramer, M. Gastpar, and P. Gupta, "Cooperative strategies and capacity theorems for relay networks," *IEEE Transactions on Information Theory*, vol. 51, no. 9, pp. 3037–3063, 2005.

[12] L. J.N., D. N. C. Tse, and G. W. Wornell, "Cooperative diversity in wireless networks: Efficient protocols and outage behavior," *IEEE Transactions on Information Theory*, vol. 50, no. 12, pp. 3062–3080, 2004.

[13] J.-w. Han, H.-j. Ju, K.-M. M. Kim, S.-Y. Chun, and K.-C. Dho, "A study on the cooperative diversity technique with amplify and forward for underwater wireless communication," in *OCEANS 2008 - MTS/IEEE Kobe Techno-Ocean*, 2008, pp. 1–3.

[14] F. Lin, Q. Li, T. Luo, and G. Yue, "Impact of relay location according to ser for amplify-and-forward cooperative communications," in *Anti-counterfeiting, Security, Identification, 2007 IEEE International Workshop on*, 2007, pp. 324–327.

[15] A. Chakrabarti, E. Erkip, A. Sabharwal, and B. Aazhang, "Code designs for cooperative communication," *IEEE Signal Processing Magazine*, vol. 24, no. 5, pp. 16–26, 2007.

[16] R. Hu and J. Li, "Practical compress-forward in user cooperation: Wyner-Ziv cooperation," in *Information Theory, 2006 IEEE International Symposium on*, 2006, pp. 489–493.

[17] Z. Liu, V. Stankovic, and Z. Xiong, "Wyner-Ziv coding for the half-duplex relay channel," in *Acoustics, Speech, and Signal Processing, 2005. Proceedings. (ICASSP '05). IEEE International Conference on*, vol. 5, 2005.

[18] A. D. Wyner and J. Ziv, "The rate-distortion function for source coding with side information at the decoder," *IEEE Transactions on Information Theory*, vol. 22, no. 1, pp. 1–10, 1976.

[19] A. Stefanov and E. Erkip, "Cooperative coding for wireless networks," *IEEE Transactions on Communications*, vol. 52, no. 9, pp. 1470–1476, 2004.

[20] Z. Zhang and T. M. Duman, "Capacity-approaching Turbo coding and iterative decoding for relay channels," *IEEE Transactions on Communications*, vol. 53, no. 11, pp. 1895–1905, 2005.

[21] ——, "Capacity-approaching turbo coding for half-duplex relaying," *IEEE Transactions on Communications*, vol. 55, no. 10, pp. 1895–1906, 2007.

[22] B. Zhao and M. C. Valenti, "Distributed turbo coded diversity for relay channel," *Electronics Letters*, vol. 39, no. 10, pp. 786–787, 2003.

[23] J. Hu and T. M. Duman, "Low density parity check codes over wireless relay channels," *IEEE Transactions on Wireless Communications*, vol. 6, no. 9, pp. 3384–3394, 2007.

[24] A. Chakrabarti, A. de Baynast, A. Sabharwal, and B. Aazhang, "Low density parity check codes for the relay channel," *IEEE Journal on Selected Areas in Communications*, vol. 25, no. 2, pp. 280–291, 2007.

[25] A. Abu Al Haija and M. Vu, "A half-duplex cooperative scheme with partial decode-forward relaying," in *Information Theory Proceedings (ISIT), 2011 IEEE International Symposium on*, 2011, pp. 1886–1890.

[26] U.-K. Kwon, C.-H. Choi, and G.-H. Im, "Full-rate cooperative communications with spatial diversity for half-duplex uplink relay channels," *IEEE Transactions on Wireless Communications*, vol. 8, no. 11, pp. 5449–5454, 2009.

[27] S. Vishwanath, S. Jafar, and S. Sandhu, "Half-duplex relays: cooperative communication strategies and outer bounds," in *Wireless Networks, Communications and Mobile Computing, 2005 International Conference on*, vol. 2, 2005, pp. 1455–1459.

[28] H. Wicaksana, S. H. Ting, Y. L. Guan, and X.-G. Xia, "Decode-and-forward two-path half-duplex relaying: Diversity-multiplexing tradeoff analysis," *IEEE Transactions on Communications*, vol. 59, no. 7, pp. 1985–1994, 2011.

[29] A. H. Bastami and A. Olfat, "Selection relaying schemes for cooperative wireless networks with adaptive modulation," *IEEE Transactions on Vehicular Technology*, vol. 60, no. 4, pp. 1539–1558, 2011.

[30] Y. Fan, C. Wang, H. V. Poor, and J. S. Thompson, "Cooperative multiplexing: Toward higher spectral efficiency in multiple-antenna relay networks," *IEEE Transactions on Information Theory*, vol. 55, no. 9, pp. 3909–3926, 2009.

[31] M. J. Abdoli, A. Ghasemi, and A. K. Khandani, "Full-duplex transmitter cooperation, feedback, and the degrees of freedom of SISO Gaussian interference and x channels," in *Information Theory Proceedings (ISIT), 2012 IEEE International Symposium on*, 2012, pp. 3120–3124.

[32] T. M. Kim and A. Paulraj, "Outage probability of amplify-and-forward cooperation with full duplex relay," in *Wireless Communications and Networking Conference (WCNC), 2012 IEEE*, 2012, pp. 75–79.

[33] I. Krikidis, H. A. Suraweera, and C. Yuen, "Amplify-and-forward with full-duplex relay selection," in *Communications (ICC), 2012 IEEE International Conference on*, 2012, pp. 3532–3537.

[34] C. G. Tsinos and K. Berberidis, "Multi-antenna cooperative systems with improved diversity multiplexing tradeoff," in *Wireless Communications and Networking Conference (WCNC), 2012 IEEE*, 2012, pp. 1093–1097.

[35] I. Krikidis, H. A. Suraweera, P. J. Smith, and C. Yuen, "Full-duplex relay selection for amplify-and-forward cooperative networks," *IEEE Transactions on Wireless Communications*, vol. 11, no. 12, pp. 4381–4393, 2012.

[36] A. Ikhlef, J. Kim, and R. Schober, "Mimicking full-duplex relaying using half-duplex relays with buffers," *IEEE Transactions on Vehicular Technology*, vol. 61, no. 7, pp. 3025–3037, 2012.

[37] S. Bakim and O. Kaya, "Power control for two user cooperative OFDMA channels," *IEEE Transactions on Wireless Communications*, vol. 12, no. 1, pp. 258–267, 2013.

[38] H. Dogan, "Maximum a posteriori channel estimation for cooperative diversity orthogonal frequencydivision multiplexing systems in amplify-andforward mode," *IET Communications*, vol. 3, no. 4, pp. 501–511, 2009.

[39] Z. Li, X.-G. Xia, and M. H. Lee, "A simple orthogonal space-time coding scheme for asynchronous cooperative systems for frequency selective fading channels," *IEEE Transactions on Communications*, vol. 58, no. 8, pp. 2219–2224, 2010.

[40] S. Ma and J.-K. Zhang, "Noncoherent orthogonal distributed space-time block codes for amplify-and-forward half-duplex cooperative relay channels," *IEEE Transactions on Vehicular Technology*, vol. 61, no. 6, pp. 2854–2858, 2012.

[41] C. Y. Ng, K. W. Shum, C. W. Sung, and T. M. Lok, "Rate allocation for cooperative orthogonal-division channels with dirty-paper coding," *IEEE Transactions on Communications*, vol. 58, no. 10, pp. 2949–2959, 2010.

[42] L. Weng and R. D. Murch, "Cooperation strategies and resource allocations in multiuser OFDMA systems," *IEEE Transactions on Vehicular Technology*, vol. 58, no. 5, pp. 2331–2342, 2009.

[43] Y. Yao and X. Dong, "Multiple cfo mitigation in amplify-and-forward cooperative OFDM transmission," *IEEE Transactions on Communications*, vol. 60, no. 12, pp. 3844–3854, 2012.

[44] G. Zheng, Y. Zhang, C. Ji, and K.-K. Wong, "A stochastic optimization approach for joint relay assignment and power allocation in orthogonal amplify-and-forward cooperative wireless networks," *IEEE Transactions on Wireless Communications*, vol. 10, no. 12, pp. 4091–4099, 2011.

[45] C.-H. Choi, Y.-J. Kim, and G.-H. Im, "Bit-interleaved coded transmission with multilevel modulation for non-orthogonal cooperative systems," *IEEE Transactions on Communications*, vol. 59, no. 1, pp. 95–105, 2011.

[46] S. Kim, S. Choi, and D.-J. Park, "Optimal beamforming with combining for the non-orthogonal amplify-and-forward (naf) protocol in cooperative communication systems," *IEEE Transactions on Wireless Communications*, vol. 10, no. 4, pp. 1038–1043, 2011.

[47] I. Krikidis, J. S. Thompson, and S. Mclaughlin, "On the diversity order of non-orthogonal amplify-and-forward over block-fading channels," *IEEE Transactions on Wireless Communications*, vol. 9, no. 6, pp. 1890–1900, 2010.

[48] Y. Bae, S. Jung, and J. Lee, "Capacity comparison of orthogonal and non-orthogonal cooperative relay systems," in *Vehicular Technology Conference, 2009. VTC Spring 2009. IEEE 69th*, 2009, pp. 1–5.

[49] A. Saadani and O. Traore, "Orthogonal or non orthogonal amplify and forward protocol: How to cooperate?" in *Wireless Communications and Networking Conference, 2008. WCNC 2008. IEEE*, 2008, pp. 368–373.

[50] I. F. Akyildiz, W. Su, Y. Sankarasubramaniam, and E. Cayirci, "A survey on sensor networks," *IEEE Communications Magazine*, vol. 40, no. 8, pp. 102–114, 2002.

[51] T. Arampatzis, J. Lygeros, and S. Manesis, "A survey of applications of wireless sensors and wireless sensor networks," in *Proc. IEEE Int. Symp. Control and Automation Mediterrean Conf Intelligent Control*, 2005, pp. 719–724.

[52] T. Ho, M. Medard, M. Effros, and R. Koetter, "Network coding for correlated sources," in *Proc. 38th Annu. Conf. Information Sciences and Systems*, Princetion, NJ, March 2004.

[53] J. Barros and S. D. Servetto, "Network information flow with correlated sources," *IEEE Transactions on Information Theory*, vol. 52, no. 1, pp. 155–170, 2006.

[54] A. R. Murugan, P. K. Gopala, and H. El Gamal, "Correlated sources over wireless channels: cooperative source-channel coding," *IEEE Journal on Selected Areas in Communications*, vol. 22, no. 6, pp. 988–998, 2004.

[55] S. Gao, "Joint distributed source and network coding for correlated information multicasting," in *Proc. 6th Int Communications and Networking in China (CHINACOM) ICST Conf*, 2011, pp. 698–702.

[56] P. L. Dragotti and M. Gastpar, *Distributed Source Coding: Theory, Algorithms and Applications*. Academic Press, 2009.

[57] R. Ahlswede, N. Cai, S.-Y. R. Li, and R. W. Yeung, "Network information flow," *IEEE Transactions on Information Theory*, vol. 46, no. 4, pp. 1204–1216, 2000.

[58] R. Joda and F. Lahouti, "Network code design for orthogonal two-hop network with broadcasting relay: A joint source-channel-network coding approach," *IEEE Transactions on Communications*, vol. 60, no. 1, pp. 132–142, 2012.

[59] T. S. Han, "Slepian-Wolf-Cover theorem for networks of channels," *Information and Control*, vol. 57, pp. 67–83, 1980.

[60] J. Del Ser, P. M. Crespo, B. H. Khalaj, and J. Gutierrez-Gutierrez, "On combining distributed joint source-channel-network coding and turbo equalization in multiple access relay networks," in *Proc. Third IEEE Int. Conf. Wireless and Mobile Computing, Networking and Communications WiMOB 2007*, 2007.

[61] Y. Wu, V. Stankovic, Z. Xiong, and S.-Y. Kung, "On practical design for joint distributed source and network coding," *IEEE Transactions on Information Theory*, vol. 55, no. 4, pp. 1709–1720, 2009.

[62] F. P. S. Luus and B. T. Maharaj, "Joint source-channel-network coding for bidirectional wireless relays," in *Proc. IEEE Int Acoustics, Speech and Signal Processing (ICASSP) Conf*, 2011, pp. 3156–3159.

[63] X. Zhou, A. O. Lim, K. Anwar, and T. Matsumoto, "Distributed joint source-channel-network coding exploiting source correlation for multiple access relay channel," in *European Wireless 2013*, Guildford, UK, 16-18 April 2013.

[64] C. E. Shannon, "A mathematical theory of communications," *Bell Systems Technical Journal*, vol. 27, pp. 379–423,623–656, 1948.

[65] X. Zhou, K. Anwar, and T. Matsumoto, "Serially concatenated joint source-channel coding for binary Markov sources," in *Communications and Networking in China (CHINACOM), 2011 6th International ICST Conference on*, 2011, pp. 53–60.

[66] L. Hanzo, R. G. Maunder, J. Wang, and L.-l. Yang, *Near-Capacity Variable-Length Coding: Regular and Exit-Chart-Aided Irregular Designs*. John Wiley & Sons, Inc., Nov. 23 2010.

[67] P. Duhamel and kieffer Michel, *Joint Source-Channel Decoding: A Cross-Layer Perspective with Applications in Video Broadcasting over Mobile and Wireless Networks*. Eurasip and Academic Press Series in Signal and Image Processing, Jan. 7 2010.

[68] L. Schmalen, M. Adrat, T. Clevorn, and P. Vary, "Exit chart based system design for iterative source-channel decoding with fixed-length codes," *IEEE Transactions on Communications*, no. 99, pp. 1–8, 2011, early Access.

[69] L. Schmalen and P. Vary, "Error resilient turbo compression of source codec parameters using inner irregular codes," in *Proc. Int Source and Channel Coding (SCC) ITG Conf*, 2010, pp. 1–6.

[70] R. Thobaben and J. Kliewer, "On iterative source-channel decoding for variable-length encoded markov sources using a bit-level trellis," in *Proc. 4th IEEE Workshop Signal Processing Advances in Wireless Communications SPAWC 2003*, 2003, pp. 50–54.

[71] ——, "Low-complexity iterative joint source-channel decoding for variable-length encoded markov sources," *IEEE Transactions on Communications*, vol. 53, no. 12, pp. 2054–2064, 2005.

[72] K. Lakovic and J. Villasenor, "Combining variable length codes and turbo codes," in *Proc. IEEE 55th Vehicular Technology Conf. VTC Spring 2002*, vol. 4, 2002, pp. 1719–1723.

[73] M. Jeanne, J. C. Carlach, P. Siohan, and L. Guivarch, "Source and joint source-channel decoding of variable length codes," in *Proc. IEEE Int. Conf. Communications ICC 2002*, vol. 2, 2002, pp. 768–772.

[74] M. Jeanne, J.-C. Carlach, and P. Siohan, "Joint source-channel decoding of variable-length codes for convolutional codes and turbo codes," *IEEE Transactions on Communications*, vol. 53, no. 1, pp. 10–15, 2005.

[75] V. Tervo, T. Matsumoto, and J. Karjalainen, "Joint source-channel coding using multiple label mapping," in *Proc. IEEE 72nd Vehicular Technology Conf. Fall (VTC 2010-Fall)*, 2010, pp. 1–6.

[76] J. Del Ser, P. M. Crespo, I. Esnaola, and J. Garcia-Frias, "Joint source-channel coding of sources with memory using turbo codes and the burrows-wheeler transform," *IEEE Transactions on Communications*, vol. 58, no. 7, pp. 1984–1992, 2010.

[77] J. Garcia-Frias and J. D. Villasenor, "Combining hidden markov source models and parallel concatenated codes," *IEEE Communications Letters*, vol. 1, no. 4, pp. 111–113, 1997.

[78] ——, "Joint turbo decoding and estimation of hidden markov sources," *IEEE Journal on Selected Areas in Communications*, vol. 19, no. 9, pp. 1671–1679, 2001.

[79] L. Yin, J. Lu, and Y. Wu, "LDPC-based joint source-channel coding scheme for multimedia communications," in *Proc. 8th Int. Conf. Communication Systems ICCS 2002*, vol. 1, 2002, pp. 337–341.

[80] R. Liu, J. Gao, and X. Zhang, "A modified iterative joint source-channel decoding algorithm based on LDPC codes and HMMs," in *Proc. ITW '06 Chengdu Information Theory Workshop IEEE*, 2006, pp. 370–374.

[81] M. Fresia, F. Perez-Cruz, and H. V. Poor, "Optimized concatenated LDPC codes for joint source-channel coding," in *Proc. IEEE Int. Symp. Information Theory ISIT 2009*, 2009, pp. 2131–2135.

[82] G.-C. Zhu and F. Alajaji, "Joint source-channel Turbo coding for binary markov sources," *IEEE Transactions on Wireless Communications*, vol. 5, no. 5, pp. 1065–1075, 2006.

[83] Z. Xiong, A. D. Liveris, and S. Cheng, "Distributed source coding for sensor networks," *IEEE Signal Processing Magazine*, vol. 21, no. 5, pp. 80–94, 2004.

[84] D. Slepian and J. Wolf, "Noiseless coding of correlated information sources," *IEEE Transactions on Information Theory*, vol. 19, no. 4, pp. 471–480, July 1973.

[85] S. S. Pradhan and K. Ramchandran, "Distributed source coding using syndromes (discus): design and construction," in *Data Compression Conference, 1999. Proceedings. DCC '99*, 1999, pp. 158–167.

[86] V. Stankovic, A. D. Liveris, Z. Xiong, and C. N. Georghiades, "Design of slepian-wolf codes by channel code partitioning," in *Data Compression Conference, 2004. Proceedings. DCC 2004*, 2004, pp. 302–311.

[87] A. D. Liveris, Z. Xiong, and C. N. Georghiades, "Joint source-channel coding of binary sources with side information at the decoder using IRa codes," in *Multimedia Signal Processing, 2002 IEEE Workshop on*, 2002, pp. 53–56.

[88] J. Garcia-Frias and Y. Zhao, "Near-shannon/slepian-wolf performance for unknown correlated sources over AWGN channels," *IEEE Transactions on Communications*, vol. 53, no. 4, pp. 555–559, April 2005.

[89] A. D. Liveris, Z. Xiong, and C. N. Georghiades, "A distributed source coding technique for correlated images using turbo-codes," *IEEE Communications Letters*, vol. 6, no. 9, pp. 379–381, 2002.

[90] ——, "A distributed source coding technique for highly correlated images using turbo-codes," in *Acoustics, Speech, and Signal Processing (ICASSP), 2002 IEEE International Conference on*, vol. 4, 2002.

[91] Z. Wang, X. Li, and M. Zhao, "Distributed coding of Gaussian correlated sources using non-binary LDPC," in *Image and Signal Processing, 2008. CISP '08. Congress on*, vol. 2, 2008, pp. 214–218.

[92] J. Ascenso, C. Brites, and F. Pereira, "Design and performance of a novel low-density parity-check code for distributed video coding," in *Image Processing, 2008. ICIP 2008. 15th IEEE International Conference on*, 2008, pp. 1116–1119.

[93] M. Sartipi and F. Fekri, "Distributed source coding in wireless sensor networks using LDPC coding: the entire slepian-wolf rate region," in *Wireless Communications and Networking Conference, 2005 IEEE*, vol. 4, 2005, pp. 1939–1944.

[94] B. Bai, Y. Yang, P. Boulanger, and J. Harms, "Symmetric distributed source coding using LDPC code," in *Communications, 2008. ICC '08. IEEE International Conference on*, 2008, pp. 1892–1897.

[95] M. Janani, A. Hedayat, T. E. Hunter, and A. Nosratinia, "Coded cooperation in wireless communications: space-time transmission and iterative decoding," *IEEE Transactions on Signal Processing*, vol. 52, no. 2, pp. 362–371, 2004.

[96] K. Anwar and T. Matsumoto, "Accumulator-assisted distributed Turbo codes for relay system exploiting source-relay correlations," *IEEE Communications Letters*, vol. 16, no. 7, pp. 1114–1117, 2012.

[97] M. Cheng, A. Irawan, K. Anwar, and T. Matsumoto, "BICM-ID for relay system allowing intra-link errors and a similarity constellation to ARQ schemes," in *Proc. Progress in Electromagnetics Research Symposium (PIERS) 2012*, 2012-03, pp. 281–286.

[98] M. Cheng, K. Anwar, and T. Matsumoto, "Outage-Analysis of Correlated Source Transmission in Block Rayleigh Fading Channels," in *2012 IEEE Vehicular Technology Conference (VTC 2012-Fall)*, Quebec, Canada, Sept. 2012, pp. 1–5.

[99] ——, "Outage probability of a relay strategy allowing intra-link errors utilizing Slepian-Wolf theorem," *EURASIP Journal on Advances in Signal Processing*, vol. 2013:34, 2013.

[100] S. Sharma, Y. Shi, J. Liu, Y. T. Hou, S. Kompella, and S. F. Midkiff, "Network coding in cooperative communications: Friend or foe?" *IEEE Transactions on Mobile Computing*, vol. 11, no. 7, pp. 1073–1085, 2012.

[101] L. Xiao, T. E. Fuja, J. Kliewer, and D. J. Costello, "A network coding approach to cooperative diversity," *IEEE Transactions on Information Theory*, vol. 53, no. 10, pp. 3714–3722, 2007.

[102] S. Fu, K. Lu, Y. Qian, and M. Varanasi, "Cooperative network coding for wireless ad-hoc networks," in *Global Telecommunications Conference, 2007. GLOBECOM '07. IEEE*, 2007, pp. 812–816.

[103] Z. Han, X. Zhang, and H. V. Poor, "High performance cooperative transmission protocols based on multiuser detection and network coding," *IEEE Transactions on Wireless Communications*, vol. 8, no. 5, pp. 2352–2361, 2009.

[104] A. Argyriou and A. Pandharipande, "Cooperative protocol for analog network coding in distributed wireless networks," *IEEE Transactions on Wireless Communications*, vol. 9, no. 10, pp. 3112–3119, 2010.

[105] A. Khlass, Y. Ghamri-Doudane, and H. Gacanin, "Combining cooperative relaying and analog network coding to improve network connectivity and capacity in vehicular networks," in *Global Telecommunications Conference (GLOBECOM 2011), 2011 IEEE*, 2011, pp. 1–5.

[106] G. Wang, W. Xiang, J. Yuan, and T. Huang, "Outage analysis of non-regenerative analog network coding for two-way multi-hop networks," *IEEE Communications Letters*, vol. 15, no. 6, pp. 662–664, 2011.

[107] A. Zhan, C. He, and L.-G. Jiang, "Outage behavior in wireless networks with analog network coding," *IEEE Transactions on Vehicular Technology*, vol. 61, no. 7, pp. 3352–3360, 2012.

[108] Z. Yi, M. Ju, and I.-M. Kim, "Outage probability and optimum power allocation for analog network coding," *IEEE Transactions on Wireless Communications*, vol. 10, no. 2, pp. 407–412, 2011.

[109] X. Bao and J. Li, "Adaptive network coded cooperation (ancc) for wireless relay networks: matching code-on-graph with network-on-graph," *IEEE Transactions on Wireless Communications*, vol. 7, no. 2, pp. 574–583, 2008.

[110] M. Xiao and M. Skoglund, "M-user cooperative wireless communications based on nonbinary network codes," in *Networking and Information Theory, 2009. ITW 2009. IEEE Information Theory Workshop on*, 2009, pp. 316–320.

[111] ——, "Design of network codes for multiple-user multiple-relay wireless networks," in *Information Theory, 2009. ISIT 2009. IEEE International Symposium on*, 2009, pp. 2562–2566.

[112] ——, "Multiple-user cooperative communications based on linear network coding," *IEEE Transactions on Communications*, vol. 58, no. 12, pp. 3345–3351, 2010.

[113] H. V. Nguyen, C. Xu, S. X. Ng, and L. Hanzo, "Non-coherent near-capacity network coding for cooperative multi-user communications," *IEEE Transactions on Communications*, vol. 60, no. 10, pp. 3059–3070, 2012.

[114] T. M. Cover and J. A. Thomas, *Elements of Information theory 2nd Edition.* USA: John Wiley & Sons, Inc., 2006.

[115] J. Proakis, *Digital Communications*, 4th ed. McGraw-Hill Science/Engineering/Math, Aug. 2000.

[116] M. Cheng, X. Zhou, K. Anwar, and T. Matsumoto, "Simple relay systems with BICM-ID allowing intra-link errors," *IEICE Trans. on Comm., Special Section on Coding and Coding Theory-Based Signal Processing for Wireless Communications*, vol. E95-B, no. 12, pp. 3671–3678, December 2012.

[117] K. Anwar and T. Matsumoto, "Very simple bicm-id using repetition code and extended mapping with doped accumulator," *Wireless Personal Communications*, pp. 1–12, September 2011.

[118] S. ten Brink, J. Speidel, and R.-H. Yan, "Iterative demapping and decoding for multilevel modulation," in *Global Telecommunications Conference, 1998. GLOBECOM 1998. The Bridge to Global Integration. IEEE*, vol. 1, 1998, pp. 579–584.

[119] X. Zhou, K. Anwar, and T. Matsumoto, "Serially concatenated joint source-channel coding for binary Markov sources," in *Communications and Networking in China (CHINACOM), 2011 6th International ICST Conference on*, Harbin, China, 17-19 Aug. 2011, pp. 53–60.

[120] S. ten Brink, "Code characteristic matching for iterative decoding of serially concatenated codes," *Annals of Telecommunications*, vol. 56, pp. 394–408, 2001.

[121] ——, "Convergence behavior of iteratively decoded parallel concatenated codes," *IEEE Transactions on Communications*, vol. 49, no. 10, pp. 1727–1737, Oct. 2001.

[122] F. Brännström, L. K. Rasmussen, and A. J. Grant, "Convergence analysis and optimal scheduling for multiple concatenated codes," *IEEE Transactions on Information Theory*, vol. 51, no. 9, pp. 3354–3364, 2005.

[123] L. Bahl, J. Cocke, F. Jelinek, and J. Raviv, "Optimal decoding of linear codes for minimizing symbol error rate (corresp.)," *IEEE Transactions on Information Theory*, vol. 20, no. 2, pp. 284–287, March 1974.

[124] W. E. Ryan, "Concatenated convolutional codes and iterative decoding," *Encyclopedia of Telecommunications*, 2003.

[125] R. Youssef and A. Graell i Amat, "Distributed serially concatenated codes for multi-source cooperative relay networks," *IEEE Transactions on Wireless Communications*, vol. 10, no. 1, pp. 253–263, 2011.

[126] T. M. Cover, "A proof of the data compression theorem of slepian and wolf for ergodic sources (corresp.)," *IEEE Transactions on Information Theory*, vol. 21, no. 2, pp. 226–228, 1975.

[127] L. R. Rabiner, "A tutorial on hidden markov models and selected applications in speech recognition," *Proceedings of the IEEE*, vol. 77, no. 2, pp. 257–286, 1989.

[128] D. Arnold and H.-A. Loeliger, "On the information rate of binary-input channels with memory," in *Communications, 2001. ICC 2001. IEEE International Conference on*, vol. 9, 2001, pp. 2692–2695.

[129] E. Ordentlich and T. Weissman, "Approximations for the entropy rate of a hidden Markov process," in *Information Theory, 2005. ISIT 2005. Proceedings. International Symposium on*, 2005, pp. 2198–2202.

[130] J. Luo and D. Guo, "On the entropy rate of hidden Markov processes observed through arbitrary memoryless channels," *IEEE Transactions on Information Theory*, vol. 55, no. 4, pp. 1460–1467, 2009.

[131] M. Tuchler, "Convergence prediction for iterative decoding of threefold concatenated systems," in *Proc. IEEE Global Telecommunications Conf. GLOBECOM '02*, vol. 2, Nov. 2002, pp. 1358–1362.

[132] X. He, "Large scale distributed decision making technique and wireless chief executive officer problem," Master thesis, Japan Advanced Institute of Science and Technology (JAIST), 2013.

[133] P.-S. Lu, V. Tervo, K. Anwar, and T. Matsumoto, "Low-complexity strategies for multiple access relaying," in *Proc. IEEE 73rd Vehicular Technology Conf. (VTC Spring)*, 2011, pp. 1–6.

[134] G. Zeitler, G. Bauch, and J. Widmer, "Quantize-and-forward schemes for the orthogonal multiple-access relay channel," *IEEE Transactions on Communications*, vol. 60, no. 4, pp. 1148–1158, April 2012.

[135] A. Gamal and Y. Kim, *Network Information Theory*. Cambridge University Press, 2011.

[136] A. D. Wyner, "On source coding with side information at the decoder," *IEEE Transactions on Information Theory*, vol. 21, no. 3, pp. 294–300, 1975.

[137] L. Shampine, "Matlab program for quadrature in 2D," *Applied Mathematics and Computation*, vol. 202, no. 1, pp. 266 – 274, 2008.

[138] J. Hagenauer, E. Offer, and L. Papke, "Iterative decoding of binary block and convolutional codes," *IEEE Transactions on Information Theory*, vol. 42, no. 2, pp. 429–445, 1996.

[139] O. Iscan and C. Hausl, "Iterative network and channel decoding for the relay channel with multiple sources," in *Proc. IEEE Vehicular Technology Conf. (VTC Fall)*, 2011, pp. 1–5.

[140] A. Irawan, K. Anwar, and T. Matsumoto, "Combining-after-decoding turbo hybrid ARQ by utilizing doped-accumulator," *IEEE Communications Letters*, vol. 17, no. 6, pp. 1212–1215, June 2013.

[141] R. H. Gohary and T. J. Willink, "Joint routing and resource allocation via superposition coding for wireless data networks," *IEEE Transactions on Signal Processing*, vol. 58, no. 12, pp. 6387–6399, December 2010.

[142] A. Zafar, M. Shaqfeh, M.-S. Alouini, and H. Alnuweiri, "On multiple users scheduling using superposition coding over Rayleigh fading channels," *IEEE Communications Letters*, vol. 17, no. 4, pp. 733–736, April 2013.

[143] L. Chen, L. Cao, X. Zhang, and D. Yang, "Integrating network coding and superposition coding in extended two-way relay networks," in *GLOBECOM Workshops (GC Wkshps), 2010 IEEE*, Miami, FL, 2010, pp. 1481–1486.

[144] E. S. Lo and K. B. Letaief, "Network coding versus superposition coding for two-way wireless communication," in *Wireless Communications and Networking Conference, 2009. WCNC 2009. IEEE*, 2009, pp. 1–5.

[145] M. Park and S. K. Oh, "A hybrid network-superposition coding for asymmetrical two-way relay channels," in *Vehicular Technology Conference Fall (VTC 2009-Fall), 2009 IEEE 70th*, Anchorage, AK, 2009, pp. 1–5.

[146] K. Fukawa, S. Ormsub, A. Tölli, K. Anwar, and T. Matsumoto, "EXIT-constrained BICM-ID design using extended mapping," *EURASIP Journal on Wireless Communications and Networking*, vol. 2012:40, 2012.

Publications

Journal Articles

[1] **X. Zhou**, M. Cheng, K. Anwar and T. Matsumoto, "Distributed Joint Source-Channel Coding for Relay Systems Exploiting Source-Relay Correlation and Source Memory", *EURASIP Journal on Wireless Communications and Networking 2012*, 2012:260.

[2] **X. Zhou**, X. He, K. Anwar and T. Matsumoto, "GREAT-CEO: larGe scale distRibuted dEcision mAking Techniques for Wireless Chief Executive Officer Problems", *IEICE Transactions on Communications*, Vol. E95-B, No. 12, pp. 3654-3662, December 2012.

[3] **X. Zhou**, P.-S. Lu, K. Anwar and T. Matsumoto, "Correlated Sources Transmission in Orthogonal Multiple Access Relay Channel: Theoretical Analysis and Performance Evaluation", *IEEE Transactions on Wireless Communications*, (Under Review).

[4] M. Cheng, **X. Zhou**, K. Anwar and T. Matsumoto, "Simple Relay Systems with BICM-ID Allowing Intra-link Errors", *IEICE Transactions on Communications*, Vol. E95-B, No. 12, pp. 3671-3678, December 2012.

[5] M. A. M. Izhar, N. Fisal, **X. Zhou**, K. Anwar and T. Matsumoto, "Exploitation of 2D Binary Source Correlation using turbo block codes with fine-tuning", *EURASIP Journal on Wireless Communications and Networking 2013*, 2013:89.

[6] X. He, **X. Zhou**, K. Anwar and T. Matsumoto, "Estimation of Observation Error Probability in Wireless Sensor Networks", *IEEE Communication Letters*, Vol. 17, No. 6, pp. 1073-1076, June 2013.

[7] P.-S. Lu, **X. Zhou**, K. Anwar and T. Matsumoto, "Joint Adaptive Network-Channel Coding for Energy-Efficient Multiple Access Relaying", *IEEE Transactions on Vehicular Technology*, (Under Review).

Conference Proceedings

[8] **X. Zhou**, K. Anwar and T. Matsumoto, "Serially Concatenated Joint Source-Channel Coding for Binary Markov Sources", *6th International ICST Conference on Communications and Networking in China (ChinaCom 2011)*, No.384, August 17-19, 2011, Harbin, China.

[9] **X. Zhou**, M. Cheng, K. Anwar and T. Matsumoto, "Distributed Joint Source-Channel Coding for Relay Systems Exploiting Spatial and Temporal Correlations", *IEEE Wireless Advanced 2012*, June 25-27, 2012, London, UK.

[10] **X. Zhou**, K. Anwar and T. Matsumoto, "EXIT Chart Based Joint Source-Channel Coding for Binary Markov Sources", *IEEE 76th Vehicular Technology Conference*, September 3-6, 2012, Quebec, Canada.

[11] **X. Zhou**, A. O. Lim, K. Anwar and T. Matsumoto, "Distributed Joint Source-Channel-Network Coding Exploiting Source Correlation for Multiple Access Relay Channel", *European Wireless 2013*, April 16-18, 2013, Guildford, UK.

[12] M. A. M. Izhar, N. Fisal, **X. Zhou**, K. Anwar and T. Matsumoto, "Utilization of 2-D Markov Source Correlation using Block Turbo Codes", *7th International Symposium on Turbo Codes and Iterative Information Processing (ISTC)*, pp. 56-60, August 27-31, 2012, Gothenburg, Sweden.

[13] X. He, **X. Zhou**, K. Anwar and T. Matsumoto, "Wireless Mesh Networks Allowing Intra-Link Errors: CEO Problem Viewpoint", *2012 International Symposium on Information Theory and Its Applications (ISITA2012)*, October 28-31, 2012, Hawaii, USA.

[14] **X. Zhou**, M. Cheng, X. He and T. Matsumoto, "Derivation of Outage Probability Expression for Decode-and-Forward Relaying System Allowing Intra-link Errors", *Globecom 2013 Workshop on Cloud-Pressing in Heterogeneous Mobile Communication Networks (IWCPM2013)*, (Submitted).